Appendix to Comparative Views of Major Regions of Active Normal Faulting and Crustal Extension on Earth

Steven G. Wesnousky
Center for Neotectonic Studies and
Nevada Seismological Laboratory
Mail Stop 174
1664 North Virginia Street
University of Nevada, Reno
Reno, Nevada 89557
email: wesnousky@unr.edu

Synopses of observations used in constructing tables and plots for each region considered and cited in the manuscript.

Each Synopsis includes sections entitled.
1. *Tectonic Setting, Geography, and Historical Context*.
2. *Physiography and Structural Character of Basins.*
3. *Distribution of Volcanics and Initiation of Rifting.*
4. *Heat Flow*
5. *Seismology*
6. *Geodesy*
7. *Crustal Structure*

The Aegean - Table 1

Tectonic Setting, Geography, and Historical Context. The region is located within the Alpide mountain belt **(Figure A1a)**. Geologists early recognized the belt to result from a northward contraction between Africa and Eurasia that commenced ~65 Ma (Argand, 1916; Heim, 1922; Staub, 1924). McKenzie (1970) and Dewey et al. (1973) followed with a plate tectonic characterization of the region. Convergence continues today and is largely accommodated by northward subduction of the Mediterranean (African Plate) beneath the Hellenic and Cyprean arcs and a westward motion of Turkey (Anatolia) along the conjugate North and East Anatolian fault systems **(Figure A1b)**. Ongoing extension within and along the margins of the Aegean is attributed to both a southward migration of the Hellenic Arc ('trench rollback' and development of a 'back-arc basin') that commenced as early as ~35 Ma ago (Le Pichon and Angelier, 1979; Le Pichon and Kreemer, 2010; Jolivet et al., 2013), and a westward migration of the right-lateral North Anatolian fault system into the Aegean region (Armijo et al., 1996; Goldsworthy et al., 2002), where strike-slip motion is partitioned to extensional displacement along the westward reaches of the fault system. The North Anatolian fault initiated ~12 Ma (Sengor et al., 2005) and extended to the northern Aegean sea by ~5 Ma, more recently than when the Hellenic Arc began its southward migration (Sengor et al., 1985; Armijo et al., 1999). Jolivet et al. (2009) comprehensively review the geodynamic evolution of the area.

Physiography and Structural Character of Basins. Normal fault bounded basins along the margins of the Aegean generally trend westward in response to north trending extension, clearly expressed by smooth water-filled and alluvial surfaces bounded abruptly at mountain rangefronts (**Figures A2**). Adjacent peaks generally rise on average 1550 m above sea level, ranging between 400 m and 2250 m. Accounting for the elevation of basin floors and the thickness of sediment and water filling the basins, the structural relief across basins ranges between 880 m and 6150 m and averages ~3700m. That the individual basins apparent on the surface are the result of the linking of smaller fault bounded basins through time is evident by presence of multiple depocenters reported along some of the grabens. Asymmetry in sediment fill thicknesses and the mapping of bounding faults shows the majority of basins are half, rather than full grabens.

Submarine basins in the Aegean are more often rhomboidal, elliptical, or trapezoidal in shape, with orientations and bounding faults and steep slopes that predominantly trend NE-SW to ENE-WSW and less so in the NW-SE to WNW- ESE directions (Sakellariou and Tsampouraki-Kraounaki, 2016). Maximum topographic reliefs across the submarine basins averages ~1700 m, falling in the range 515 m and 3550 m. Measures of structural relief fall between 1075 m and 5160 m, and average about 3100 m, when accounting for thicknesses of basin fill reported largely from seismic reflection surveys across the basins,

Distribution of Volcanics and Initiation of Rifting. The arcuate alignment of active volcanoes extending across the Aegean from Turkey to Greece is the South Aegean Volcanic Arc (**Figure A2**). Older fields of volcanic rocks are conspicuous to the north of the Arc, largely in Turkey and less so within the Aegean and Greece (**Figure A3**). The older volcanics show a trend of ages that increase northward in Plio-Quaternary to Eocene time. The progression is surmised to record the southward migration of the Hellenic subduction system (Fytikas et al., 1984; Ersoy and Palmer, 2013). Volcanic rocks are largely absent from the numbered extensional basins in **Figures A2**, but for those along the volcanic arc and the presence of Miocene fields adjacent to the Kucuk-Menderes (basin 11), Buyuk-Menderes (basin 12) and Aleshir-Gediz grabens (basin 10) in Turkey.

Interpretations of seismic reflection profiles, geological cross sections, and observations of the oldest sediments resting on basement show rifting across the region initiated ~3 Ma to ~23 Ma. Most common are Pliocene (3.8 Ma to 5.3 Ma) ages for basins within Greece and the Aegean, whereas basins in Turkey and the southeastern most Aegean are more broadly bracketed between about 5.3 and 23 Ma. The major exceptions to these generalities are the older Eocene age sediments reported at the bottom of the Thessoloniki Basin and North Aegean Trough.

Heat flow. Fytikas and Kolios (1979) use 37 measurements onshore and an additional 22 offshore measurements from Jongsma (1974), Erickson (1970), and Hsu et al. (1975) to produce the heat flow map of the Aegean and coastal Greece in **Figure A3**. Heat flow contours range between 80-120 mWm^{-2} along the volcanic arc and 60-100 mWm^{-2} elsewhere across the Aegean and coastal regions of Greece. (The same map is reproduced in Papadakis et al. (2016)). Heat flow along the Aegean coastal regions of Turkey is described in the heat flow map of Balkan-Pazvantoglu et al. (2021) also reproduced in **Figure A3** that is based on ~70 measurements, including those previously published by Pfister et. al. (1998) and Erkan (2015). Values across the area generally fall between 60 and 100 mWm^{-2}. The resolution of the maps is limited by irregular and wide spacing of measurement sites (on average one per ~2.5 to 10 km^2).

Seismology. The principal characteristics of seismicity around the Aegean were first charted more than 50 years ago (Caputo et al., 1970; McKenzie, 1970; 1972; 1978) and since refined in numerous seismicity analyses and reviews (e.g., Jackson, 1994; Jolivet et al., 2013; Bocchini et al., 2018). Earthquake hypocenters north of the Hellenic arc are generally limited to depths between 5 and 25 km and focal mechanisms of such events are normal (Shaw and Jackson, 2010), reflecting north-south extension, but for in the northernmost Aegean along the west to southwest trending North Anatolian faults system where displacements are more often strike-slip.

The 1969-03-28 Mw 6.8 Alesehir (Eyidogan and Jackson, 1985) and the 1970-03-28 Mw 7.2 Gediz earthquakes (Ambraseys and Tchalenko, 1970; Ambraseys and Jackson, 1998; Gürboga, 2013) in Turkey, the 1981-02-24 Mw 6.5 earthquake in the Gulf of Corinth, Greece (Jackson et al., 1982a; Jackson et al., 1982b), and the 2020-10-30Mw 7.0 Samos (Ganas et al., 2021; Ren et al., 2022) and 1956-07-09 Amorgos earthquakes within the Aegean Sea (Okal et al., 2009; Leclerc et al., 2024) are the largest instrumentally recorded earthquakes in the area (**Figure A2**). The normal fault ruptures are all limited to depths less than about 25 km.

Geodesy. Global Positioning System (GPS) studies across the region are numerous (Straub and Kahle, 1994; Reilinger et al., 1997; Straub et al., 1997; Clarke et al., 1998; Cocard et al., 1999; Kahle et al., 1999; Kahle et al., 2000; McClusky et al., 2000; Ayhan et al., 2002; Goldsworthy et al., 2002; Meade et al., 2002; Avallone et al., 2004; Nyst and Thatcher, 2004; Reilinger et al., 2006; Hollenstein et al., 2008; Aktug et al., 2009; Le Pichon and Kreemer, 2010; Nocquet, 2012; Chousianitis et al., 2015; Ozdemir and Karslioglu, 2019).

The southward increase in length of GPS vectors that are plotted in an Anatolia-fixed reference frame and reported by McClusky et al. (2000) conveniently illustrates the northerly extension that is ongoing across the Aegean (**Figure A2**).

The Bergama (basin 9), Aleshir-Gediz (basin 10), Kucuk-Menderes (basin 11), Buyuk-Menderes (basin 12), and Gokova Basins (basin 13-ob) each trend easterly and are located along an ~300 km long span of the *Aegean-Turkey coast* **(Figure A2)**. The geodetically derived strain field presented in Figure 7 of Aktug et al. (2009) shows principal axes of extension northerly directed with values between ~40-60 nstrain/yr, equivalent to an extension rate of ~12 to 18 mm/yr when multiplied by 300 km. Calculated values of strain are locally higher when models assume basin are bounded by rigid blocks. The block modeling of Aktug et al. (2009), for example, shows extensional strain and extension rates across the Aleshir-Gediz graben equal to 85 nstrain/yr and 4-6 mm/yr, 140 nstrain/yr and 3-8 mm/yr across the Buyuk-Menderes graben, and ~4-7 mm/yr across the Gokova basin.

The size of principal extensional strains varies markedly along the *western margin of Greece* (Chousianitis et al., 2015). The maximum rates of north directed extensional strain are in the range of 100 – 150 nstrain/yr over the ~100 km distance encompassing the Gulf of Corinth (Basin 1) and the Evoikos Gulf (Basin 2) **(Figure A2)**, equivalent to a rate of extension between about 10 - 15 mm/yr. Values of northerly directed range are a lesser 20-40 nanostrain/yr along a ~200 km transect that crosses basins 3 to 7 add another ~4 to 8 mm/yr extension along the coast.

Strain rates in the *Aegean* south of the latitude of Corinth and north of the island of Crete are negligible in comparison to those observed along the coastal regions of Greece and Turkey (Kahle et al., 1999; Le Pichon and Kreemer, 2010; Chousianitis et al., 2015) . The observation is in concert with the general absence of seismicity as compared to along the adjacent coasts. The same studies show the northern Aegean crust in the vicinity of ~40°N is dominated by the strike-slip motions of the Anatolian fault system with principal extensional strains approaching 150 nstrain/yr.

Crustal Structure. Active source seismic reflection and refraction studies in concert with inversion of gravity field measurements to assess Moho thickness began in the 1970's (e.g., Makris, 1977; Makris and Vees, 1977), continued in the decades following (e.g., Papoulia and Makris, 2010), and are summarized in the analysis of Makris et al. (2009). More recently passive seismic techniques, including Pn-tomography and P and S-wave receiver analysis have complemented and contributed to characterizing the depth of Moho across the Aegean (e.g., Saunders et al., 1998; Sodoudi et al., 2006; Wang et al., 2014). The findings generally agree. The map of Sodoudi et al (2006) based on P and S receiver functions encompasses the entire region and shows Moho depths generally between ~25 -33 km, with values generally increasing within the central Aegean to greater values along the coasts and inland, but for depths as low as 21 km for basins immediately north of Crete (Basins 18-0B and 19-0B in **Figure A2**). The crustal thicknesses fall between those of oceanic and continental crust and are attributed to extreme crustal thinning of continental crust that occurred with southward migration of the Hellenic arc (Jolivet et al., 2013)

Africa - Table 2

Tectonic setting, geography, and historical context. Physical descriptions of the East African Rift System **(Figure A4)** began with nineteenth century European explorers seeking the source of Nile and Congo rivers (among them David Livingstone (1813-1873), Richard F. Burton (1821-1890), John H. Speke (1827-1864), and Henry M. Stanleys (1841-1904) - see McConnell, 1972). The largely Neogene Eastern and Western Branches of the rift system trend southerly across >3000 km of eastern Africa. The Eastern Branch (sometimes also referred to as the Gregory Rift) extends southward from near Addis Ababa through the Lake Eyasi basin and southward to the latitude of Lake Rukwa. The Western Branch encompasses Lake Mobutu basin in the north and extends southward to Lake Rukwa. The Lake Malawi (Nyasa) rift is considered to be the southern extension of the Western Branch based on continuity of topographic, free-air gravity and seismicity trends (Ebinger et al., 1987), and possibly farther south through Mozambique beneath sedimentary cover (Domingues et al., 2016).

The entire extent of the Eastern Branch of the rift system is first addressed by Suess (1891), following yet earlier explorations of the area by the Hungarian explorer Count Samuel Teleki (von Hohnel, 1894; Teleki, 1895; McConnell, 1972; Kent, 1978). Subsequent explorations by Gregory (1896) included the

Western Branch. Therein arose the interpretion that the basins of the rift are fault bounded grabens indicative of crustal extension. Ensuing decades brought forth some disagreement with the idea that the rift system is extensional. Bullard (1936) and Willis (1936), for example, suggested the rift was the result of thrust faulting. Heezen's (1960) recognition of the global seafloor rift system and the ensuing development of plate tectonics removed the idea of thrusting from discussion. The East African Rift System in that plate tectonic framework is the landward continuation of mid-ocean ridges and the result of incipient seafloor spreading. Research in the vicinity of the rift has since focused on documenting the temporal evolution of the system, the geophysical and seismological characteristics of the region, and structural development of the rifts basins (e.g., McConnell, 1967; McConnell, 1972; Bosworth et al., 2005; Chorowicz, 2005; Corti, 2009; d'Oreye et al., 2011; Macgregor, 2015).

Physiography and Structural Character of Basins. The *East African Rift* system is a relatively continuous alignment of elongate sediment and often water-filled grabens developed largely in Precambrian crust (Chorowicz, 2005; Corti, 2009) (**Figure A4**). Basin widths generally fall between 20 and 50 km, but for the Ethiopian and Luangwa rifts that surpass 60 km. Basin lengths are most common between ~50 km and 300 km with exception of the water-filled Lakes Malawi and Tanganyika that approach 600 km to 700 km, respectively. For those basins affording observations of basin fill depths, structural reliefs range from ~4000 m to >10,000m. Peaks adjacent to basins commonly reach 2000 to 4000 m.

Basins are generally asymmetric half grabens, characterized on one side by a normal high angle border fault that accommodates the majority of extension and, on the opposite side, lesser normal faults accompanying flexure and rollover of the hanging wall into the main high angle border fault (Ebinger, 1989; Morley et al., 1992; Chorowicz, 2005). Main border faults reach to >100 km length and are generally limited to one side of the larger valleys and basins (Ebinger et al., 1987; Jackson and Blenkinsop, 1997; 1999). Reversals in basin asymmetry less frequently lead to a segmentation of the larger valleys into accordingly smaller structural sub basins (Ebinger, 1989). The broad flanks of the rift system are commonly uplifted 1-2 km above surrounding topography of the East African Plateau. The uplift is generally highest along rift edge defined by a main border fault and attributed to flexural isostatic compensation resulting from displacement on the main border faults (Ebinger et al., 1991; 1999). East African graben faults generally cut preexisting structures and basement fabric (Ebinger et al., 1999).

Distribution of Volcanics and Initiation of Rifting. Large volumes of Eocene and younger volcanic rocks are observed along the *Eastern Branch* whereas volcanism is limited to a few isolated centers along the *Western Branch (***Figure A5***)*. Given that the ultimate phase of continental rifting is effusive volcanism and sea-floor spreading, the *Eastern Branch* appears to be at a more advanced stage of rifting than the *Western Branch*. Rocks on which the East African Rift is developed and on which the volcanics are extruded are no younger than Jurassic to Precambrian age, indicating hundreds of millions of years of tectonic quiescence before rifting.

The history of rifting is largely derived from chronostratigraphic sections of basin fill sediments derived from drilling (e.g., Macgregor, 2015). The present day rift system is considered to have initiated with vulcanism ~35 Ma (latest Eocene) along the *Eastern Branch* near the present day Kenyan settlement of Lokichar (**Figures A4 and A5**). The subsequent initiation and development of individual basins elsewhere along the *East African Rift* generally post-dates the early to mid-Miocene (~12-23 Ma).

Heat Flow. Heat flow measurements are few within and around the East African rift system (Davies, 2013). VonHerzen and Vacquier (1967) report 22 measures of heat flow within Lake Malawi. Ebinger et al. (1987) corrected the values for sedimentation effects and interpret heat flow across the entire lake basin averages about 75.3 mW/m^2, with values ranging from about 137.5 when attention is limited to the central portion of the lake, and lesser average values of about 28 to 40 mW/m^2 toward the northern and southern limits of the lake, respectively. Chapman and Pollack (1977) report eleven widely spaced sites in Zambia to register heat-flow values between 54 to 76 $mW\ m^{-2}$ (average 66). Values of heat flow reported by Wheildon et al. (1994) on the western and eastern flanks of the Kenyan rift are 40 to 60 $mW\ m^{-2}$ and 50 to 100 $mW\ m^{-2}$ on the rift floor. When taken together, the observations of heat flow show little to no elevation of geotherms beneath the rift flanks, and heat flow measurements along the rift floors are locally elevated and somewhat higher (e.g., Nyblade et al., 1990; Wheildon et al., 1994). Wheildon et al. (1994) concluded from their observations in the Kenya rift that any deep-seated heat anomaly associated with the Kenya rift has not yet been conducted to the surface. Nyblade (1997) with four additional measurements similarly concludes that heat flow in the interior of East Africa is not elevated relative to undisturbed Precambrian terrains of similar age. Mohamed and Al Deep (2021) most recently incorporate gravity and magnetic data in presenting a regional model to interpret heat flow averages between 40 and 50 mWm^{-2} in the vicinity of the rifts **(Figure A6)**.

Seismology and Geodesy. Rates of extension across the rift assessed by GPS range from 1 to 3 mm/yr along branches of the rift located south of about Lake Turkana (**Figure A7)**, and as high as 5 mm/yr within the Ethiopian Rift and Afar (Saria et al., 2014; Stamps et al., 2018). Accordingly, focal mechanisms of earthquakes are mostly normal with P-axis oriented transverse to the trend of the basins (Shudofsky, 1985; Foster and Jackson, 1998; Yang and Chen, 2010; Lindenfeld et al., 2012). Seismicity along the rift system **(Figure A7)** occurs to depths of 25 to 42 km along the *Eastern* and *Western Branches* of the rift (e.g., Craig et al., 2011; Lavayssiere et al., 2019). Locally seismicity has been observed to extend continuously with no gap from near the surface to depths of ~42 km (Lavayssiere et al., 2019).

The largest instrumentally analyzed events along the rift occurred in 1990 (Mw 7.1; Giardini and Beranzoli, 1992) and 2006 (Mw 7.0; Yang and Chen, 2008) **.** The shocks initiated at depths of about 15 km and along extensions of the *Western Branch.* (**Figure A4 and A7)**. The northernmost of these exhibited left-lateral slip on a northwest striking fault plane (Gaulon et al., 1992), and the southern displays normal displacement indicating near east-west extension (Yang and Chen, 2008). The only known earthquake to have produced surface rupture is the M6.9 Subukia Valley earthquake of 1928 in the Kenyan rift (Ambraseys, 1991). Zielke and Strecker (2009) report the fault has produced six similar earthquakes in the last ~50,000 years.

Crustal Structure. Estimates of Moho depth about the East and West Branches derived from analysis of body-wave receiver functions and surface wave group velocity analyses are about 40 ± 2 km, similar to the observed maximum depth of seismicity. (Dugda et al., 2007; Craig et al., 2011; Hodgson et al., 2017; Wang et al., 2021; Baranov et al., 2023).

Baikal Rift System - Table 3

Tectonic setting, geography, and historical context. Baikal Rift basins trend ~1700 km northwestward from Mongolia into Russia **(Figure A8)**. The largest of the basins are filled by Lake Baikal**.** Rift research has its origins in the 18th century geographic expeditions of the Russian Academy of Sciences (Mats, 1993). Earliest nineteenth century investigators attributed the Rift to synclinal warping of the crust. The Rift, and in particular Lake Baikal, was subsequently ascribed to the pulling apart of tectonic blocks (Obrutchev, 1938). Geological and geophysical study of the rift escalated rapidly with establishment of Russia's Institute of the Earth's Crust (IEC) in Irkutsk in the 1960's (e.g., Florensov, 1960; Vvedenskaya, 1961; Misharina, 1963; Florensov, 1965b; Khil'ko, 1966; Kurushin et al., 1966; Lubimova and Shelyagin, 1966; Zorin, 1966; Misharina, 1967). Florensov (1969) introduced the research to the English literature and investigations are numerous since (e.g., Logatchev, 1984; Baljinnyam et al., 1993; Ivanov, 2004; Petit and Déverchère, 2006; Ivanov and Demonterova, 2009).

The tectonic similarities between the Baikal and African rift systems were first addressed by Pavlovsky (1948). Earlier studies attribute the initiation and development of the Baikal Rift to local thermal processes in the underlying mantle (e.g., Lubimova, 1969; Artemjev and Artyushk, 1971; Logatchev et al., 1983). The idea that the Baikal Rift system formed in response to plate tectonic movements, specifically the northward advance of the India subcontinent into Asia, arose with the research of Molnar and Tapponnier (1975) (**Figure A9**). Normal faults of Baikal Rift system in this interpretation are accommodating extension produced by left-lateral strike-slip motion on east-west striking faults that serve to accommodate northward collision of India into Asia. The relative contribution of the two processes that have contributed to rift development remains a point of discussion today (e.g, Ivanov, 2004; Ivanov et al., 2015).

Physiography and Structural Character of Basins. The north-trending Busingol, Dharkhart, and Hovsgol (Khuvsgul) basins of the Sayan highlands comprise the southwestern limit of the Baikal Rift system (**Figure A8**). The remaining basins strike northeast. The Lake Baikal basins are the largest of the system with widths and lengths reaching upwards of of 40-50 km and 200-250 km, respectively. Maximum elevations along the rift commonly approach and surpass 3000 m, and topographic relief locally reaches to between 2 and 2.5 km. The basins are invariably bounded by abrupt and steep rangefronts. Thicknesses of basin-filling sediment are reported for all but the Busingol and Darkhat basins (Logatchev, 1974; Hutchinson et al., 1992; Logatchev and Zorin, 1992; Mazilov et al., 1993; Prokopenko et al., 2005; Shchetnikov et al., 2012). Sedimentary fill is generally greatest on the north and northwest sides of the basins, giving reason to interpret that the basins are chiefly the result of displacement on normal faults that dip south and southwest from the north and northwest edges of the basins, respectively (e.g., Hutchinson et al., 1992; Logatchev and Zorin, 1992; Shchetnikov et al., 2012). The reported thicknesses of basin fill with measures of the highest adjacent of mountain peaks indicate values of structural relief that range from 2000 to 4000 meters across basins at the southwestern and northeastern end of the rift system and to over an 10000 meters in the central basins filled by Lake Baikal.

Distribution of Volcanics. Significant attention has been placed in study of the spatial, temporal, and petrological characteristics of volcanism across the region (e.g., Florensov, 1969; Logatchev and Florensov, 1978; Logatchev et al., 1983; Kiselev, 1987; Rasskazov et al., 1997; Rasskazov et al., 2002; Johnson, 2005; Ivanov and Demonterova, 2009; Ivanov et al., 2015). Pre-Cenozoic volcanic rocks are not observed. Cenozoic volcanic rocks are limited to (1) numerous distributed small volcanic fields encompassing the southwestern end of the rift system, (2) the larger Vitim and Udokan volcanic fields to the northeast (**Figure A10**).. The volcanism, mostly basaltic, commenced as early as Late Oligocene, was common to the areas by Early Miocene, and persistent though not continuous into the Pliocene and Quaternary. Holocene volcanism is limited to a few volcanoes at the very northeastern and southwestern limits of the rift system (Rasskazov et al., 2002; Ivanov and Demonterova, 2009).

Initiation of Rifting: Zorin (1999) and Petit & Déverchère (2006) address in detail the tectonic evolution of the Rift. The rift resides along the boundary of Siberian Platform and the Sayan-Baikal fold belt (**Figures A8 and A10)**. Paleozoic and Mesozoic sedimentary cover on the Platform overlies Archaean basement. Episodes of Paleozoic and Mesozoic deformation are recorded in the Paleozoic and Mesozoic sediments. The Sayan-Baikal fold belt is composed of rocks accreted to the craton during the early Paleozoic and reactivated by northeast contraction during the Mesozoic. The northwest directed alignment of hills of the Sayan-Baikal fold belt are remanent of the Mesozoic contraction. This contraction is the youngest episode of crustal deformation preceding development of the Baikal rift.

The temporal evolution of Baikal Rift basins is recorded in the age, texture, and depth of sediments to crystalline basement observed in each (e.g., Florensov, 1969; Logatchev and Florensov, 1978; Logatchev, 1984; Nikolayev et al., 1985; Logatchev and Zorin, 1987). Krivonogov and Safonova (2017) use the observations to interpret initiation of rifting in the Tunka and south and central Lake Baikal basins to be as old as late Cretaceous (65ka-100ka), Oligocene (23-38 Ma) in the north basin of Lake Baikal, and Miocene (5-23 Ma) and younger for remaining basins of the rift. The earlier stages of basin formation appear older than the main stage of India-Asia collision which commenced about 25- 20 Ma (Hall, 2002).

Heat Flow. Lubimova and Shelyagin (1966) and Lubimova (1969) first interpreted on the basis of 18 measurements the presence of a regional heat flow anomaly along the Baikal rift. Lysak (1975a; 1978) in contrast and with a larger ~150 measurements observe the pattern of heat flow within Lake Baikal to be irregular and not to reflect a regional anomaly. They rather interpret relatively high values within the rift to redistribution of heat by hydrothermal circulation along active fault structures. A subsequent assessment of ~500 measurements by Lysak (1984) arrives at the same conclusion and reports mean values of heat flow between 50-75 mWm^{-2} along the rift system, 25-50 mWm^{-2} in the Siberan Platform, and 50-75 mWm^{-2} in the Zayan-Baikal fold belt. More recent measurements and data summaries are in accord with these values (Lysak and Sherman, 2002; Poort and Klerkx, 2004; Rychkova and Mongush, 2018).

Seismology. Seismicity in the area **(Figure A10)** concentrates in a zone along the rift (Radziminovich et al., 2013). Earthquakes along the zone exhibit normal mechanisms and T-axes oriented perpendicular to the trend of the rift (Vvedenskaya, 1961; Misharina, 1963; Florensov, 1969; Golenetsky and Misharina, 1978; Golonetski, 1990; Doser, 1991; Déverchère et al., 1993; Petit et al., 1996; Emmerson et al., 2006; Radziminovitch et al., 2006). Regional relocation of small earthquakes and aftershocks of moderate sized events show most seismicity is located at depths of 15 to 25 km and persistent to depths of ~30 km (Golonetski, 1990; Deverchere et al., 2001; Radziminovitch et al., 2005; Radziminovich, 2010; Mel'Nikova et al., 2012). Deverchere et al. (2001) conclude with a relocation study of small earthquakes along the rift that the seismogenic thickness is ~35-40 km. Emmerson et al.'s (2006) waveform analysis shows hypocentral depths of ~25 moderate size (Mw 5 -6) earthquakes along the Rift to reach ~30 km.

Earthquakes of M > 6.5 are common to the 270 year historical record (Solonenko, 1977; Doser, 1991). The Mw 7.1 Muya earthquake of May 27, 1957 (Emmerson et al., 2006) and Mw 6.7 Khovsgol (Liu et al., 2021; He et al., 2022; Ovsyuchenko et al., 2024) are the largest instrumentally recorded events, located near the northwestern and southeastern limits of the rift system, respectively.

Geodesy. Estimates of extension rates across regions of the rift **(Figure A10)** bracketed by GPS stations generally fall in the range of 3 – 5 mm/yr (Calais et al., 2003; Sankov et al., 2014). Assuming the extension is accommodated across the width of the individual basins, equivalent average strain rates across the individual basins range between ~40 - 170 nanostrain. The values are maximum if some of the measured strain is accommodated outside the rift basins. For example, Sankov (2014) interprets the strain is spread over ~190 km, wider than the geomorphic expression of the Baikal Rift basins, and accordingly interprets a lesser average strain rate of ~$1.8 \pm 0.4 \times 10^{-8}$/yr.

Crustal Structure. The first 'deep seismic sounding' (seismic refraction) profiles of Puzirev et al. (1970; 1973; 1978) revealed a Moho depth and thus crustal thickness of about 40 km in the region around Lake Baikal. Additional terrestrial and marine refraction lines (ten Brink and Taylor, 2002), gravity (Zorin et al., 1989; Zorin and Cordell, 1991; Burov et al., 1994; Petit et al., 1997; Petit and Déverchère, 2006) , seismic tomography and ray-tracing (Suvorov et al., 2002; Yakovlev et al., 2007; Nielsen and Thybo, 2009a; 2009b), receiver function analysis (Gao et al., 1994; Gao et al., 2004; Emmerson et al., 2006; Vinnik et al., 2017), and velocity inversion of earthquake arrival times (Gao et al., 1994; Petit and Deverchere, 1995) have since generally confirmed, refined, and expanded on Puzirov's early results. Withstanding variations of several kilometers or more between results, average estimates of crustal thickness increase from ~40 km in the Siberian Craton to ~45 km below the Baikal folded area.

It remains unclear if not controversial the exact manner of transition and variability directly below the rift. The most recent (Nielsen and Thybo, 2009a; Nielsen and Thybo, 2009b) analysis of a 360-km-long refraction profile with ~2 km spacing across southern Lake Baikal interprets that Moho depths of 41 km beneath the Siberian Platform transition smoothly in the vicinity of Lake Baikal to 46 km southward into the Sayan-Baikal Fold Belt. A receiver function analysis of (Gao et al., 2004) suggests crust may thin to 35 km beneath the central portion of the rift, though this is not observed in refraction profiles.

Basin and Range, Western North America - Table 4

Tectonic setting, geography, and historical context. The province extends ~600 km from the Wasatch mountains in the east to the Sierra Nevada and northwest trending faults and ranges of the Walker Lane in the west **(Figure A11)**. Geological accounts of the Basin and Range trace back to government sponsored explorations of the territory that took place after the United States Civil War of 1861-1865 (King, 1870 - 1878; Powell, 1874; Wheeler, 1875; 1876). Therein the reports of G. K. Gilbert and others described and interpreted the system of regularly spaced northerly trending mountain ranges of the region to be the result of uplift and rotation of crustal blocks resulting from displacement on active range bounding normal faults (Gilbert, 1874; Gilbert, 1875) (Russell, 1885; Davis, 1903; Wallace, 1984). C. King (1878) at the same time showed that rocks within the fault blocks record yet earlier periods of intense faulting and folding.

The ongoing deformation is generally attributed to a combination of (1) gravitational stresses reflecting the relatively high elevation of the area produced by an earlier period convergence across the region and (2) distributed shear imparted by transform motion between the Pacific and North America (Jones et al., 1992; Jones et al., 1996; Thatcher et al., 1999; Thatcher, 2003). Earlier evolution of thought on causative explanations of the basin and range topography are recounted in Nolan (1943).

Physiography and Structural Character of Basins. The province is distinguished by 'isolated nearly parallel mountain ranges and intervening plains made in the main by subaerial deposits of waste from the mountains' (Fenneman, 1928) (**Figure A11**). The mountain ranges are generally on the order of ~15-20 km across and separated by valleys of similar dimension (Hamilton and Meyers, 1966; Stewart, 1971; 1978; 1980; 1989; 1998), albeit there are exceptions such as the Carson Desert and Bonneville basins which are significantly broader.

Ranges most commonly exhibit a tilted monoclinal structure resulting from displacement on a fault on one side of the range in the absence of significant displacement on the other, while some are bounded by parallel faults of opposite dip, each with significant displacement. Tilt in most ranges is less than about 32°, though greater dips and overturning of beds in some mountain blocks occurs locally (Anderson, 1971; Proffet, 1977; Stewart, 1980). Valley floor elevations and topographic relief across the ranges are prevalently between 1,000 to 2000 m.

Planar, steeply dipping normal faults are reportedly most abundant (Thompson et al., 1989). Some have pointed to the presence of listric normal and very low-angle detachment faults as well (Anderson et al., 1983; Smith and Bruhn, 1984; Mohapatra and Johnson, 1998). Direct measures of the thickness of deepest sediments in valleys via drilling or seismic reflection are apparently absent from most valleys. Shah et al. (2018c) have inferred the thickness of valley fill sediments across the entire region from measurements of gravity. The maximum values of fill on crystalline basement are diverse among the ranges, reaching maximum values >7000 m. Jachens and Moring (1990) compare similarly estimated values to those measured in 225 boreholes that penetrate basement before exceeding 1200 m. Some 85% of the gravity measures fall within 300 m of the drill hole depths. Observations are fewer and uncertainties are greater and less well defined for those wells reaching basement at greater depths. That said, the gravity measures provide a systematic view of the relative depths of sediments present in Basin and Range valleys. The maximum values of structural relief surpass 8000 m when considering maximum values of basin fill reported by Shah et al. (2018c).

Distribution of Volcanics and Initiation of Rifting. Basin and Range structure is developed on (1) lower Paleozoic and uppermost Precambrian strata that record sedimentation along the western edge of a passive continental margin that approximately paralleled the eastern boundary of today's Basin and Range province (e.g., Stewart and Pool, 1974), (2) subsequently accreted terrains emplaced along an evolving and apparently north-trending convergent boundary during the Late Devonian Antler (Roberts, 1968; Speed and Sleep, 1982; Trexler et al., 2003) and Permo-Triassic Sonoma orogenies (Gabrielse et al., 1983; Trexler et al., 2004), large volumes of Oligocene ash-flow tuffs erupted from numerous calderas, and subsequent late Oligocene-Miocene basaltic lava flows **(Figure A12)** (Armstrong et al., 1969; McKee and Silberman, 1970; McKee, 1971; Christiansen and McKee, 1977; Coney, 1978; McKee and Noble, 1986; Henry and John, 2013). Faulting of the once continuous Oligocene and Miocene volcanic flows that are today found separated on adjacent Basin and Range mountaintops marks the initiation of the modern Basin and Range topography (Louderback, 1904; Cooke, 1965; Gromme et al., 1972),

The initiation of modern Basin and Range topography (**Figure A13**) correlates to inception of the San Andreas fault that accompanied the cessation of subduction along the west coast of the United States during the Miocene~17 my ago (Atwater, 1970; Dickenson and Snyder, 1979; Severinghaus and Atwater, 1990; Atwater and Stock, 1998). The inception was preceded since Jurassic time by eastward subduction of the Pacific Plate beneath the present western edge of North America, for with the associated volcanic arc is now recorded by the batholith of the Sierra Nevada (Bateman, 1988). Paleobotannical observations indicate regions east of the arc were elevated (Wolfe and Molnar, 1997) and relatively flat (Garside et al., 2005; Henry et al., 2012) when the transition from subduction to strike slip began. Normal faulting responsible for the physiographic expression of the Basin and Range is generally attributed to the cessation of crustal contraction that accompanied subduction, the gravitational load attendant to the region's high elevation, and crustal drag arising from shear motion along the San Andreas that commenced ~17 Ma (Jones et al., 1996; Sonder and Jones, 1999; Thatcher et al., 1999).

Heat Flow. Borehole heat flow measurements collected over the last ~50 years approach 1000 in number. Data compilations and attendant maps show regional heat flow generally ranging between ~60 and 100 mWm^{-2} (e.g., Sass et al., 1971; Lachenbruch and Sass, 1978; Blackwell et al., 1991; Blackwell and Richards, 2004; Sass et al., 2005; Blackwell et al., 2011; DeAngelo et al., 2022) *(1 cal/cm2/s = 1 HFU = 41.8 mW/m2).*

Seismology. Instrumentally recorded seismicity is less within the interior of the province relative to higher rates at the margins adjacent to the Wasatch and within the Walker Lane **(Figure A12)**. Upwards of 98% of seismicity recorded across the region occurs at depths less than 15 to 17 km, with the remainder largely above depths of 20 km (Pancha et al., 2006).

The largest historical earthquakes have produced surface rupture. These include adjacent to and in the Walker Lane the Mw 6.8 Cedar Mountain (Doser, 1988), Mw 7.0 Fairview Peak (Caskey et al., 1996) and M6.2-6.5 Fallon Stillwater events **(Figure A12)**. Each exhibits a focal mechanism and surface rupture displaying right-lateral and right-oblique motion. The Mw 6.9 Dixie Valley (Caskey et al., 1996) and Mw 7.2 Pleasant Valley (Wallace, 1984) events interior to the province display normal fault mechanisms. Similar size normal earthquakes have also occurred in a like portion of Basin and Range just to the north of **Figure 12**: the 1983 Borah Peak Mw 6.8 (Doser and Smith, 1985) and 1959 Hebgen Mw 7.3 earthquakes (Doser, 1985).

Geodesy. Global Positioning System (GPS) derived surface velocities from UNAVO (2020) are reproduced in **Figure A12**. At 39°N approximately 2-3 mm/yr of east-west extension is being accommodated across the Wasatch whereas only a total of 1-2 mm/yr cumulative east-west extension distributed across the ~450 km between the Wasatch and Central Nevada Seismic Belt. At the northerly alignment of large earthquakes, geodetic vectors increase markedly and rotate northwesterly to reflect a component of strike-slip deformation and deformation rates of 3-5 mm/yr (Thatcher et al., 1999; Kreemer et al., 2012; UNAVCO, 2020). The northwestward rotation and increase in magnitude of geodetic vectors reflects the superposition of lateral density gradients associated with the relatively high elevation of the Basin and Range and shear tractions exerted by relative motions between the Pacific and North American plates shown schematically in **Figure A13** (Jones et al., 1996; Sonder and Jones, 1999). The transtensional strike-slip fault system of the Walker Lane that bounds the west edge of the Basin and Range province accommodates a yet higher 6-8 mm/yr.

Crustal Structure. Seismic refraction profiles dating since the 1960s consistently show the depth to Moho across the Basin and Range at latitude ~39°N-40° N is in the range of 30 to 35 km (Pakiser, 1963; Thompson and Burke, 1974; Prodehl, 1979; Klemperer et al., 1986; Allmendinger et al., 1987; Thompson et al., 1989). Analysis of higher mode surface waves crossing the same area (Klemperer et al., 1986; Allmendinger et al., 1987) and surface wave and teleseismic receiver function analyses (Priestley et al., 1982; Gilbert and Sheehan, 2004) yield similar results.

Italy - Table 5

Tectonic setting, geography, and historical context. Italy like the Aegean is situated within the Alpine - Himalayan belt **(Figure A14)**. The Apennine mountains trend southeastward along the length of the Italian peninsula **(Figure A15)**. The fold and thrust deformation leading to uplift of the mountains commenced in late Cretaceous (Argand, 1916; Heim, 1922; Staub, 1924). Dewey et al. (1973) later placed the deformation in the framework of plate tectonics. Malinverno and Ryan (1986) more specifically attributed the fold and thrust structure to westward subduction of the Adriatic Plate beneath Italy and the Tyrrhenian Sea **(Figure A15)**.

The fold and thrust structure is overprinted by active normal fault-bounded basins that follow the trend of the Apennines **(Figure A16)**. The bounding normal faults follow the same trend to accommodate southwest directed crustal extension. Factors considered in explanations of the transition from contraction along the Adriatic Margin to extension along and west of the Apennine crest **(Figure A17)** include the increased gravitational load associated with high elevation of the Apennines (e.g., D'Agostino et al., 2014), the weak coupling across the Adriatic plate margin (e.g. Uyeda and Kanamori, 1979; Scholz and Campos, 1995), slab retreat (Doglioni, 1991; 1992), the westward migration of the Adriatic margin since the Miocene (e.g., Carminati et al., 2010), and postulated forces attendant to the subducting slab and surrounding flow of the mantle (e.g., Cavinato and De Celles, 1999; Bennett et al., 2012).

Physiography and Structural Character of Basins. Active normal fault bounded basins are generally limited to the highest elevations of the Apennines **(Figure A16)**. Fault bounded basins are generally oriented with long axes oriented parallel to the northwest trending. Principal basin bounding faults generally strike to the northwest along the long axes of the basins and dip to the southwest, form asymmetric half-grabens. Basin lengths and widths tend to be greater along the southwestern edge of the zone as compared to those closer to the crest of the Apennines to the northeast. The length and width of basins is on average about 13 and 5 km, respectively, with maximum values reaching 30-43 km and 15-17 km, respectively. Thickness of sediment fill within basins is generally less than 500 m, with notable exceptions of the Avenzano-Fucino and Vallo di Diano basins where fill thicknesses reportedly reach 1000 m. The two latter basins are located along the southwestern edge of the distribution of normal fault basins.

Distribution of Volcanics and Initiation of Rifting. Pleistocene and Holocene volcanic centers are located along the southwest edge of the Italian peninsula (Global_Volcanism_Program, 2023). The larger volcanic edifices and craters on the west side of the peninsula are visible on the shaded relief map of **Figure A16**. Most are considered to reflect ongoing or vestiges of subduction of the Adriatic Plate along the Calabrian arc (Doglioni and Flores, 1997). The volcanic centers are located southwest of the active normal fault bounded basins. The active normal fault bounded basins occur largely within Tertiary and older sedimentary rocks of marine origin, generally absent of volcanic rocks.

Basin fill sediment ages are interpreted to indicate extensional basins began formation in the Plio-Pleistocene between 1 m.y. and 3.5 m.y. ago (Martini and Sagri, 1993; Cavinato and De Celles, 1999). Catchment areas, thicknesses of sedimentary fill, and initiation ages increase westward from the Apennine crest. (Larger submarine basins bounded by apparently inactive normal faults exist yet farther to the southwest). The zone of active normal fault bounded basins was preceded by active thrusting as recently as 3.5- 7.5 Ma (Cavinato and De Celles, 1999).

Heat Flow. Heatflow measurements are compiled and summarized by, among others, Mongelli et al. (1989), Della Vedova et al. (1991) and Cataldi et. al. (1995). Values of heat flow exhibit a general gradient between < 30 mW/m^2 along the northeastern coast of Italy to > 100 mW/m^2 along the southwest coast. The active normal fault bounded basins of Italy generally fall in regions of heat flow between 30 mW/m^2 to 70 mW/m^2. Values of heat flow listed for each basin in **Table 5** are from the map of Della Vedova et al. (1991).

Seismology and Geodesy. Seismicity beneath the active basins is largely confined to depths of 15 km or less (Chiarabba et al., 2005; Chiarabba and Di Stefano, 2010; Chiarabba and De Gori, 2016). The shallow depth of the seismogenic layer is highlighted with the aftershock distributions and surface ruptures of basin bounding faults accompanying the region's largest well documented earthquakes, included among them the 1915-06-13 Mw 7.0 Fucino (Oddone, 1915; Michetti et al., 1996), the 1980-11-23 Mw 6.9 Campania-Basilicate (Irpinia) (Westaway and Jackson, 1984; Pantosti and Valensise, 1993), the 1997-09-26 Mw 6.7 Umbria-Marche (Galli and Galadini, 1999), the 2009-04-06 Mw 6.3 L'Aquila (Chiarabba et al., 2009; Alessio et al., 2010), and the 2016-10-30 Mw 6.5 Norcia (Civico et al., 2018; Gori et al., 2018) earthquakes. The distribution of these large quakes is in agreement with Westaway's (1992) assessment of intensity data for historical earthquakes since the 17th century that shows no earthquakes of Mw 6.5 north of 42.5°N, whereas numerous magnitude ~7 events are registered to the south. The value of seismogenic depth assigned to each basin in **Table** 5 is from visual examination of Chiarabba and De Gori's (2016) contour map of seismogenic depth from analysis of ~150,000 crustal earthquakes over the period 2005-2015. Most microseismicity occurs west of the Apennine crest and above the Alto Tiberina low-angle normal fault (**Figure A17** and (Lavecchia et al., 2024)).

Geodesy. Analyses of first-order triangulation measurements taken between 1867 and 2001 were among the first to document northeast directed extension across the Apennines (Hunstad and England, 1999; Hunstad et al., 2003). The observations are confirmed and refined in more recent Global Positioning Surveys (GPS) (Serpelloni et al., 2005; Serpelloni et al., 2006; Serpelloni et al., 2007; D'Agostino, 2014; D'Agostino et al., 2014). Observations show ~3 mm/yr extension between the Tyrrhenian and Adriatic coasts and a continuous ~50 km wide zone deforming at 40-60 nstrain/yr (D'Agostino, 2014; D'Agostino et al., 2014).

Crustal Structure. Integrating, di Stefano et al. (2011) show the depth of Mojo beneath active Apennine extensional basins is generally between 25 and 30 km, using controlled source seismic and teleseismic receiver function data. The values are in accord with the Moho map of Nicolich 1989 that is reproduced in Doglione and Flores (1997). Yet earlier estimates deduced from seismic refraction profiles and gravity are similar (e.g., Elter et al., 1975; Gasparini et al., 1985; Keller et al., 1994).

The Ordos Table 6

Tectonic setting, geography, and historical context. The loess-covered Ordos plateau extends northeastward from the edge of the Tibetan plateau **(Figure A18)**. Major active faults and earthquake activity are largely absent within the plateau (Lee et al., 1976; Tapponnier and Molnar, 1979; Wesnousky et al., 1984; Peltzer et al., 1985; Qin et al., 1999; Qin, 2002). The normal fault bounded basins along the northwestern and southeastern margins of the Ordos define the Yinchuan-Hetao and Weihe-Shanxi graben systems, respectively.

The genesis of the graben systems is commonly attributed to Indian-Asian plate collision (Tapponnier and Molnar, 1977). The ongoing collision is in part accommodated by large left-lateral Haiyuan and Kunlun fault systems within the Asian continent. The Yinchuan-Hetao and Weihe-Shanxi graben systems are near the eastern ends of the left lateral fault systems. Much like tension cracks occurring at the end of shear cracks, the northeast trending graben systems are correctly oriented to accommodate tension expected near the eastern limits of the Haiyuan, Ganshu, and Kunlun faults **(Figures A18 and A19**, and see Zhang et al., 1998).

Physiography and Structural Character of Basins. The smooth alluvial surfaces of individual basins of the graben systems are clearly expressed in the slope-shade map of **Figure A19**. The larger basins commonly exhibit lengths and widths greater than 100 km and 30 km, respectively. Active basin-bounding normal faults are generally prominent on only one side of the basins (Ma and Wu, 1987; Ye et al., 1987). Rangefronts are steeper and basin deposition greater adjacent to the principal active bounding normal faults. Observations of dips of active rangebound faults are reportedly between 40° and 75° (Wang et al., 1982-cited by ; Ye et al., 1987). Normal fault displacement has resulted in a basin fill sequences that reach the range of 7000 m to 10,000 m in the Weihe, Yinchuan, and Hetao grabens. Thicknesses are less in the smaller basins that occur toward the northeast limit of Weihe-Shanxi system (Zhang et al., 1998). Structural relief across the larger basins surpasses 10,000 m.

Distribution of Volcanics and Initiation of Rifting The grabens have developed in near absence of volcanism. Volcanic rocks are limited to the early to middle Pleistocene volcanic craters in the Datong graben of the Weihe-Shanxi system. Ye et al. (1987) suggest that the volcanism is not directly linked to graben development but rather to volcanic processes ongoing to the north of the Ordos plateau.

The commencement of collision of India into Eurasia ~45 Ma ago places a maximum bound on the beginning of graben development (Molnar and Tapponnier, 1977). The temporal evolution of the graben systems is recorded by the age of sediments that fill the basins (Ye et al., 1987). Rifting commenced in the Yingchuan-Hetao and the southern part of the Weihe-Shanxi graben system in Early Oligocene or Late Eocene (~45 Ma), with major extension and rapid subsidence occurring later in the Neogene and Quaternary. The middle and northern basins of the Weihe-Shanxi graben initiated later in the Pliocene, reflecting a northward migration of graben development. The age of basal beds in the grabens correspondingly correlates to the cessation of sedimentary deposition and uplift on the intervening Ordos block (Ye and Zhang, 1983).

The Ordos block was the locus of sedimentation from the Cambrian to Cretaceous (e.g., Gao et al., 2018). The perimeter of the Ordos plateau experienced contractional deformation in the Late-Jurassic-Early Cretaceous (Darby and Ritts, 2002; Middleton et al., 2017). The surrounding crust may be considered stable for ~100 my or more before development of the graben systems.

Heat Flow. Heat flow measurements number in the thousands in China (Tao and Shen, 2008), of which several dozen are located within the Ordos Plateau and the Weihe-Shanxi graben system. Tao and Shen's (2008) map based on interpolation of measured values in and around the Ordos plateau average between 62.5 ± 12.5 mW/m^{-2}. Gao et al. (2018) combine 13 steady-state deep borehole temperature measurements with earlier reported measurements to interpret heat flow in the Ordos plateau to range from 43.3 to 88.7 mWm-2 with a mean of 64.7 ± 8.9 mWm-2. Values within the range tend to increase from west to east across the block.

Seismology. Seismicity is distributed along the graben systems and largely absent from the Ordos plateau (e.g., Qin, 2002; Middleton et al., 2017). Instrumentally recorded seismicity, while most abundant at depths < ~25 km is observed to extend to depths of 35-40 km along the perimeter of the plateau. (Qin, 2002; Cheng et al., 2014).

There are no instrumentally recorded normal fault earthquakes >M6 in either the Shanxi or Weihe graben systems, though much larger earthquakes are found in the historical and geological record. For example, normal surface displacements of the 1739 earthquake interpreted to be M~7.4 remain preserved within the Yinchuan basin (Deng and You, 1985; Zhang et al., 1986; Zhang et al., 1998; Middleton et al., 2016). Xu et al.(2018) with fault mapping and trenching interpret the occurrence of a Mw 7.2-7.6 earthquake within the Southern Shanxi (Xinxian) graben in 1303. Numerous other similarly large earthquakes though lacking direct evidence of fault mechanism are suggested around the Ordos plateau on the basis of felt reports (Wesnousky et al., 1984; Zhang et al., 1998).

Geodesy. Contemporary deformation across the basins bounding the Ordos are assessed directly by Zhao et al. (2017) with GPS data collected between 1999 to 2014. Rates of extension across the major basins range between 0.1 mm/yr and 1.6 mm/yr, and generally accompanied by a similar amount of strike-slip motion.

Crustal Structure. Ambient noise tomography (Zheng et al., 2011) indicates the depth to Mojo beneath the Ordos plateau is 40-50 km depth. Yu et al. (2012) interpret deep seismic soundings and crustal receiver function analysis to show the Moho at 50-60 km depth beneath the Ordos block, and shallowing to 40 km across the Shanxi graben system. Teleseismic receiver function analysis shows crustal thickness beneath basins surrounding the Ordos block averages 40-45 km (Pan and Niu, 2011; Wang et al., 2014), but locally within the Linhe and Weihe rifts thickness are a lesser 35 - 40 km. The values agree with the older map of Moho depth presented by the Research Group of the State Seismological Bureau (Research Group of SSB, 1988 (in Chinese)) that is also reproduced in Qin (2002). Likewise in accord are values of Moho depth estimated from seismic refraction profiles and gravity earlier published by Ye, Zhang, and Mao (1987).

Tibet Table 7

Tectonic setting, geography, and historical context. Basins bounded by active normal faults are common in the portion of Tibetan Plateau extending several hundred kilometers northward from the crest of the Himalaya mountains **(Figure A20).** The normal faults and basins strike northerly, transverse to the trend of the Himalayan arc, and are located mostly south of the easterly striking Bangon-Jujang Suture **(Figure A21)**. The northerly strike of faults and basins record east-west oriented extension of the underlying crust. A left-stepping en-echelon pattern is apparent in the arrangement of individual basins located immediately north of the Indus - Tsangpo suture.

Recognition of normal faulting in the area came with the early studies of Gansser (1964) and Chang (1973). The region gained further attention with ensuing focal mechanism studies enabled with a new World Wide Standardized Seismographic Network (WWSSN) in 1968 (Molnar et al., 1973) and terrain analysis facilitated by the Landsat satellite imagery acquisition system that began in 1972 (Tapponnier and Molnar, 1977). Today's discussions of the region originated with these and similar seismological studies (Molnar and Tapponnier, 1978; Ni and York, 1978; Molnar and Chen, 1983; Seeber and Armbruster, 1984), analyses of landsat imagery (Molnar and Tapponnier, 1978; Ni and York, 1978), and field observation (Tapponnier et al., 1981; Armijo et al., 1982; Armijo et al., 1986) that followed soon after.

Molnar and Tapponnier (1976; 1978) attribute the spatial distribution and orientation of normal faults to gravitational collapse of a thick crust resulting from the collision of India and Asia **(Figure A22)**. Normal faulting in this context dissipates potential energy more than possibly supported by convergent forces. Subsequent discussions introduce additional variables that may affect or control development of the rifts, among them the curvature of the arc (e.g., Seeber and Armbruster, 1984), bending of the arc with time (e.g., Klootwijk et al., 1985), and the obliquity of subduction (e.g., Armijo et al., 1989), basal shear beneath Tibet attendant to oblique subduction (e.g., McCaffrey and Nabelek, 1998), and processes of mantle flow (Yin and Harrison, 2000).

Physiography and Structural Character of Basins. The normal fault-bounded basins manifest as smooth basin floors sharply juxtaposed to steep range fronts **(Figure A21)**. The fault bounded rangefronts are described to exhibit triangular facets and wineglass canyons (Tapponnier et al., 1981; Armijo et al., 1986). The basin floor elevations average ~4700 m. Topographic relief across the basins average around 1250 m, locally approaching ~2 km. Both symmetric and asymmetric fault grabens are suggested by the presence of steep rangefronts on one or both sides of respective basins.

Observations bearing on the depth of sediment and structural relief across the basins are limited. Armijo et al. (1986) put forth a number of interpretive structural cross-section along basins extending between Yadong and Gulu **(Figure A21)**. Maximum ~1500 m and ~3000 m depths of Quaternary basin fill and structural relief, respectively, are shown near Yanbajain (basins 24 and 15 in Figure A21), with significantly lesser values elsewhere along the alinement of basins. Similar values are assessed from refraction and reflection surveys along the range (Cogan et al., 1998). Reports of sediment depth in other basins are not known to the author.

Distribution of Volcanics and Initiation of Rifting. Widespread volcanism in the area between the Indu-Tsangpo (Indus-Yalu) and Bangon-Nujiang sutures is recorded by the Paleogene Linzizong formation. The volcanism ceased ~ 40 Ma (Chung et al., 2005; Taylor and Yin, 2009). Younger Late Oligocene to Mid-Miocene (~8 - 25 Ma) intrusive rocks are also locally present within and adjacent to the volcanic field. Miocene leucogranite intrusives are also scattered south of the Indus-Tsangpo suture (Ding et al., 2007). The area is also home to batholithic rocks of the Trans Himalaya emplaced 110-40 Ma. That said, volcanism has been absent from the area for ~40 Ma.

Observations bearing on the inception of normal faulting are few. Armijo et al. (1986) refer to sedimentary stratigraphy reported by (Wang and Li, 1982 (in Chinese)) to interpret a late Pliocene-early Pleistocene lower bound on the age of inception for 'most basins'. Mercier et al. (1987) interpret that sediments in the Gyirong and Thakkhola basins were active in the Pliocene and that extension in the region 'probably' started 10 – 5 Ma. Mineral cooling ages in shear zones and dikes along the margins of a number of basins (e.g. Yangbajian, Thakula, Pabai Zong, Daggyai basins) have been the basis to place initiation of extension at between ~5 and 18 Ma (Pan and Kidd, 1992; Coleman and Hodges, 1995; Harrison et al., 1995; Williams et al., 2001). Blisniuk et al's. (2001) analysis of mineralization post-dating normal faulting in the Shuang-hu basin obtains a similar initiation age of at least 13.5 Ma. Thermochronometry of Maheo et al. (2007) applied to a pluton suggests initiation of the Kung Co half graben post dates 4 Ma, and older ages of initiation interpreted by dating of dikes (i.e., Coleman and Hodges, 1995; Williams et al., 2001) may be overestimates because the presence of vertically oriented dikes doesn't require the vertical stress be minimum. Initiation of the currently active normal fault across the region is broadly constrained to between 4 and 18 Ma.

Heat Flow. Direct measures of heat flow in Tibet are few and generally concentrated around the longitude of Lhasa (~92°E). Measures of heat flow in two lakes southeast of Lhasa (Francheteau et al., 1984) average 96 mWm^{-2} (Lake Pumung 90°30'E 28°30'N) and 146 mWm^{-2} (Lake Yangzhouyun (28°45'N 90°32'). A half-dozen measures reported further to the north just west of Lhasa range between 60 mWm^{-2} and 110 mWm^{-2} (Wang et al., 2017). Lucazeau (2019) applies a global correlation of heat flow measurements (IHFC-DataViewer, 2023) to geological and geophysical observations at measurement sites to assess a regional picture of heat flow across the area. The analysis concludes heat flow in southern Tibet varies with values varying regionally within between ~70 mWm^{-2} and ~120 ° mWm^{-2}.

Seismology and Geodesy. Normal fault earthquake mechanisms within the Tibetan Plateau are reported in Molnar et al. (1973). Correlation of normal fault mechanisms indicating east-west extension to the northerly trending normal faults of Tibet is found in Ni and York (1978). Molnar and Chen's (1983) analysis of long period P- waveforms shows moderate sized normal earthquakes in the region are limited to depths less than 15 km. The depth limit of the seismogenic layer is confirmed in Elliot et al.'s (2010) application of Insar and P-waveform modeling of the largest normal earthquakes in the 43 years preceding 2008, as does the more recent compilation of earthquake depths registered in Bai et al. (2017) for the period preceding ~2014. Normal fault events in these studies are of Mw no larger than ~6.3. The largest instrumentally recorded event on record is the Mw 7.1 Xizang earthquake of Jan 7, 2005 near Dingye (**Figure A21**).

Crustal Structure. Molnar's (1988) review of prior surface wave dispersion and reflection seismology studies concludes the crust beneath Tibet is thick : "nowhere less than 50 km, at least 65 km, in most areas, but less than 80 km in all areas that have been studied". Ensuing seismic reflection, receiver function, deep seismic sounding, gravity and seismic tomographic analyses confirm that the Moho in the region of southern Tibet encompassing the north trending normal faults is generally between 70 km and 80 km thick (e.g., Zhang et al., 2004; Nábelek et al., 2009; Gao et al., 2013; Zhang et al., 2013; Singh et al., 2017; Zhao et al., 2020).

Rates of Extension. Molnar and Lyon-Caen (1989), building on earlier observations of Seeber and Armbruster (1981; 1984) and Baranowski et al. (1984), use geometrical arguments to suggest the rate of easterly extension in southern Tibet should be equal to about 18 ± 9 mm/yr, comparable to the rate at which India is subducting beneath the Himalaya. Wang et al.'s (2001) analysis of global positioning system (GPS) measurements yields confirmatory results: showing extension across southern Tibet between 80° and 90 is 20 ± 3 mm/yr . Zhang et al's (2004) subsequent GPS analysis interprets a similar 21.6 ± 2.5 mm/yr of eastward stretching between 79° and 93°. The extension is equivalent to about 20 ± 2 nanostrain/yr when dividing the extension rate by the ~1300 km between longitudes 79° and 93°. Summations of instrumentally recorded moment tensors are able to account for only ~15-20% of easterly extension measured by geodesy (Molnar and Lyon-Caen, 1989; Elliott et al., 2010).

Japan Trench Table 8

Tectonic setting, geography, and historical context. Normal fault bounded basins occur on the seafloor to the seaward side of the Japan trench (**Figure 1 and A23)** and many other subduction zones were early attributed to crustal extension oriented perpendicular to the trench axes (e.g., Raitt et al., 1955; Ewing and Ewing, 1962; Fisher and Raitt, 1962; Ludwig et al., 1966). The long-axes of the basins trend parallel to the subduction zones as do the basin-bounding faults. Earthquake foci below are additionally observed to be at shallow depths, generally display axes of tension aligned normal to the local axis of the trench (Stauder, 1968), and capable of producing earthquakes reaching M8 and greater (Kanamori, 1971). The extension is now generally attributed to bending of the oceanic lithosphere where it curves downward to subduct below the oceanic trenches (Jones et al., 1978; Chapple and Forsyth, 1979; Forsyth, 1982).

Physiography and Structural Character of Basins. Global collection of seismic reflection data provides the most comprehensive picture of the physiographic expression of faults in outer trench walls (Tozer et al., 2019; GEBCO, 2024). The trends of outer wall trench faults are generally oriented parallel to the strike of adjacent trenches, in some cases reoriented by features on the seafloor, such as sea mounts and fracture zones, and the original spreading fabric of the subducting seafloor (e.g., Masson, 1991). The characteristics are well manifest in the outer wall of the Japan Trench **(Figures A23 and A24)**.

The topographic relief across the across individual basins in **Figure A24 and A25** ranges from ~70 m to 600 m, with the relief across individual basins tending to systematically increase toward the trench **(Figure A25)**. Sediment accumulation within and postdating formation of the grabens is absent or minimal (Nakamura et al., 2023), and so structural relief here is equal the topographic relief. The most prominent basins shown in **Figure A24** approach 60 km in length and are limited in width to between 2 km and 6 km (Nakamura et al., 2023).

Distribution of Volcanics and Initiation of Rifting. Volcanism post-dating the creation of the subducting oceanic plate is absent along the section of outer rise pictured in **Figure A24**. Subduction of seafloor here is ~90 mm/yr near perpendicular to the Japan Trench strike (Tectonics_Observatory, 2009). The increasing relief across graben bounding faults toward the trench is reason to assume that the age of the grabens also increases toward the trench (Boston et al., 2014). The grabens span a zone of about 70 km in an east-west direction. Dividing the 70 km width by the ~90 mm/yr subduction rate places the age (or inception) of the oldest grabens near the trench at ~0.8 Ma. It may be surmised that the region of faulting has been tectonically quiescent over the last ~140 Ma, the age of the subducting seafloor on which the grabens are developed (Müller et al., 2008; Tectonics_Observatory, 2009; Liu et al., 2017).

Heat Flow. Two transects of heat flow measurements across the region of faulting extending ~150 km eastward of the trench axis are reported by Yamano et al. (2008; 2014). Reported values fall between ~40 – 100 mW/m^2 and average ~ 70 ± 20 mw/m^2. The values generally fall above the ~50 mW/m^2 typical of ocean basins (Hasterok et al., 2011) with seafloor ages similar to that now being subducted along the Japan trench. The relatively higher values are attributed to heat transport that accompanies hydrothermal circulation (Kawada et al., 2014; Yamano et al., 2014).

Seismology and Geodesy. Gamage et al's. (2009) examination of sP depth phases for >1000 M>3 events recorded between 2000 and 2006 reveals a double planed seismic zone beneath the area with events extending to depths of ~35 - 40 km, with those above and below ~25 km exhibiting extension and contraction oriented perpendicular to the trench, respectively. Earlier and sparser collections of large teleseisms here and along other major convergent plate boundaries show the same pattern (Chapple and Forsyth, 1979; Forsyth, 1982; Seno and Gonzalez, 1987; Seno and Yamanaka, 1996). Authors attribute the reversal of horizontal stress at shallower depth to contraction at deeper depths to bending of the subducting plate, whereby the upper portion of the downward bending plate is subjected to extension while that deeper subject to contraction. Deployments of ocean bottom seismometers subsequent to the great Mw 9.0 earthquake of March 11, 2011 show the same depth distribution but in contrast show extension through the entirety of the seismogenic layer (Obana et al., 2012; Obana et al., 2019; Obana et al., 2021), leading the investigators to conclude that stresses in the subducting plate are modulated by the accumulation and release of stress that accompanies great thrust earthquakes along the trench. Finally, assessment of the depth to which outer rise faults may propagate is complicated by the occurrence of the great 1933 normal fault for which analysis of seismograms has led to the conclusion that it ruptured upwards of 100 km through the entirety of the subducting plate (Kanamori, 1971; Okal et al., 2016).

The largest normal fault earthquake along this section of the trench occurred March 2, 1933 and shows an Mw of 8.5 (Okal et al., 2016). A similarly large event of Mw 8.3 normal faulting occurred on August 19, 1977 near the island of Sumba in Indonesia. Rupture extended to depths of 30 to 50 km (Lynnes and Lay, 1988). These are to my knowledge the largest such instrumentally recorded normal fault earthquakes along the global system of subduction zones.

Crustal Structure. Seismic surveys over several decades show the depth of Moho extending seaward of the Japan trench to the crest of the outer rise is between 7 and 10 km beneath the seafloor, which is about 5 km below the surface (Shor and Fisher, 1961; Fisher and Raitt, 1962; Ludwig et al., 1966; Fujie et al., 2016; Obana et al., 2019). The largest normal fault earthquakes appear to produce rupture well below the crust-mantle boundary.

Mid-Atlantic Ridge -Table 9

Tectonic setting, geography, and historical context. The interconnected system of mid-ocean ridges extends ~60,000 km through major ocean basins around the globe**(Figure 1)**. Plate tectonic theory evolved from the collection of geophysical observations across the ridge system. Reviews of investigators, observations, and ideas leading to development of the theory are many, extensive, and beyond recounting here (e.g., Ewing and Heezen, 1956; Heezen et al., 1959; Cox and Hart, 1986; Smith and Cann, 1993; Macdonald, 1998; Oreskes, 2003; Felt, 2012; Sykes, 2019). Most simply, the mid-ocean ridges are considered to be the loci of seafloor spreading. They comprise the globe's largest area of extensional tectonics. Basis of comparison to other extensional environments is here limited to the section of mid-Atlantic ridge that is outlined in **Figure 1** and shown as a shaded relief map in **Figure A26**.

Physiography and Structural Character of Basins. The Mid-Atlantic ridge outlined in **Figure A26** rises gradually from abyssal depths of 4–5 km over distances of 500-1500 km to its crest at 2-3 km beneath the ocean surface **(Figures A27).** Basins at the ridge crest are bounded by steep 2-3 km high escarpments attributed to active normal faulting (e.g., Heezen et al., 1959; Atwater and Mudie, 1968). The basin widths generally rang between 10 - 20 km (Sandwell et al., 2002; GEBCO, 2024). The rate of seafloor spreading here is 2 - 2.5 cm/yr (e.g., DeMets et al., 2010). An axial rift is generally absent elsewhere along the mid-oceanic rift system where spreading rates are greater than ~4 cm/yr (Macdonald and Atwater, 1978).

Relief across the axial rift in **Figure A26** ranges between 1800m and 3000m with an average of about 2500 m. The 21 individual basins marked in **Figure 26** are bounded by closed contours at depths ranging from 3000 to 4000 m, respectively, except for where they are interrupted and open at the intersection of fracture zones. Sediment accumulation is negligible near and within the rift basins (Ewing et al., 1964; 1966; e.g., Ballard and Vanandel, 1977). The lengths of the basins range from about 20 km to nearly 600 km. Lesser faults and shears (Ballard and Vanandel, 1977; Sempere et al., 1990; Shaw, 1992), smaller basins (Ballard and Vanandel, 1977; Smith et al., 2006), volcanos (Smith and Cann, 1992; Smith and Cann, 1993), detachment faults (MacLeod et al., 2002; Smith et al., 2006; Simao et al., 2010), and metamorphic core complexes (Blackman et al., 1998; Brothers et al., 2009) occur between major escarpments that bound the basins. Extension at the ridge is thus complex, accommodated by processes of both magma accretion and faulting (Smith and Cann, 1993; Tucholke et al., 2008; Simao et al., 2010). Forces in models explaining the mechanisms driving extension include increased gravity due to higher elevation of the mid-ocean ridges relative to distal abyssal portions of the seafloor and shear at the base of the crust imposed by mantle convection (**Figure A28)**

Distribution of Volcanics and Initiation of Rifting. Circular volcanoes, volcanic flows and fissures are typically reported within the inner rift valley (Smith and Cann, 1993). The ages of volcanic rocks sampled from the seafloor range between several to 300 thousand years, and upwards of about one million years on adjacent ridgecrests (Fleischer et al., 1968; Aumento, 1969; Hekinian et al., 1976; Bryan and Moore, 1977). The ages are in accord with paleomagnetic observations that show rocks within and adjacent to the rift to occur close in time to the Brune-Matayama reversal of the Earth's magnetic field about 780k years. The portions of the ridge system exhibiting active normal faulting are apparently limited to oceanic crust less than several hundred thousand to a million years old.

Geophysical imaging of magma chambers along the rift is challenging (Calvert, 1997) and examples apparently few. Among the earlier in the mid-Atlantic arise the seismic reflection studies of Sinha et al. (1997), Navin et al. (1998), and Singh et al. (2006) that interpret the presence of magma chambers of lengths and widths <10 km extending upwards to about 2.5 - 3.0 km beneath the seafloor. Sinton and Detrick (1992) report seismic refraction studies elsewhere along the mid-Atlantic ridge showing velocity anomalies (<10-20%), interpreted to possibly reflect regions of hot rock that is predominantly solid and possibly with small pockets of melt, but not molten magma chamber. Elsewhere in the Pacific, the most recent study of Kent et al. (2025) along the ridge separating the Pacific and Juan De Fuca plates utilizes higher resolution multi-channel reflection methods to show magmatic crystal rich mush migrating upward through the crust to within ~1 - 2 km of the seafloor wherein melt sills are also manifest.

Heat Flow. Original efforts to assess heat flow along the mid-Atlantic ridge include those of Bullard and Day (1954), Nason and Lee (1962), Von Herzen and Simmons (1972), Hyndman et al. (1976), and Hyndman and Rankin (1972). Subsequent global summaries by Stein and Stein (1994) and Elderfield and Schultz (1996) of heat flow versus age show heat flow averaging ~150 ± 100 mW m^{-2} along oceanic spreading centers. Lucazeau et al. (2006) with additional observations from a transect of measurements across the mid-Atlantic ridge at 37°N more recently interpret heat flow near the ridge axis to average about 100 ± 58 mW/m^2, with some individual measures reaching to ~400 mW/m^2. At larger distances from the ridge, Khutorski and Teveleva (2020) use a traverse of 565 measurements across the ridge at ~30°N to interpret that heat flow values are similar at larger distances from the ridge.

Seismology. Sykes' (1967) first-motion analysis and Huang et al.'s (1986) waveform analyses were the first to document mid-Atlantic ridge earthquakes were of normal mechanism. Huang and Solomon (1988) and Huang et al. (1986) using similar methods established that fault displacement during ridge-axis earthquakes is limited to between ~2-10 km and observed events no greater than Mw 6.0 in magnitude. Ocean bottom seismometer deployments at numerous sites along the ridge similarly reveal microseismicity limited to depths between 3-10 km (e.g., Cessaro and Hussong, 1986; Wolfe et al., 1995; Barclay et al., 2001; Tilmann et al., 2004; Dusunur et al., 2009). Submarine hydroacoustic monitoring along the ridge between 15°N and 35°N shows seismicity is limited to within 20 km on either side of the ridge (Ichinose et al., 2003).

Crustal Structure. Normal faulting along the mid-Atlantic ridge is occurring in recently created and evolving crust. Numerous seismic reflection and seismic refractions studies reported within and near the rift valley nonetheless show crustal structure with characteristics similar to older oceanic crust (Keen and Tramontini, 1970; Fowler, 1976; Fowler, 1978; Fowler and Keen, 1979; Purdy and Detrick, 1986; Dunn et al., 2005; Planert et al., 2009; Dannowski et al., 2010; Sauermilch et al., 2018). P-wave velocities immediately below the Moho at 6 to 10 km depths are generally ~8 km/s and locally as slow as 7.5 km in the middle of the rift valley **(Figure A28)**. The observations are attributed to the idea that any melt beneath the ridge axis is confined to very small and thin lenses (Sinton and Detrick, 1992), and that characteristics of ocean crust are generally formed in a time period less than that separating major volcanic injection events (Purdy and Detrick, 1986).

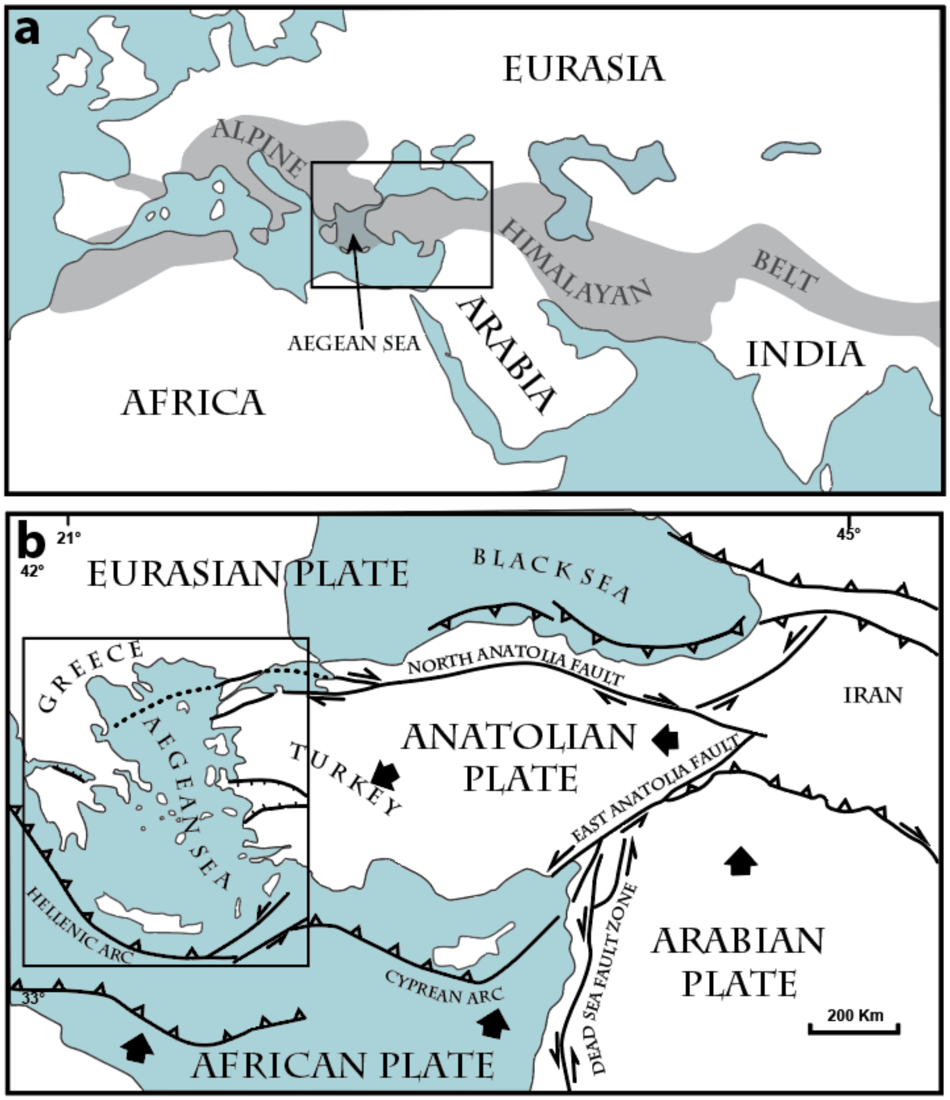

Figure A1. (a) Aegean region (box) is within Alpine-Himalayan belt (shaded). (b) Regional tectonic framework of Aegean region. Box outlines region of **Figure A2**.

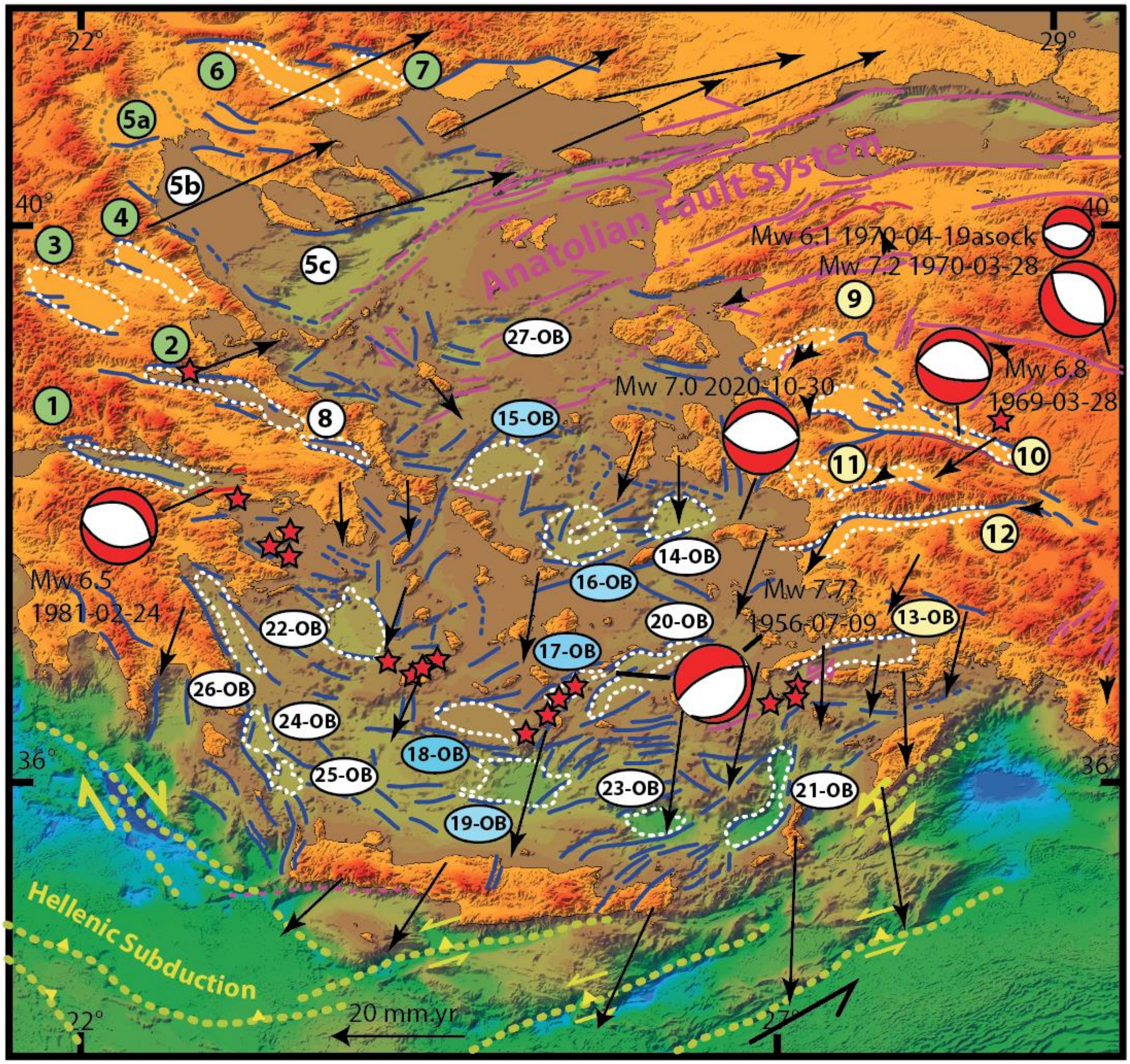

Figure A2. Shaded relief image of Aegean Sea and adjacent coastal areas of Greece and Turkey to the west and east, respectively. Normal and strike-slip faults are blue and magenta, respectively. Faults of Hellenic subduction zone are yellow. Active normal fault-bounded basins are outlined with white dashed lines. Numbers adjacent to basins correspond to **Table 1**. Red stars are active volcanoes. Date, moment magnitude, and focal mechanisms of largest historical earthquakes are also shown. Faults locations adapted from from the National Observatory of Athens database of active faults in Greece (NOAFAULTS, 2024), the Active Fault Map of Turkey (Emre et al., 2013), and the marine study of Sakellariou and Tsampouraki-Kraounaki (2022). Earthquake data from Eyidogan and Jackson (1985), Jackson et al. (1982a; 1982b), and Ganas et al. (2021). Shaded relief model constructed with global terrain model of GEBCO (2024). GPS velocity vectors (arrows) are with with respect to central - eastern Anatolia reported in McClusky et al. (2000).

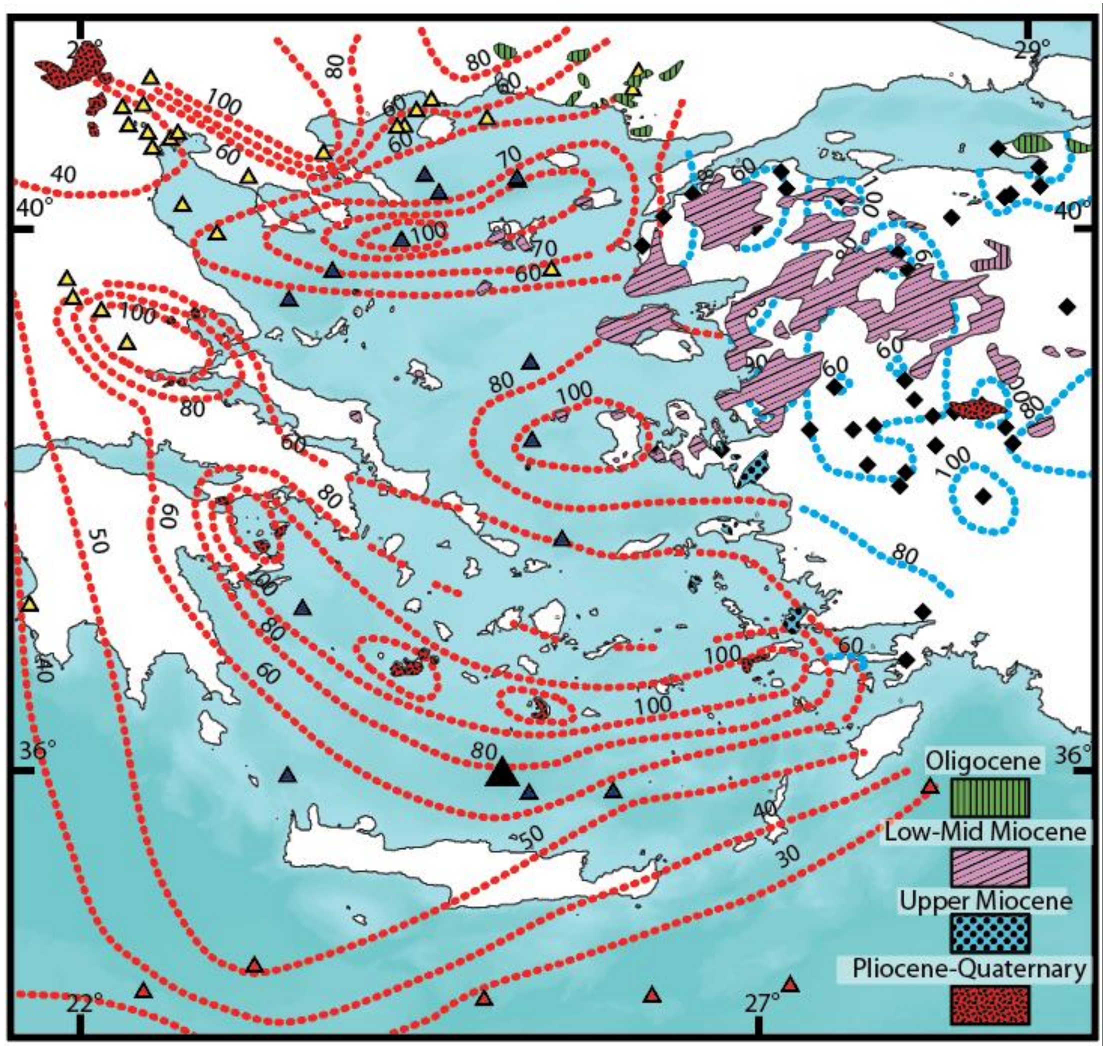

Figure A3. Contours of heat flow (mWm^{-2}) from Fytkas and Kolios (1979) and Balkan-Pazvantoglu et. al. (2021) are red and blue, respectively. Control points: Yellow triangles from Fytkas and Kolios (1979), Blue triangles from Jongsma (1974), Red triangles from Erickson (1970), and black diamonds from Balkan-Pazvantoglu et. al. (2021). Locations of volcanic rocks color coded by age from Fytikas (1984) and Ersoy and Palmer (2013).

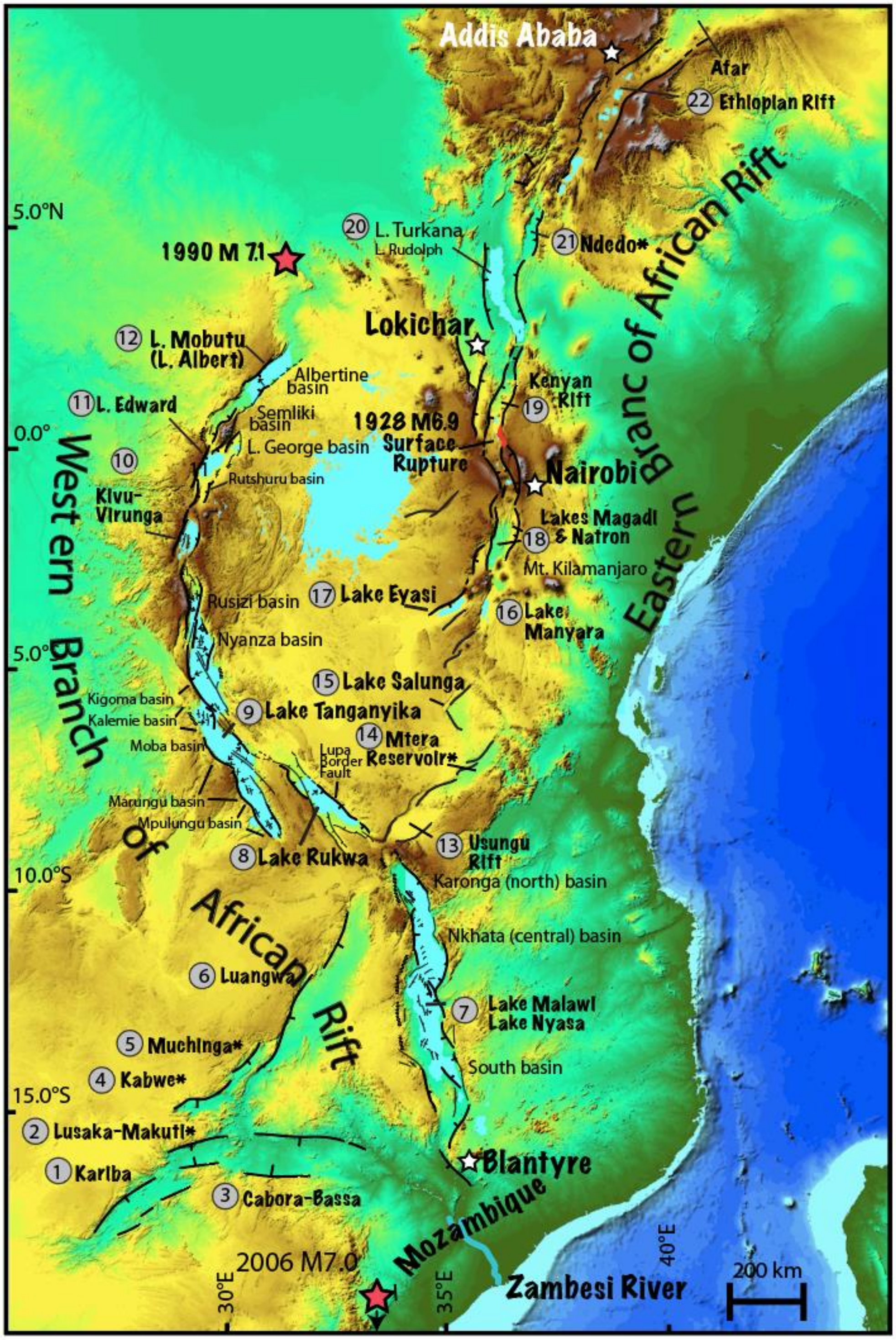

Figure A4. Geography of East African Rift System. Major rift bounding faults are black. Structural basins included in text and tables are labeled and often named for the lakes that fill them. Basin numbers are indexed to basin names in **Table 2**. The two largest instrumentally recorded earthquakes subject to waveform analyses are shown by red stars. Shaded relief constructed with elevation data from Becker et al. (2009a)

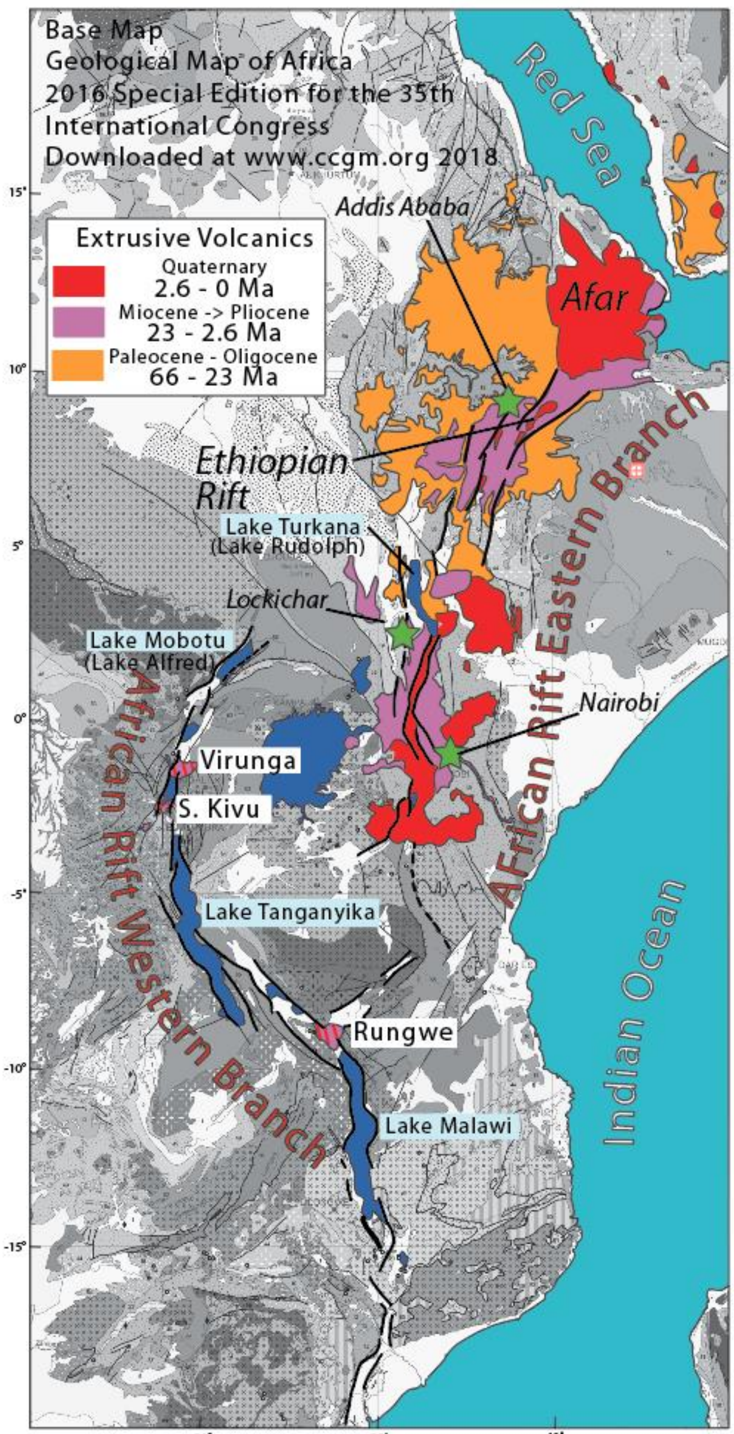

Figure A5. Distribution of extrusive volcanics along African Rift are highlighted in color on grayscale geological base map of eastern Africa (Thieblemont, 2016) . Volcanic rocks are voluminous along the *Eastern Branch*. The *Western Branch* is amagmatic, but for the isolated Virunga, South Kivu, and Rungwe volcanic fields. Areas of gray are Mesozoic to Proterozoic age rocks. Cenozoic sedimentary rocks are white.

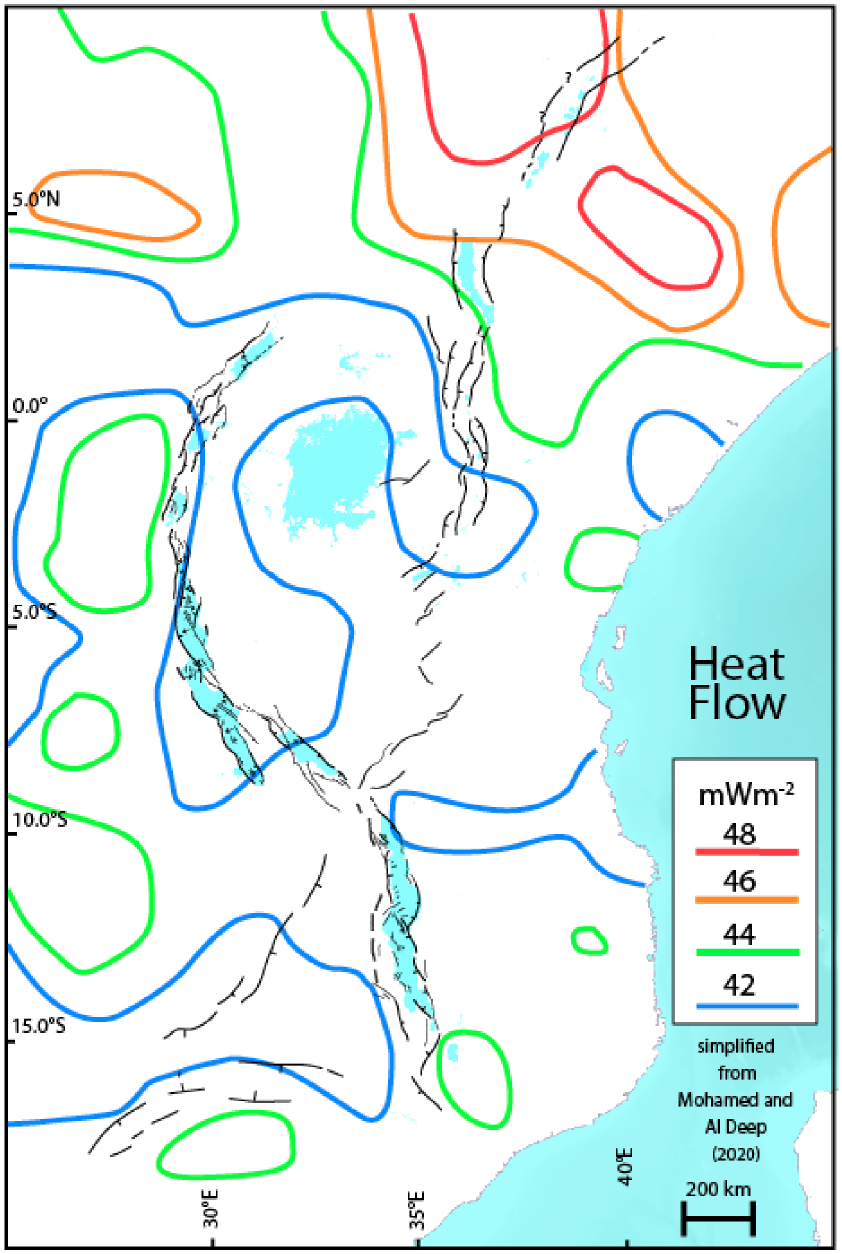

Figure A6. Heat flow contours simplified from Mohamed and Al Deep (2020)

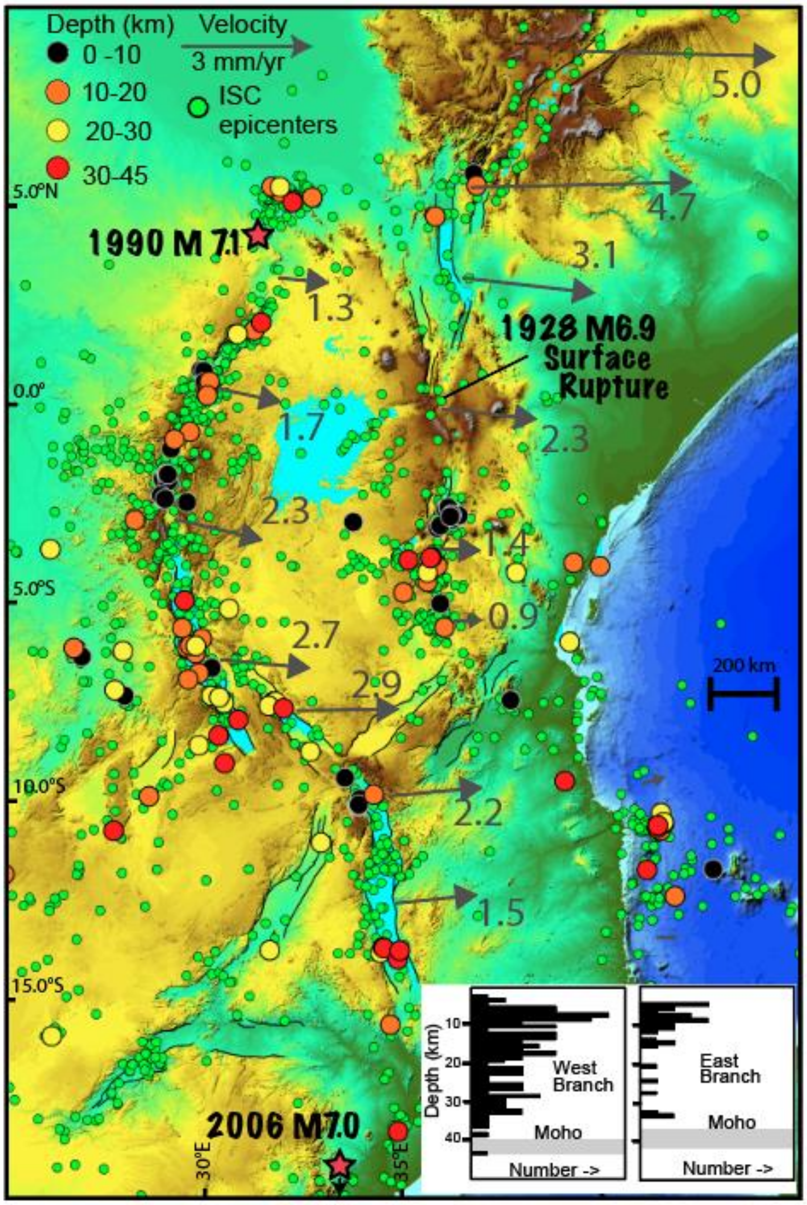

Figure A7. Geodetic velocity vectors and seismicity along *East African Rift from Saria et al. (2014)*. Green dots are epicenters of all earthquakes recorded by International Seismological Centre 1905 to 2018. Epicenters in other colors represent depths of earthquakes determined by Craig et al. (2011) using body waveform analyses. Inset shows distribution of the seismicity as function of depth. Gray bars are average depth of Moho from Dugda et al. (2007) .

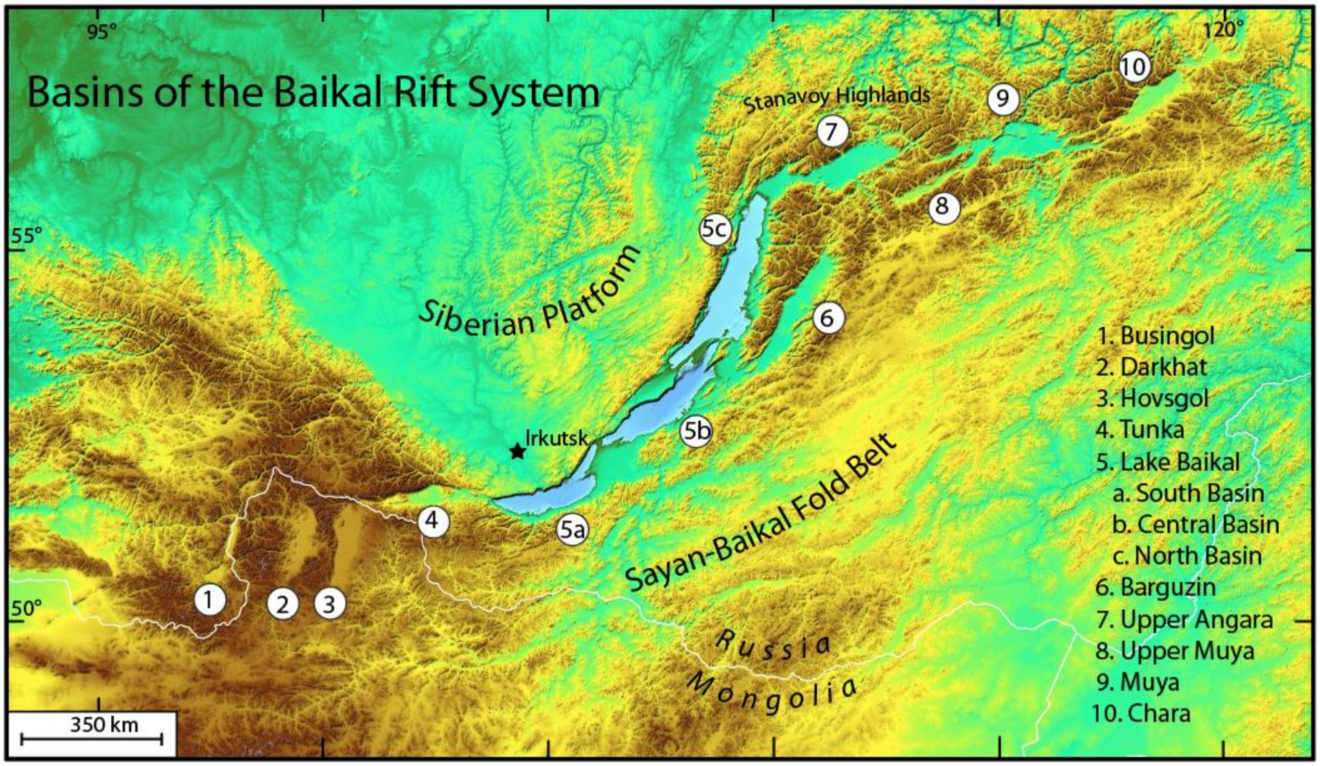

Figure A8. (upper) Shaded Relief Map region of Baikal Rift. Basin numbers and names correspond to **Table 3**.

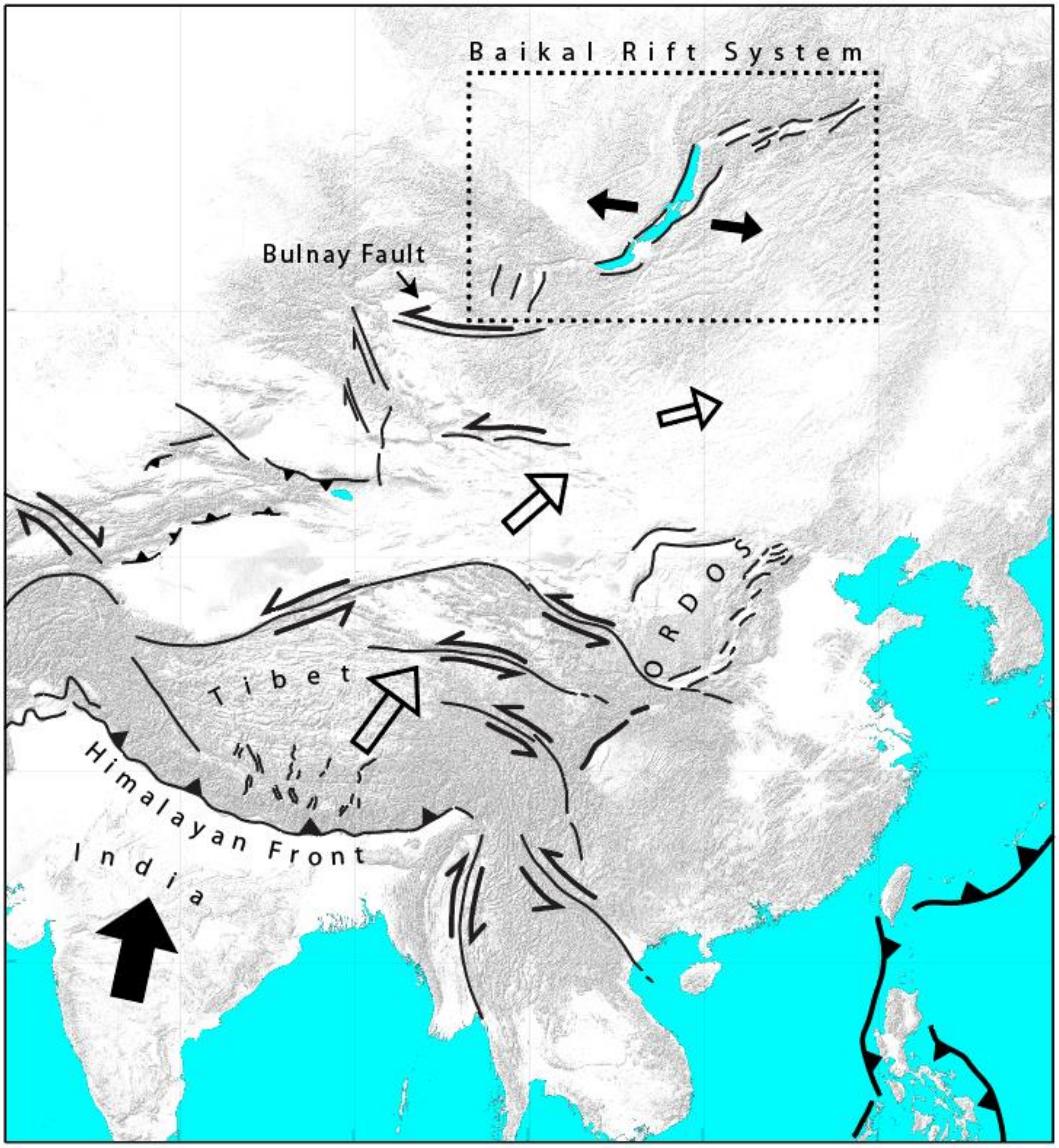

Figure A9. Baikal Rift system is often considered to accommodate extension (small black arrows) resulting from the northeastward crustal displacements (open arrows) resulting from northward impingement of India into Eurasia (large black arrow) and, more locally, the accommodation of left lateral displacement on the Bogd fault. Sketch is developed from observations and ideas of Tapponnier (1975), Petit and Déverchère (2006), Calais and Amarjargal (2000), and Zhang et al. (2004).

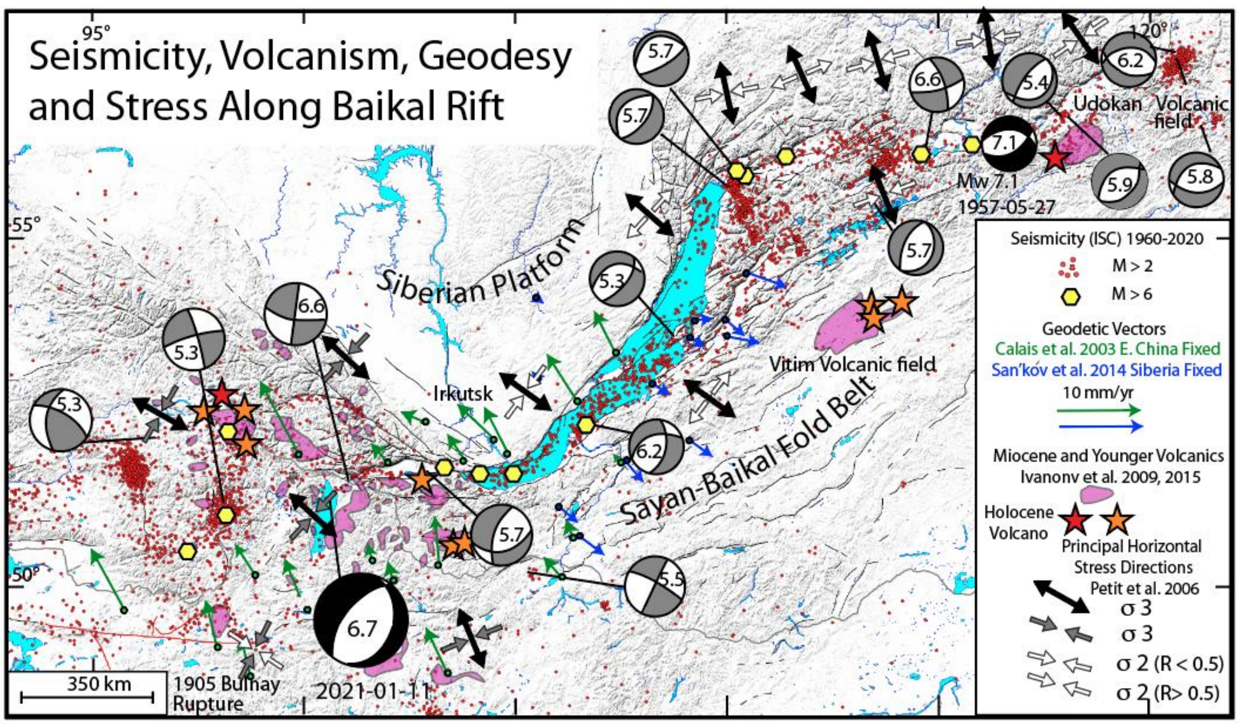

Figure A10. Observations of seismicity, geodesy, and volcanism along the Baikal Rift. See key for data sources. All focal mechanisms are from body-waveform modeling of Emmerson et al. (2006) but for recent Hovsgol Mw 6.7 event of Jan 11, 2021 reported from USGS. The two largest events show black mechanisms rather than gray. Other features and their sources annotated in figure index. Topography from Becker et al. (2009b).

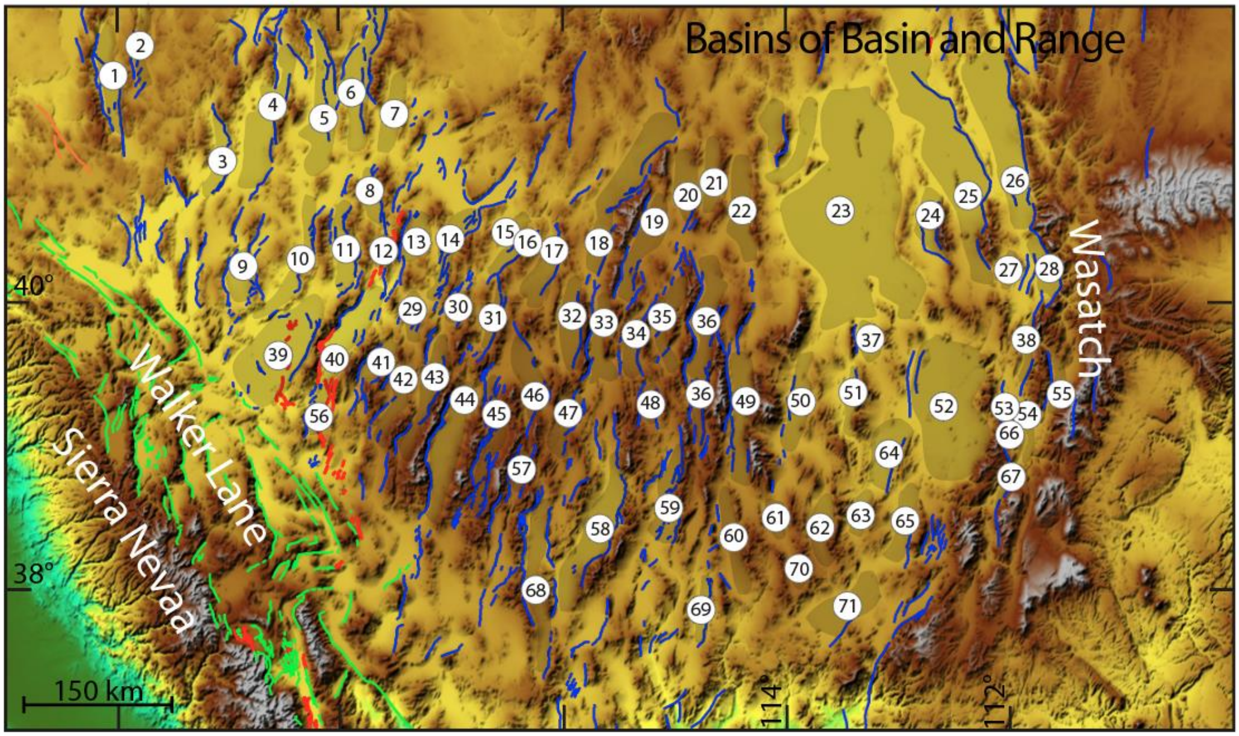

Figure A11. Physiographic map encompassing Basin and Range province of western North America. Topographic basins number labels correspond to **Table 4.** Quaternary fault traces of Walker Lane and Basin and Range provinces are green and blue, respectively. Red faults are those for which historical earthquakes have produced surface rupture. Fault traces from U.S. Geological Survey Quaternary Fault and Fold Database website https://earthquakes.usgs.gov/ hazards/qfaults. Shaded relief constructed with digital elevation data from Becker et al. (2009a): https://topex.ucsd.edu/ WWW_html/srtm30_plus.html .

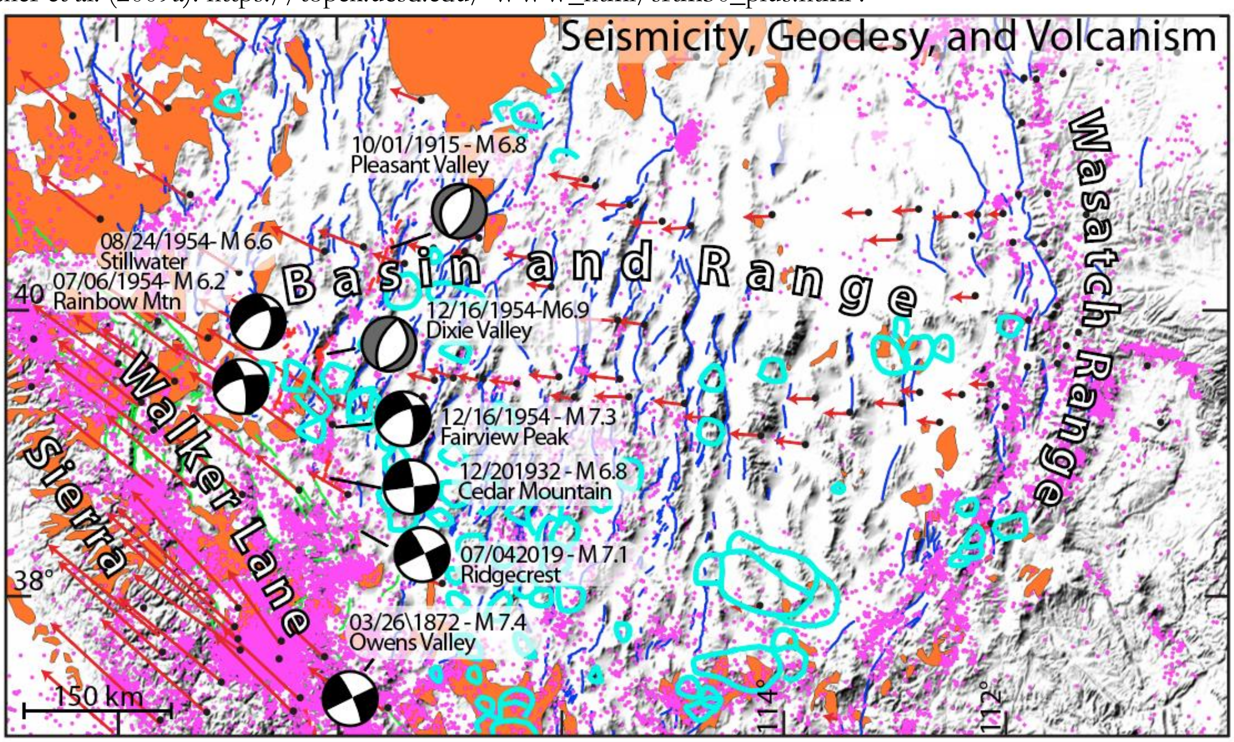

Figure A12. Same area as **Figure A11**. Distribution of M2 and greater seismicity since 1980 (magenta epicenters), focal mechanisms of historical earthquakes accompanied by surface rupture, and velocity vectors plotted with respect to stable North America, distribution of volcanism (orange) since ~17 Ma, and Henry and John's (2013) locations of major calderas that were source of voluminous siliceous ash-flow tuffs during the preceding Oligocene period (~23 - 34 Ma). The large earthquakes of 1915, 1932, and 1954 define the Central Nevada Seismic Belt. *Shaded relief constructed with digital elevation data from Becker et al. (2009a): https://topex.ucsd.edu/ WWW_html/srtm30_plus.html. Seismicity from Advanced National Seismic System (ANSS): https:// earthquake.usgs.gov/data/comcat/. Geodetic velocity vectors (light blue) from UNAVCO (2020). Focal mechanisms from Caskey et al (1996) and (gray and white) interpreted from surface rupture distributions reported Wallace (1984).*

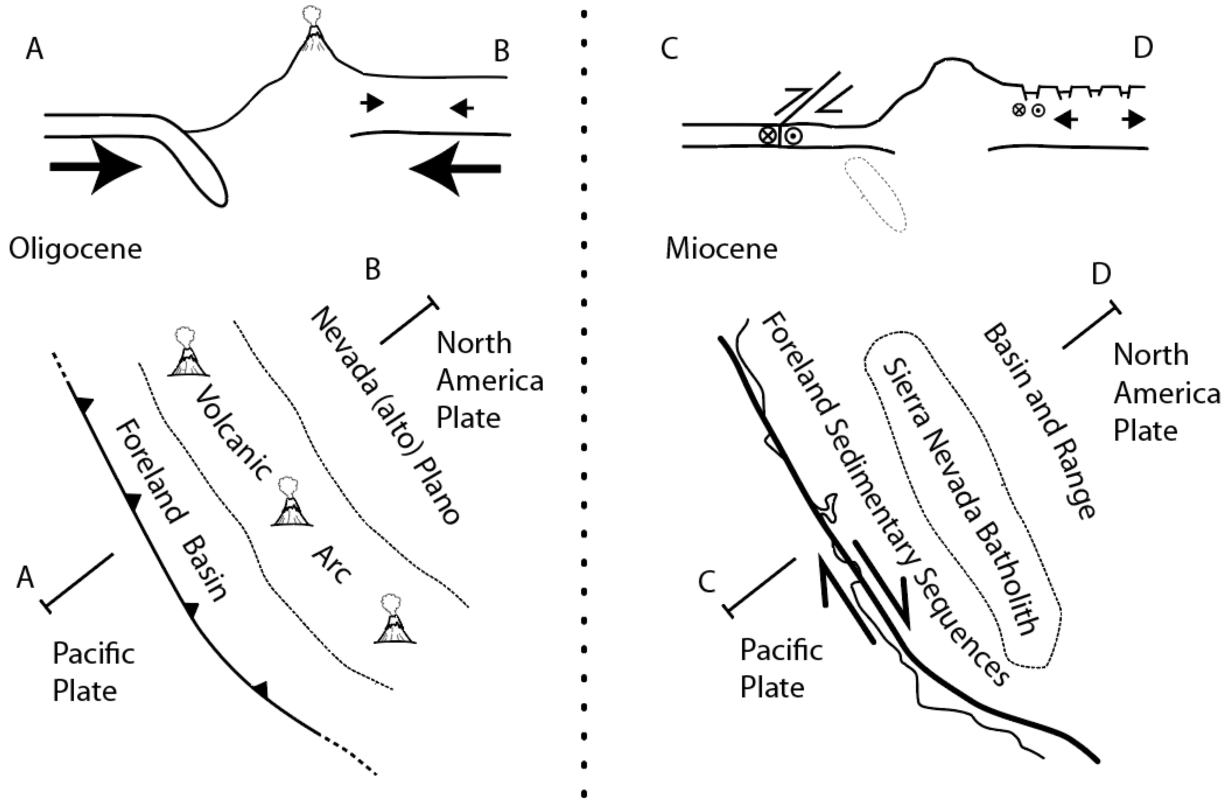

Figure A13. Crustal extension in the Basin and Range is ascribed to a transition from Oligocene and earlier subduction (left) that resulted in a thickening and elevation increase of crust on the over-riding North American Plate to create a high plateau to (right) the transform of subduction to strike-slip motion across the Pacific-North American Plate boundary in the Miocene that served to release compression across the margin and allow gravity as well as right-lateral shear to drive extension across the region. Sources of interpretation cited in text.

Figure Italy A14. Location of Italy in Alpine Himalyan belt. Box outlines **Figure A15**.

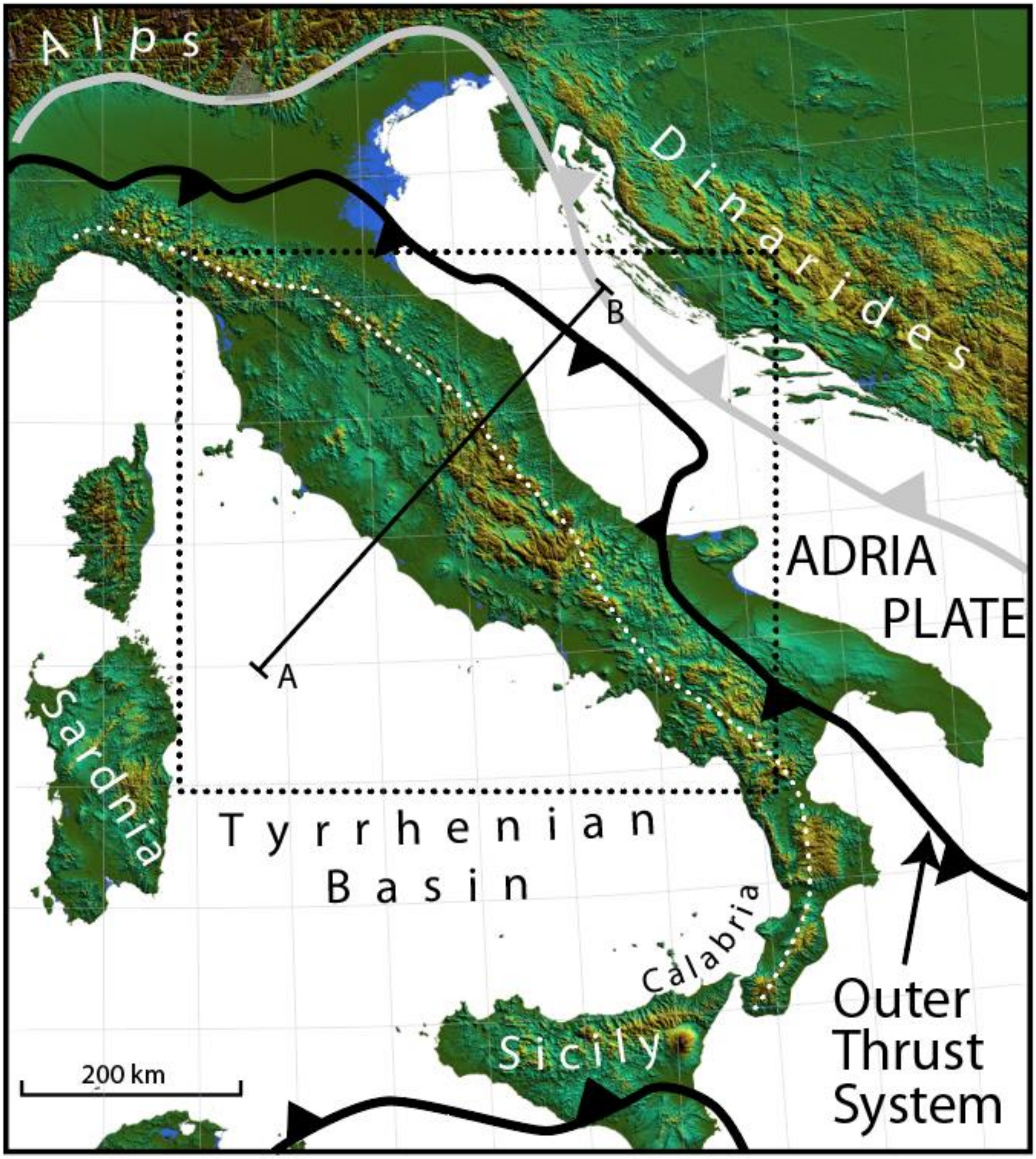

Figure A15. The Apennine mountains strike southeasterly along the peninsula of Italy. The mountains are structurally a northeast verging fold and thrust belt formed in concert with the southwestward subduction of the Adriatic plate. The northeastward front of thrusting associated with subduction of Adria plate beneath Italy is shown by black line with teeth placed on the hanging wall and adapted from Carminati et al. (2012). Box outlines **Figure A16**.

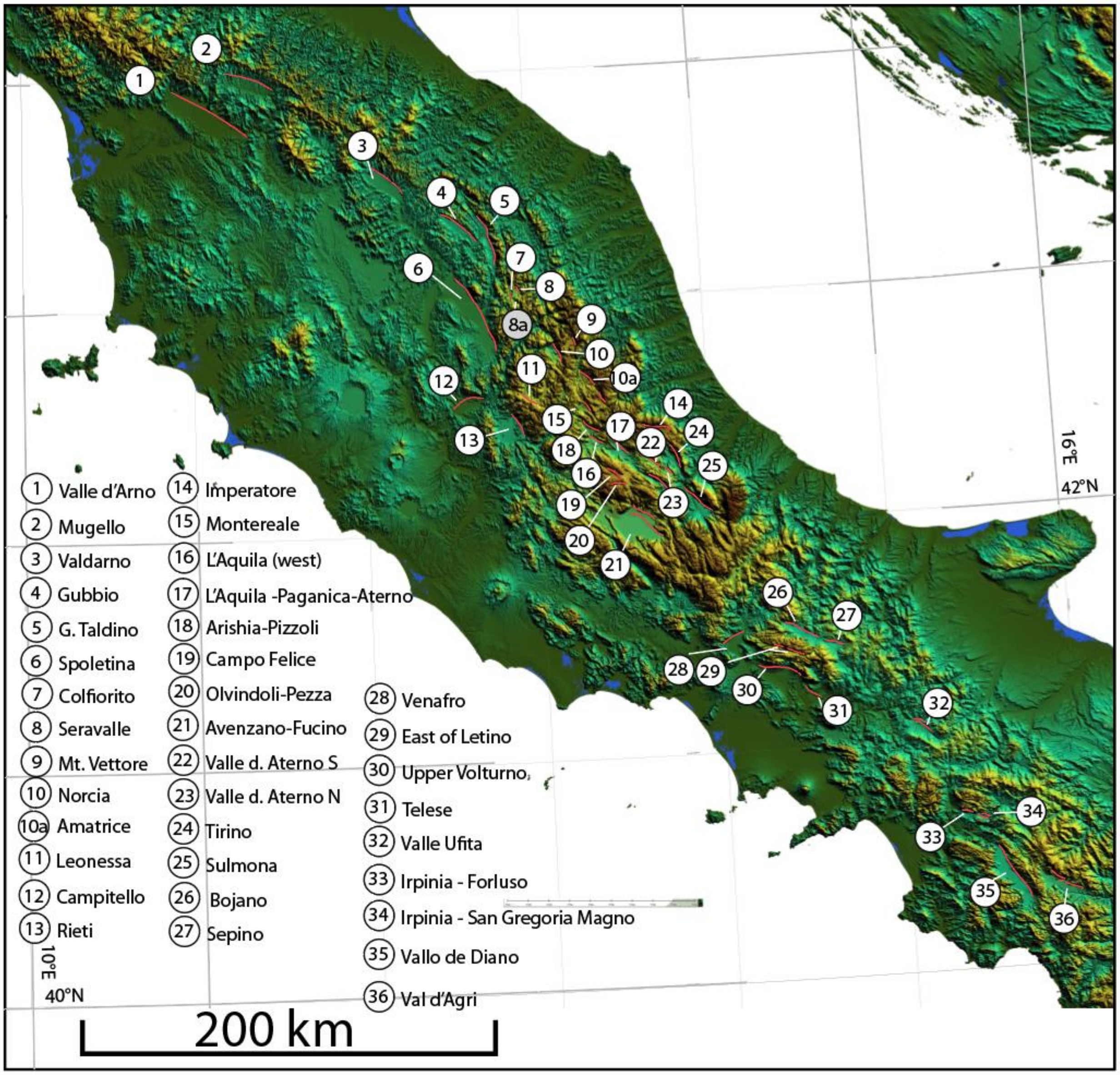

Figure Italy A16. Basins (labeled) and bounding active normal faults (red lines) occur along the length of the Apennines. Basin numbers correspond to **Table 5**.

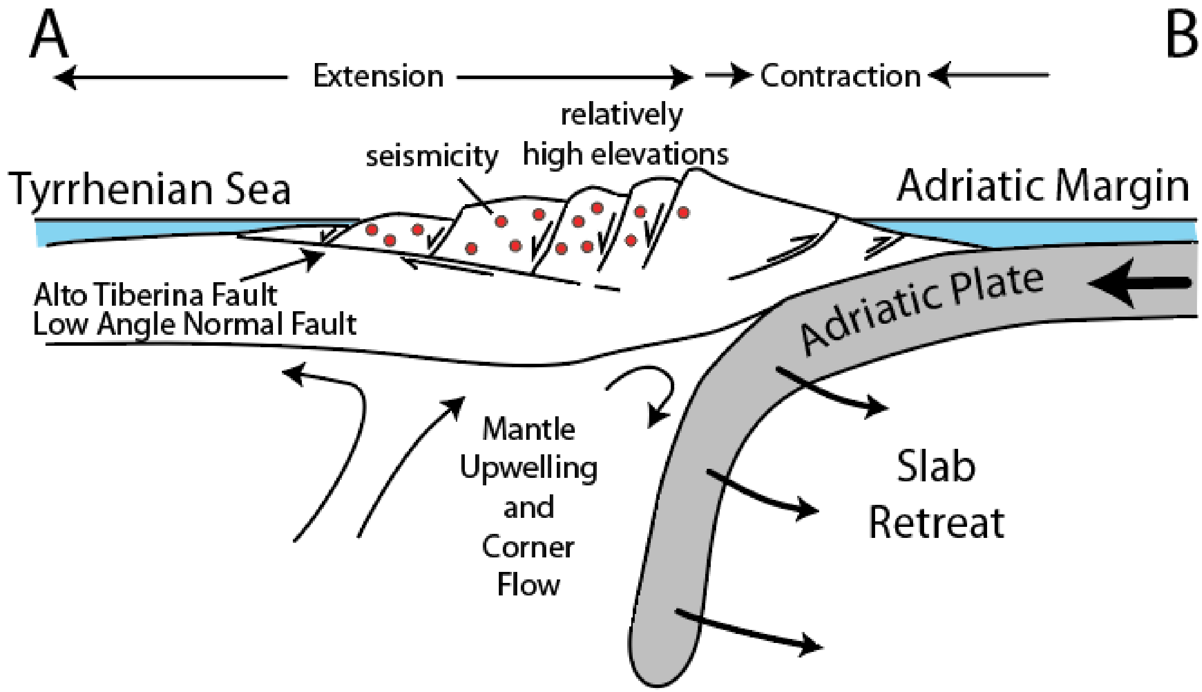

Figure A17. Schematic cross-section (from A to B in **Figure A15**) illustrating factors that play role in presence of normal faulting and crustal extension in the Apennines. Most seismicity (red dots) is located above the Alto Tiberina low angle normal fault (Lavecchia et al., 2024).

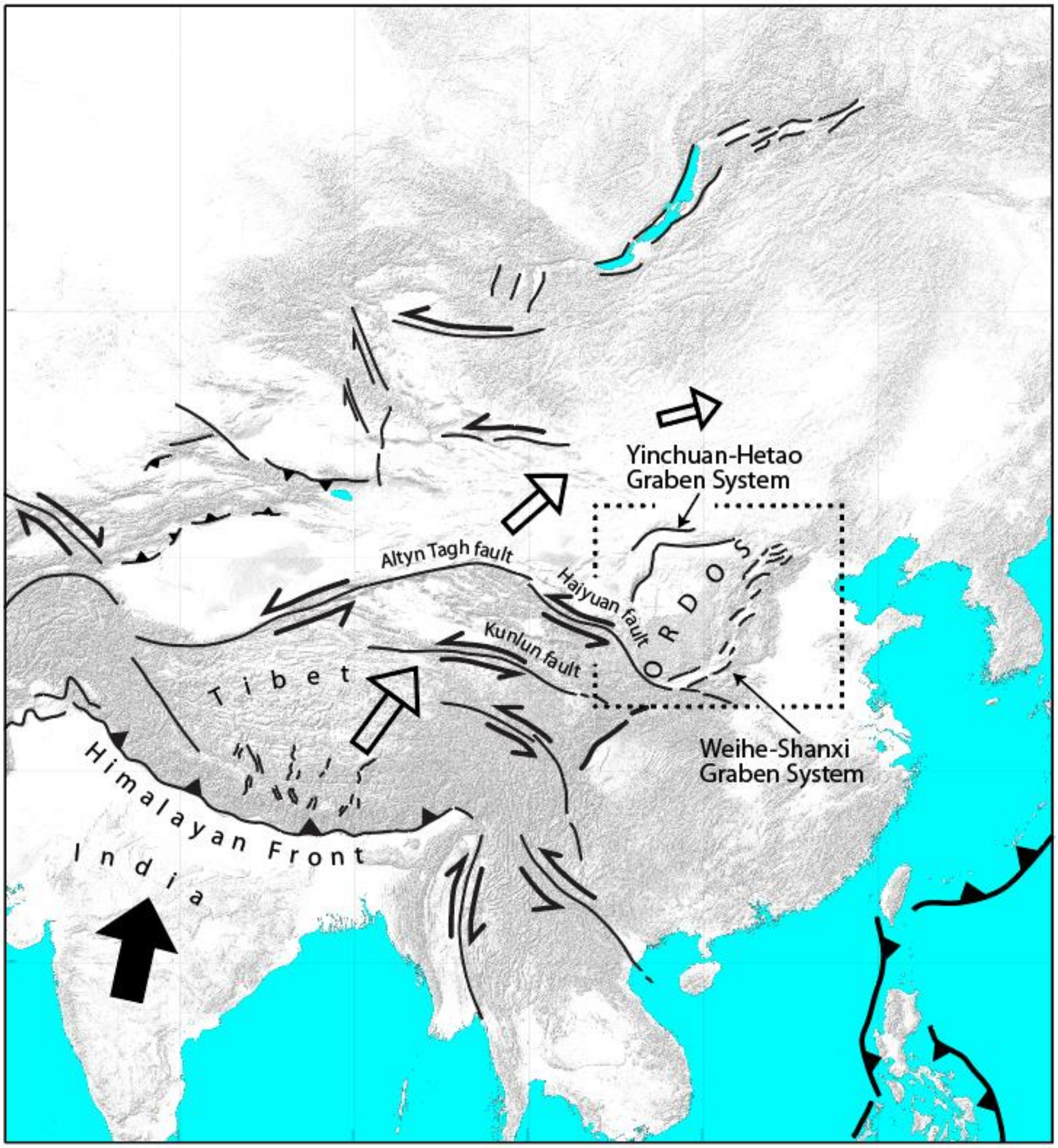

Figure A18. Normal fault bounded basins on the margins of the Ordos plateau accomodate left-lateral displacement along the Haiyuan and Kunlun fault systems resulting from the northeastward crustal displacements (open arrows) resulting from northward impingement of India into Eurasia (large black arrow). Sketch is developed from observations and ideas of Tapponnier (1975).

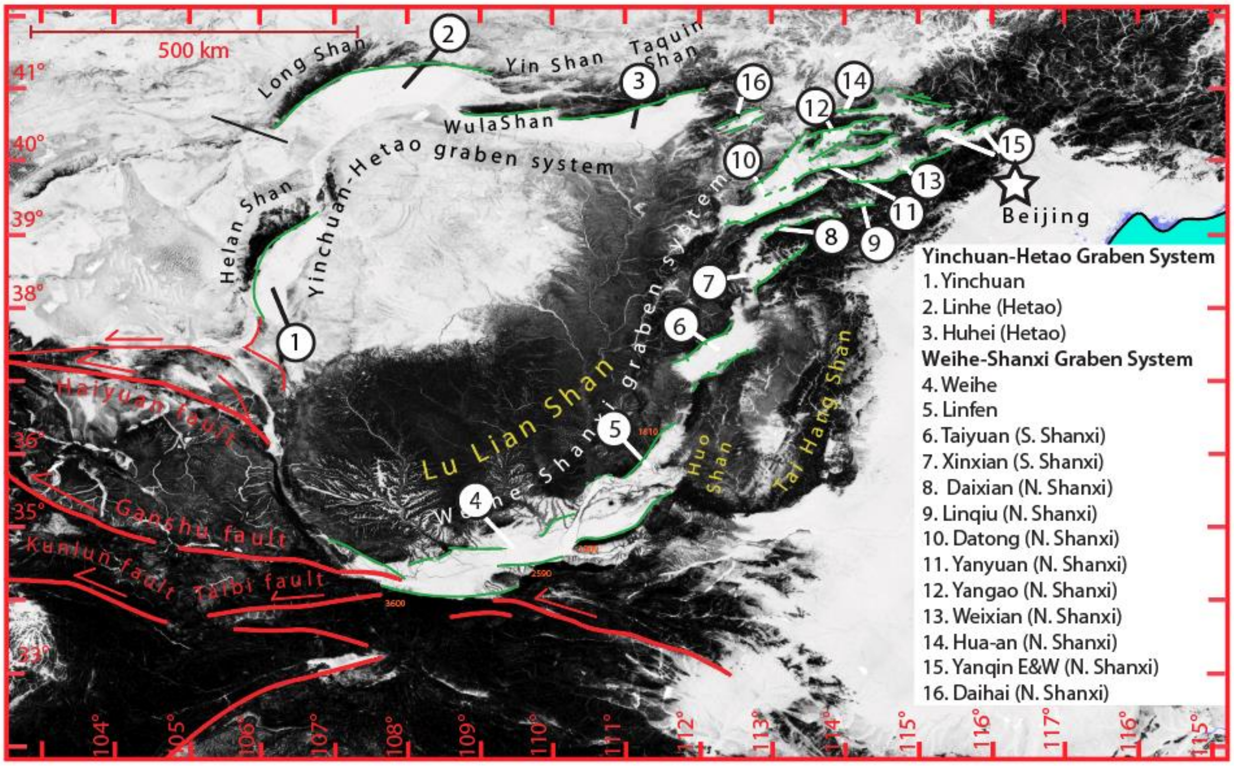

Figure A19. Slope shade map of major fault normal fault bounded basins along the margins of Ordos Plateau. Basin numbers correspond to **Table 6**. Map constructed with data from Tozer et al. (2019).

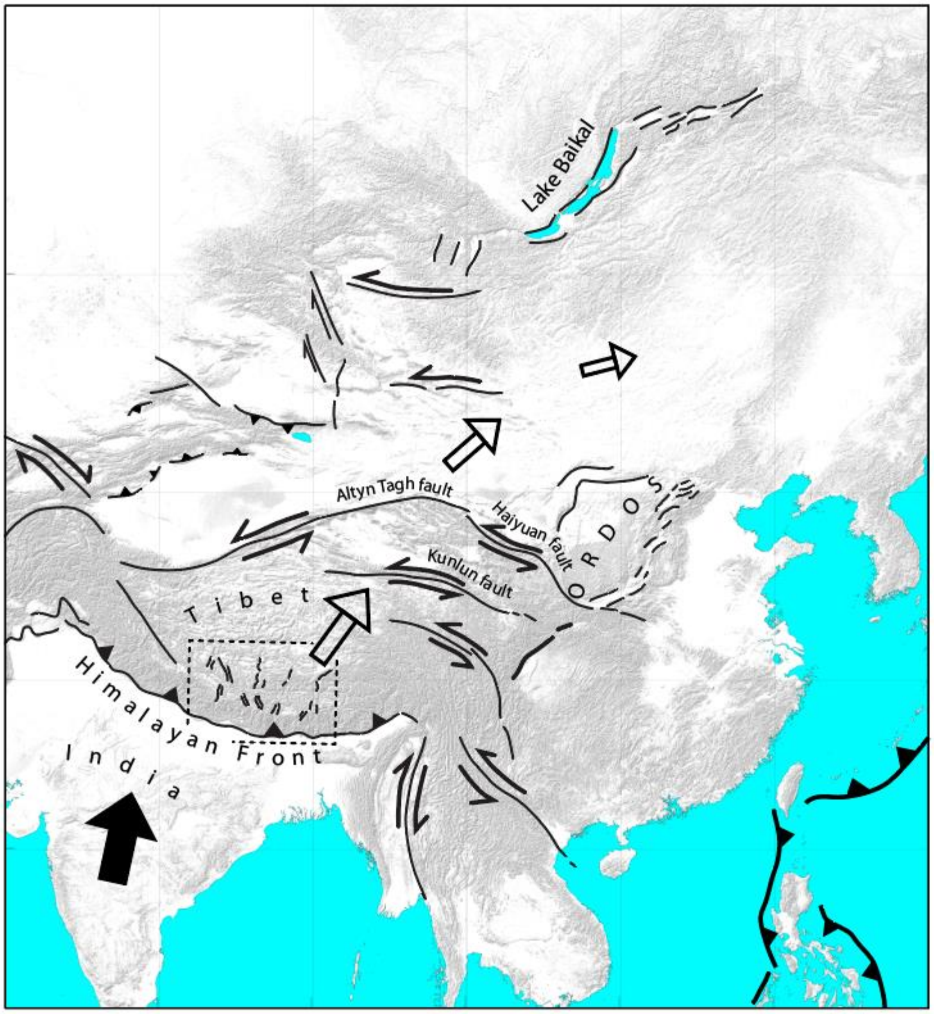

Figure A20. Box outlines region of north trending active normal fault bounded basins present north of the Himalayan front. Area of box shown in **Figure A21**.

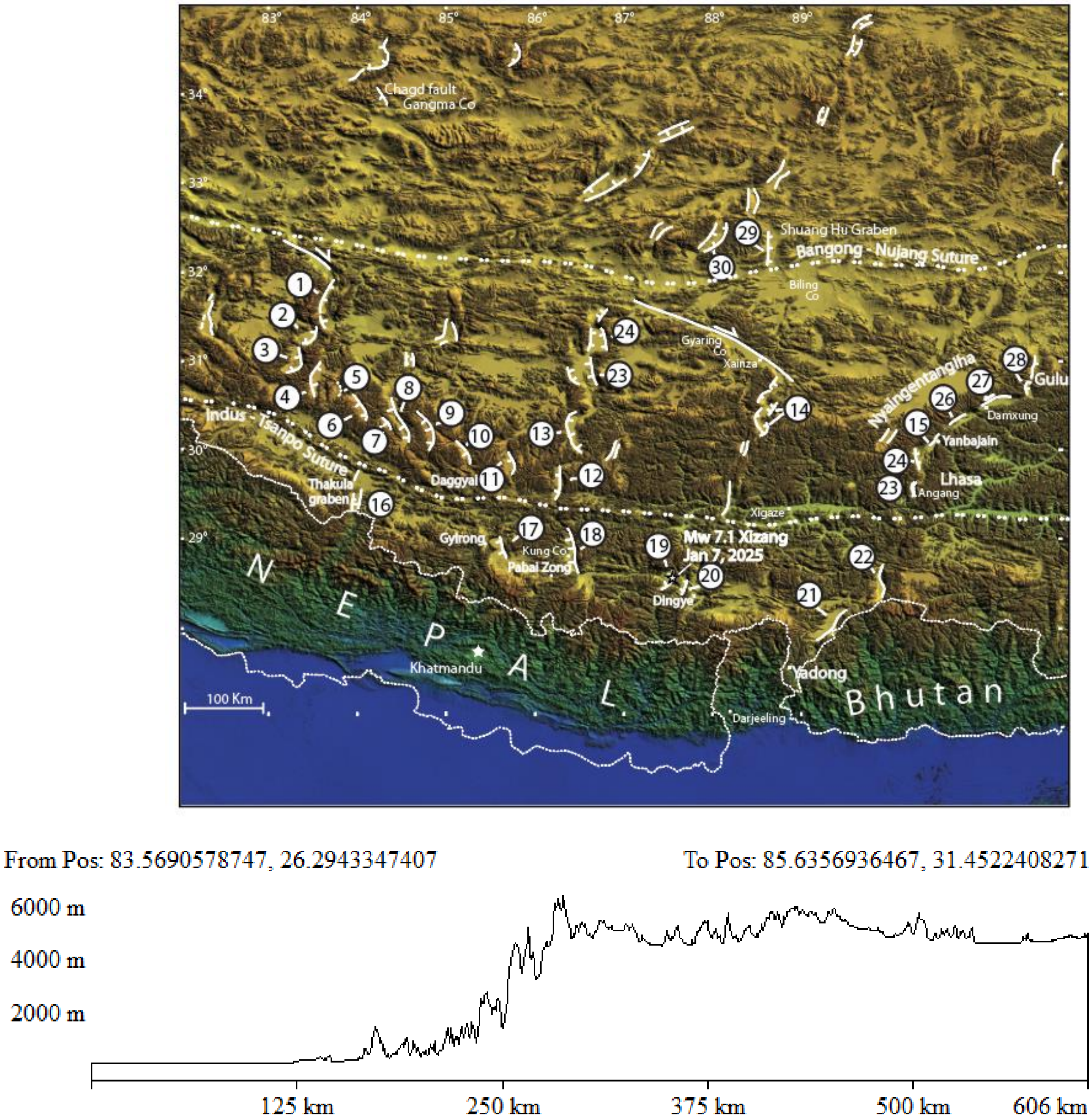

Figure A21. (upper) Active normal fault bounded basins of Tibet are numbered on physiographic map. Numbers correlate to **Table 7.** Places cited in text are labeled as is location of 2025 Mw 7.1 earthquake. (lower) Topographic profile transverse to Himalaya.

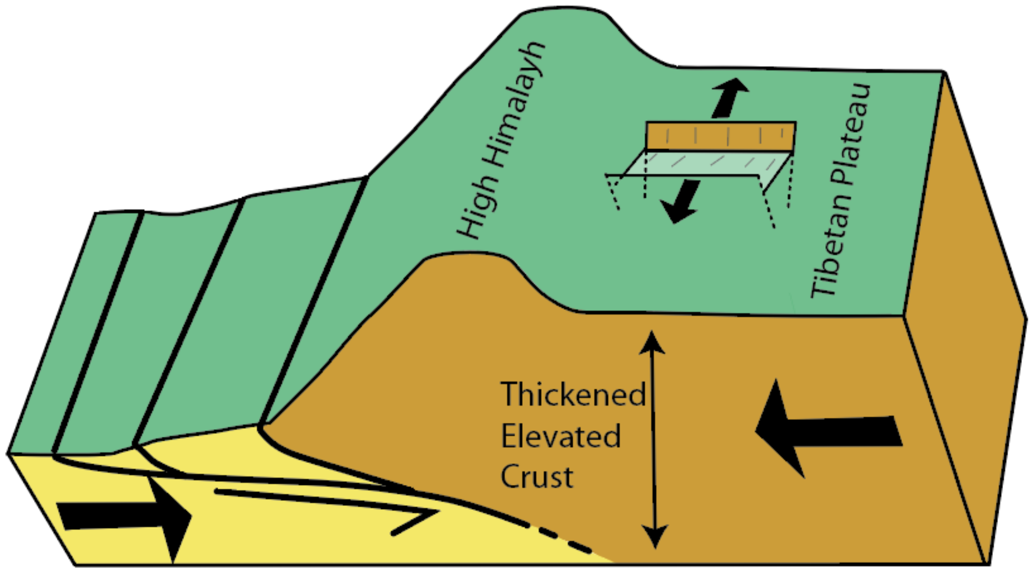

Figure A22. Sketch illustrating idea grabens are caused by overthickening of crust and increase in elevation resulting from convergence of India into Tibet.

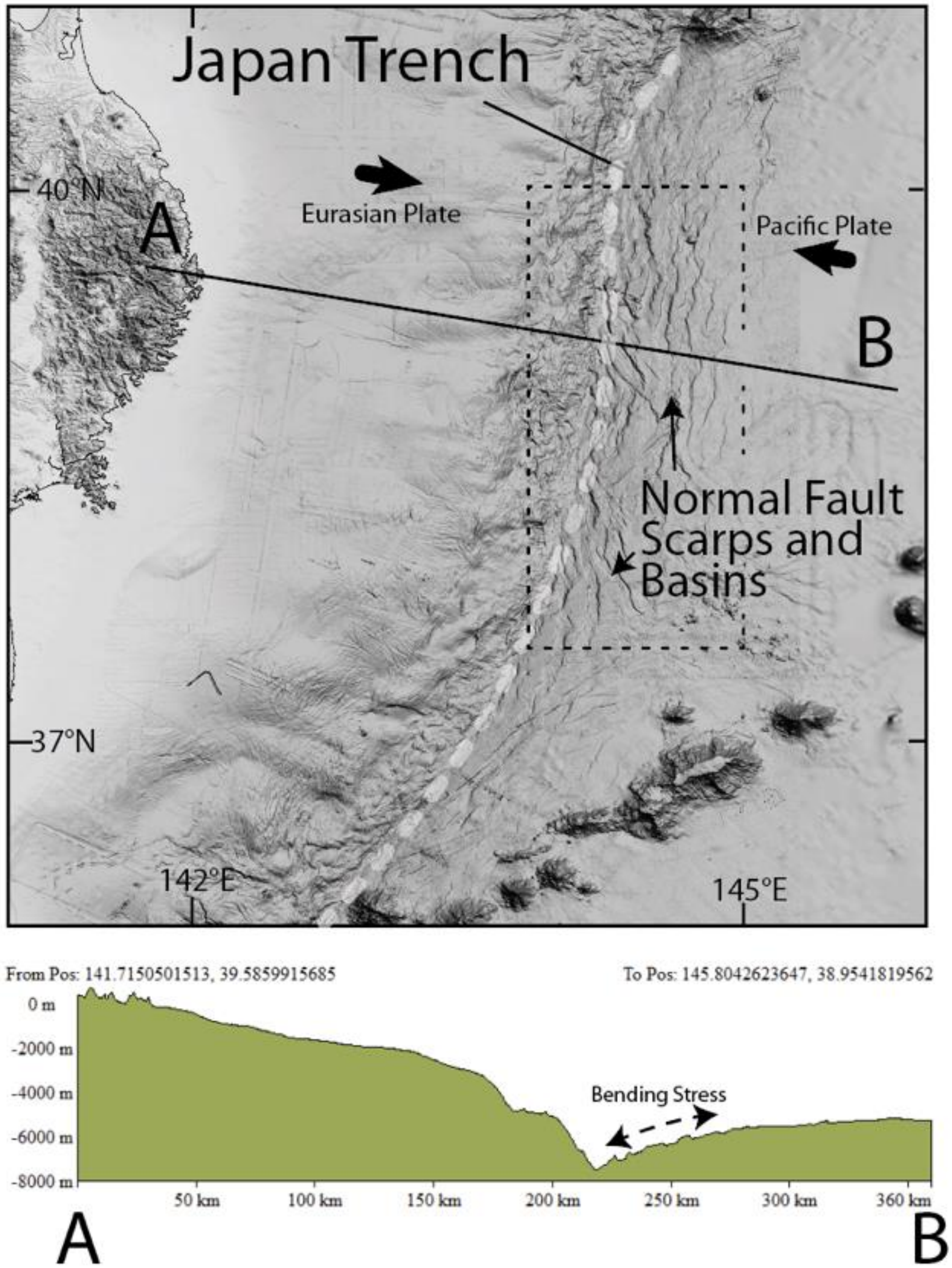

Figure A23. Digital elevation model and topographic cross section across portion Japan Trench outlined in **Figure 1** of main text. Normal fault basins east of Japan Trench on Pacific Plate are attributed to bending stresses as Pacific Plate subducts beneath Eurasian Plate. Enlargement of area in dashed box shown is **Figure A24.** See text for discussion and citations of original research. Digital elevation model from GEBCO (2024).

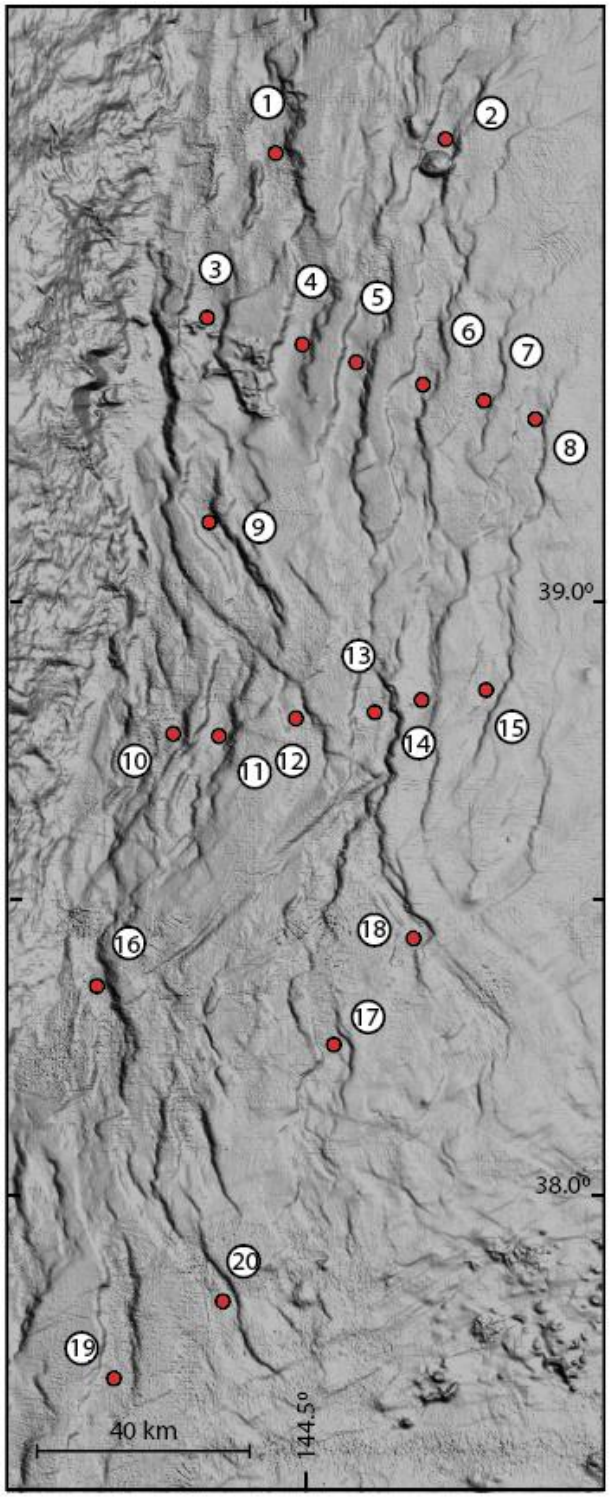

Figure A24. Digital elevation model of area outlined by dashed box in Figure **A23**. Fault bounded basins are numbered and numbers correspond to **Table 8**

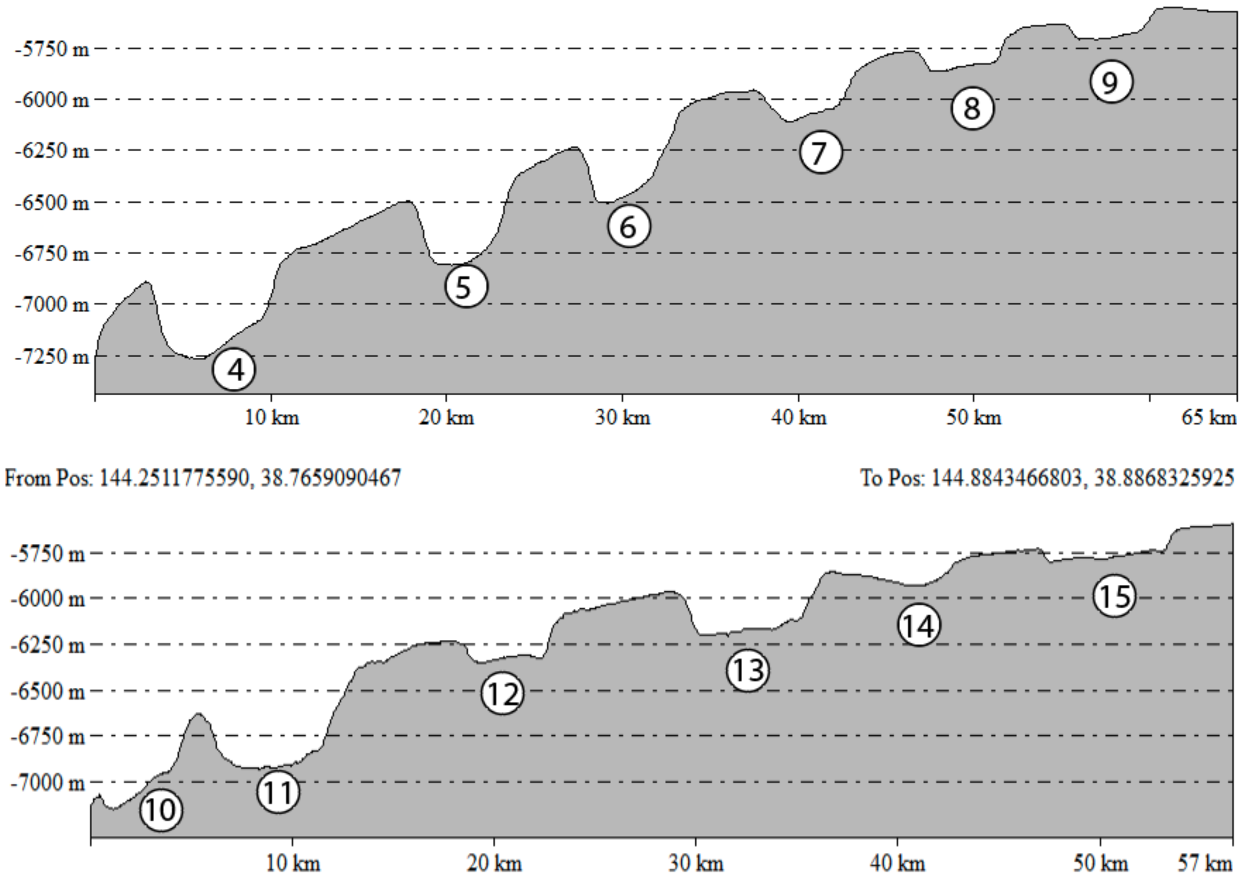

Figure A25. Topographic profiles across fault bounded basins 4 to 9 and 10 to 15. Basin locations shown in map view in **Figure A24**.

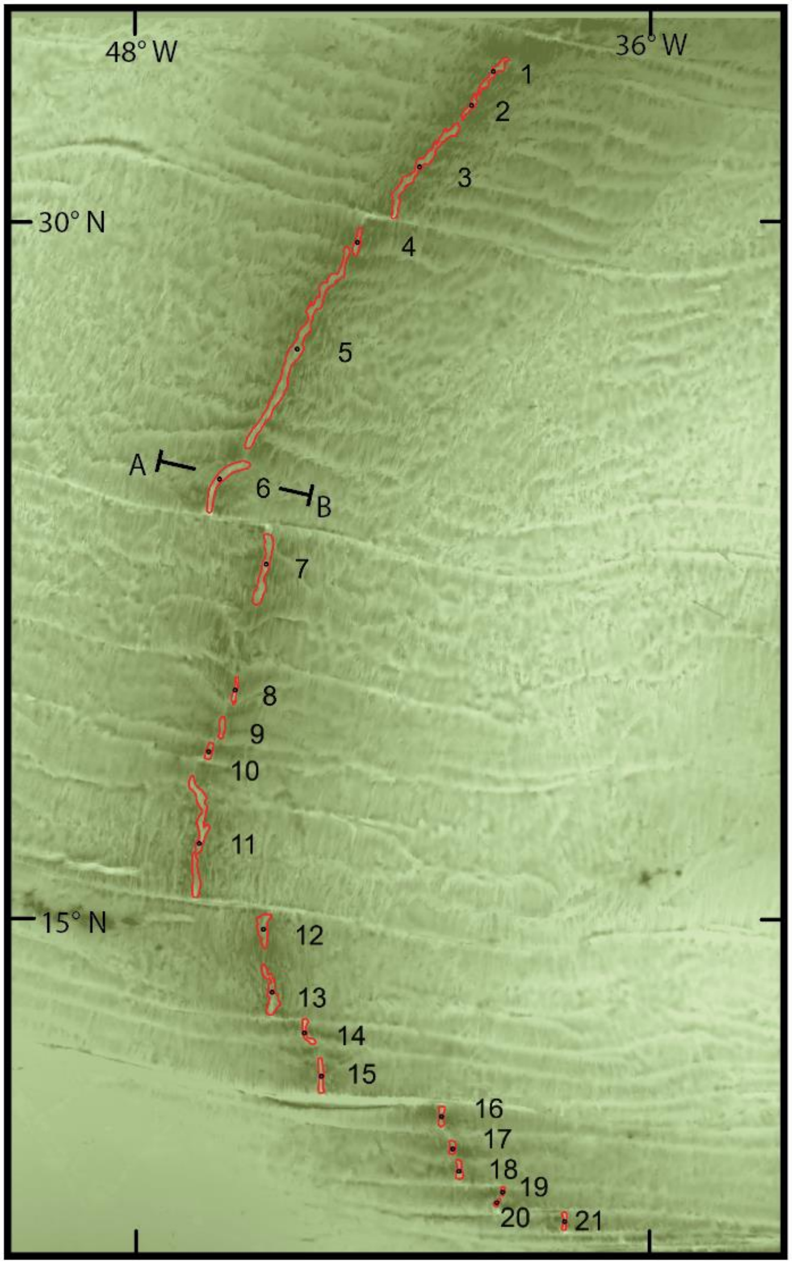

Figure A26. Shaded relief map of section of Mid-Atlantic Ridge outlined in **Figure 1**. Enclosed basins along the axial rift and those ending at fracture zones outlined in red. Numbers are keyed to geological and geophysical observations listed in **Table 9**. Constructed with GEBCO (2024) elevation model. Elevation profile from A to B shown in **Figure A27**.

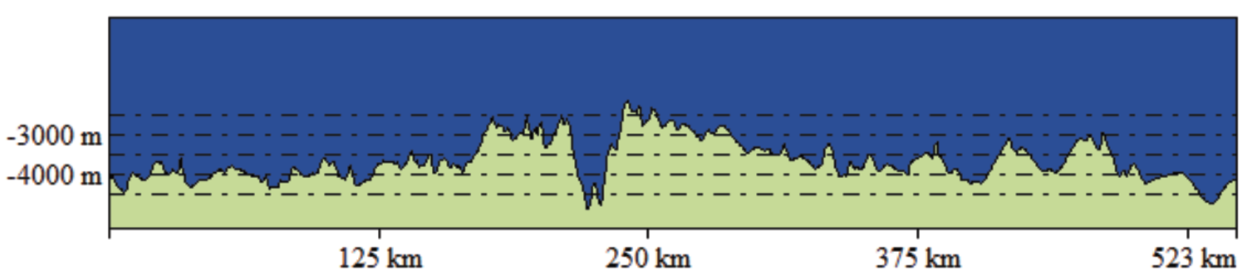

Figure A27. Elevation profile between points A and B in **Figure A26**

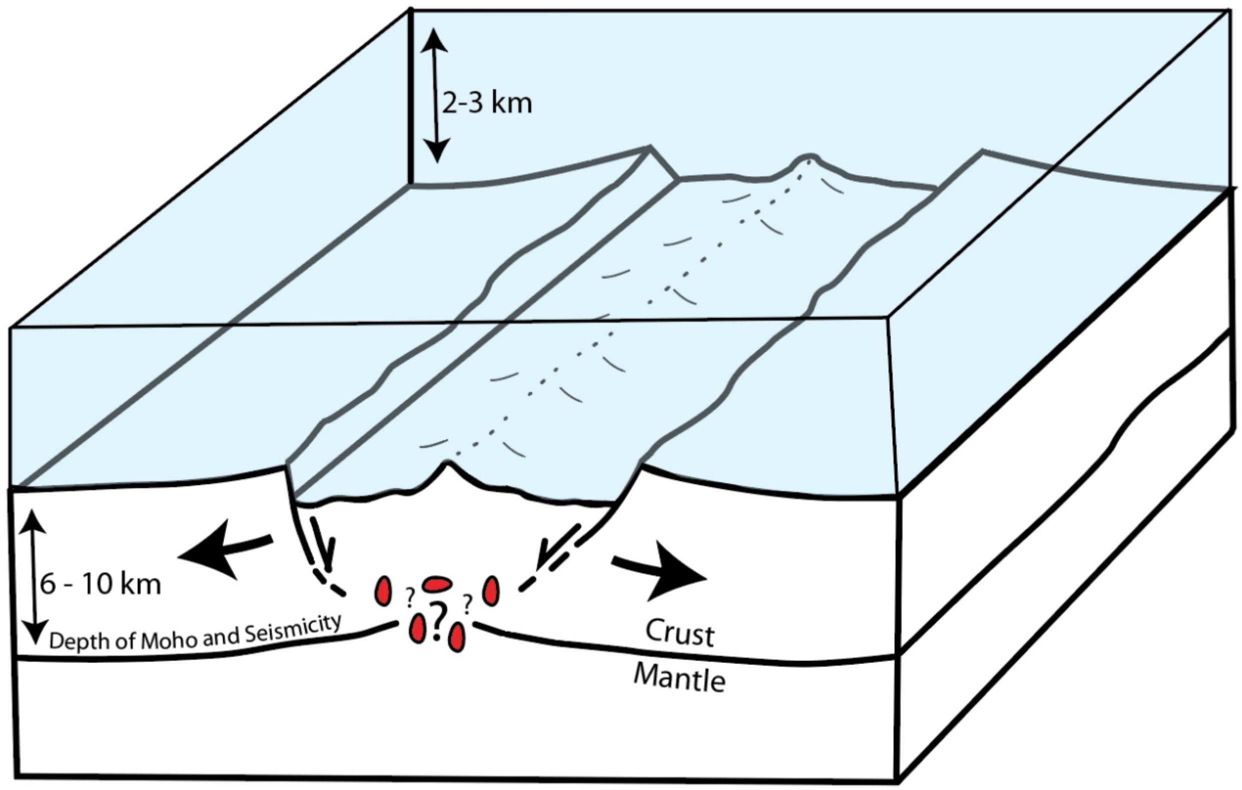

Figure A28. Simplified sketch (not to scale) to show major geophysical characteristics of crust along mid-oceanic ridge and emphasize extension at the ridge is accommodated by processes of both magma accretion and faulting.

References Cited in Appendix

Akinci, A., et al. 2009. Effect of Time Dependence on probabilistic seismic-hazard maps and deaggregation for the central Apennines, Italy. Bulletin of the Seismological Society of America, 99, 2A, 585-610.

Aktug, B., et al. 2009. Deformation of western Turkey from a combination of permanent and campaign GPS data: Limits to block-like behavior. Journal of Geophysical Research, 114, B10404, Article Number B10404 pp. 22.

Alessio, G., et al. 2010. Evidence for surface rupture associated with the Mw 6.3 L'Aquila earthquake sequence of April 2009 (central Italy). Terra Nova, 22, 1, 43-51.

Allmendinger, R. W., et al. 1987. Overview of the COCORP 40°N transect, western United-States - the fabric of an orogenic belt. Geological Society of America Bulletin, 98, 3, 308-319.

Ambraseys, N. N. 1991. Earthquake hazard in the Kenya Rift - The Subukia Earthquake 1928. Geophysical Journal International, 105, 1, 253-269.

Ambraseys, N. N., and J. A. Jackson. 1998. Faulting associated with historical and recent earthquakes in the Eastern Mediterranean region. Geophysical Journal International, 133, 2, 390-406.

Ambraseys, N. N., and J. S. Tchalenko. 1970. Gediz (Turkey) earthquake of March 28, 1970. Naure, 227, 5258, 592-593.

Anastasakis, G., et al. 2006. Upper Cenozoic stratigraphy and paleogeographic evolution of Myrtoon and adjacent basins, Aegean Sea, Greece. Marine and Petroleum Geology, 23, 3, 353-369.

Anderson, R. E. 1971. Thin skin distension in tertiary rocks of southeastern Nevada. Geological Society of America Bulletin, 82, 1, 43-58.

Anderson, R. E., et al. 1983. Implications of selected subsurface data on the structural form and evolution of some basins in the Northern Basin and Range Province, Nevada and Utah. Geological Society of America Bulletin, 94, 9, 1055-1072.

Argand, E. 1916. Sur l'arc des Alpes occidentales: . Eclogae Geol. Helvetiae, 14, 145-191.

Armijo, R., et al. 1999. Westward propagation of the North Anatolian fault into the northern Aegean: Timing and kinematics. Geology, 27, 3, 267-270.

Armijo, R., et al. 1996. Quaternary evolution of the Corinth Rift and its implications for the Late Cenozoic evolution of the Aegean. Geophysical Journal International, 126, 1, 11-53.

Armijo, R., et al. (1982). A field study of Pleistocene rifts in Tibet of. In Anonymous (Ed.s.), A field study of Pleistocene rifts in Tibet of Book (pp. 1093). Washington, DC, United States: American Geophysical Union.

Armijo, R., et al. 1986. Quaternary extension in southern Tibet - field observations and tectonic implications. Journal of Geophysical Research, 91, B14, 13803-13872.

Armijo, R., et al. 1989. Late Cenozoic right-lateral strike-slip faulting in southern Tibet. Journal of Geophysical Research, 94, B3, 2787-2838.

Armstrong, P. A., et al. 1969. Space-time relations of cenozoic silicic volcanism in the Great Basin of the western United States. American Journal of Science, 267, 478-490.

Artemjev, M. E., and E. V. Artyushk. 1971. Structure and isostasy of Baikal Rift and mechanism of rifting. Journal of Geophysical Research, 76, 5, 1197-&.

Atwater, T. 1970. Implications of plate tectonics for the Cenozoic tectonic evolution of western North America. Bulletin of the Geological Society of America, 81, 3513-3536.

Atwater, T., and J. Stock. 1998. Pacific North America plate tectonics of the Neogene southwestern United States: An update. International Geology Review, 40, 5, 375-402.

Atwater, T. M., and J. D. Mudie. 1968. Block faulting on Gorda Rise. Science, 159, 3816, 729-&.

Aumento, F. 1969. The Mid-Atlantic Ridge near 45 °N. V. Fission track and ferro-manganese chronology. Canadian Journal of Earth Sciences, 6, 6, 1431-1440.

Avallone, A., et al. 2004. Analysis of eleven years of deformation measured by GPS in the Corinth Rift Laboratory area. Comptes Rendus Geoscience, 336, 4-5, 301-311.

Ayhan, M. E., et al. 2002. Inter-seismic strain accumulation in the Marmara Sea region. Bulletin of the Seismological Society of America, 92, 1, 216-229.

Bai, L., et al. 2017. Focal depths and mechanisms of shallow earthquakes in the Himalayan-Tibetan region. Gondwana Res., 41, 390-399.

Baljinnyam, I., et al. 1993. Ruptures of major earthquakes and active deformation in Mongloia and it's surroundings. Geological Society of America Memoir, 181, 62.

Balkan-Pazvantoglu, E., et al. 2021. Surface heat flow in bestern Anatolia (Turkey) and implications to the thermal structure of the Gediz Graben. Turkish Journal of Earth Sciences.

Ballard, R. D., and T. H. Vanandel. 1977. Morphology and tectonics of inner rift valley at lat 36°50'n on Mid-Atlantic Ridge. Geological Society of America Bulletin, 88, 4, 507-530.

Baranov, A., et al. 2023. A new Moho map of the African continent from seismic, topographic, and tectonic data. Gondwana Res., 124, 218-245.

Baranowski, J., et al. 1984. Focal depths and fault plane solutions of earthquakes and active tectonics of the Himalaya. Journal of Geophysical Research, 89, NB8, 6918-6928.

Barclay, A. H., et al. 2001. Microearthquake characteristics and crustal Vp/<i>Vs structure at the Mid-Atlantic Ridge, 35°N. Journal of Geophysical Research, 106, B2, 2017-2034.

Bateman, P. C. 1988. Constituion and genesis of the central Sierra Nevada batholith, California. U. S. Geological Survey Open-file Report 88-382, 284 p.

Becker, J. J., et al. 2009a. Global Bathymetry and Elevation Data at 30 Arc Seconds Resolution: SRTM30_PLUS: https://topex.ucsd.edu/WWW_html/srtm30_plus.html. Marine Geodesy, 32, 4, 355-371.

Becker, J. J., et al. 2009b. Global bathymetry and elevation data at 30 arc seconds resolution: SRTM30_PLUS https://topex.ucsd.edu/WWW_html/srtm30_plus.html. Marine Geodesy, 32, 4, 355-371.

Bennett, R. A., et al. 2012. Syn-convergent extension observed using the RETREAT GPS network, northern Apennines, Italy. Journal of Geophysical Research, 117, B04408, Article B04408.
Blackman, D. K., et al. 1998. Origin of extensional core complexes: Evidence from the Mid-Atlantic Ridge at Atlantis Fracture Zone. Journal of Geophysical Research, 103, B9, 21315-21333.
Blackwell, D. D., and M. Richards. 2004. Geothermal Map of North America. AAPG Map, scale 1:6,500,00, Product Code 423.
Blackwell, D. D., et al. 2011. SMU Geothermal Laboratory heat flow map of the conterminous United States. supported by Google. org, Available at http://www.smu.edu/geothermal.
Blackwell, D. D., et al. (1991). Chapter 23: Heat-flow patterns of the North American continent; A discussion of the Geothermal Map of North America of. In D. B. Slemmons, E. R. Engdahl, M. D. Zoback and D. D. Blackwell (Ed.s.), Chapter 23: Heat-flow patterns of the North American continent; A discussion of the Geothermal Map of North America of Book (pp. 423-4435). Boulder, Colorado: Geological Society of America.
Blisniuk, P. M., et al. 2001. Normal faulting in central Tibet since at least 13.5 Myr ago. Nature, 412, 6847, 628-632.
Bocchini, G. M., et al. 2018. Tearing, segmentation, and backstepping of subduction in the Aegean: New insights from seismicity. Tectonophysics, 734, 96-118.
Boston, B., et al. 2014. Outer-rise normal fault development and influence on near-trench decollement propagation along the Japan Trench, off Tohoku. EARTH PLANETS AND SPACE, 66, 135.
Bosworth, W., et al. 2005. The Red Sea and Gulf of Aden basins. Journal of African Earth Sciences, 43, 1-3, 334-378.
Brichau, S., et al. 2008. Timing, slip rate, displacement and cooling history of the Mykonos detachment footwall, Cyclades, Greece, and implications for the opening of the Aegean Sea basin. Journal of the Geological Society, 165, 263-277.
Brothers, D. S., et al. 2009. New Constraints on Deformation, Slip Rate, and Timing of the Most Recent Earthquake on the West Tahoe-Dollar Point Fault, Lake Tahoe Basin, California. Bulletin of the Seismological Society of America, 99, 2A, 499-519.
Bryan, W. B., and J. G. Moore. 1977. Compositional variations of young basalts in mid-atlantic ridge rift valley near lat 36°49'N. Geological Society Of America Bulletin, 88, 4, 556-570.
Bullard, E. C. 1936. Gravity measurements in East Africa. Royal Society of London Philosophic Transactions, A235, 445-531.
Bullard, E. C., and A. Day. 1954. The flow of heat through the floor of the Atlantic Ocean. Proceedings of Royal Society A., 177, 4708-429.
Burov, E. B., et al. 1994. A broken plate beneath the North Baikal Rift Zone revealed by gravity modelling. Geophysical research letters, 21, 2, 129-132.
Calais, E., and S. Amarjargal. 2000. New constraints on current deformation in Asia from continuous GPS measurements at Ulan Baatar, Mongolia. Geophysical Research Letters, 27, 10, 1527-1530.
Calais, E., et al. 2003. GPS measurements of crustal deformation in the Baikal-Mongolia area (1994-2002): Implications for current kinematics of Asia. Journal of Geophysical Research, 108, B10.
Calvert, A. J. 1997. Backscattered coherent noise and seismic reflection imaging of the oceanic crust: An example from the rift valley of the Mid-Atlantic Ridge at 23 degrees N. Journal of Geophysical Research, 102, B3, 5119-5133.
Caputo, M., et al. 1970. Deep structure of Mediterranean-basin. Journal of Geophysical Research, 75, 26, 4919-+.
Carminati , E., et al. (2010). Tectonics, magmatism and geodynamics of Italy: What we know and what we imagine of. In M. Beltrando, A. Peccerillo, M. Mattei, S. Conticelli and C. Doglioni (Ed.s.), Tectonics, magmatism and geodynamics of Italy: What we know and what we imagine of Book (pp. paper 9). Journal of Virtual Explorer, Electronic Edition.
Carminati, E., et al. 2012. Geodynamic evolution of the central and western Mediterranean: Tectonics vs. igneous petrology constraints. Tectonophysics, 579, 173-192.
Caskey, S. J., et al. 1996. Surface faulting of the 1954 Fairview Peak (M(S), 7.2) and Dixie Valley (M(S) 6.8) earthquakes, central Nevada. Bulletin of the Seismological Society of America, 86, 3, 761-787.
Cataldi, R., et al. 1995. Geothermal ranking of Italian territory. Geothermics, 24, 1, 115-129.

Cavinato, G. P., and P. G. De Celles. 1999. Extensional basins in the tectonically bimodal central Apennines fold-thrust belt, Italy: Response to corner flow above a subducting slab in retrograde motion. Geology, 27, 10, 955-958.
Cessaro, R. K., and D. M. Hussong. 1986. Transform seismicity at the intersection of the Oceanographer Fracture-Zone and the Mid-Atlantic Ridge. Journal Of Geophysical Research, 91, B5, 4839-4853.
Chang, C.-F., and H.-L. Cheng. 1973. Some tectonic features of the Mt. Jolmo Lungma area, southern Tibet. Sci. sinica, 16, 257-265.
Chapman, D. S., and H. N. Pollack. 1977. Heat-flow and heat-production in Zambia - evidence for lithospheric thinning in Central-Africa. Tectonophysics, 41, 1-3, 79-100.
Chapple, W. M., and D. W. Forsyth. 1979. Earthquakes and bending of plates at trenches. Journal of Geophysical Research, 84, NB12, 6729-6749.
Cheng, B., et al. 2014. Seismic structure of the Helan-Liupan-Ordos western margin tectonic belt in North-Central China and its geodynamic implications. Journal of Asian Earth Sciences, 87, 141-156.
Chiarabba, C., et al. 2009. The 2009 L'Aquila (central Italy) Mw 6.3 earthquake: Main shock and aftershocks. Geophysical Research Letters, 36, L18308.
Chiarabba, C., and P. De Gori. 2016. The seismogenic thickness in Italy: constraints on potential magnitude and seismic hazard. Terra Nova, 28, 6, 402-408.
Chiarabba, C., and R. Di Stefano. (2010). Seismicity and deep structure of the northern-central Apennines of. In M. Beltrando, A. Peccerillo, M. Mattei, S. Conticelli and C. Doglioni (Ed.s.), Seismicity and deep structure of the northern-central Apennines of Book (pp. paper 13). Journal of Virtual Explorer, Electronic Edition.
Chiarabba, C., et al. 2005. A new view of Italian seismicity using 20 years of instrumental recordings. Tectonophysics, 395, 3-4, 251-268.
Chorowicz, J. 2005. The East African rift system. Journal of African Earth Sciences, 43, 1-3, 379-410.
Chousianitis, K., et al. 2015. Strain and rotation rate patterns of mainland Greece from continuous GPS data and comparison between seismic and geodetic moment release. Journal of Geophysical Research, 120, 5, 3909-3931.
Christiansen, R. L., and E. H. McKee. 1977. Late Cenozoic volcanic and tectonic evolution of the Great Basin and Columbia intermontane regions. Geological Society of America Memoir, 152, 283-311.
Chung, S. L., et al. 2005. Tibetan tectonic evolution inferred from spatial and temporal variations in post-collisional magmatism. Earth-Science Reviews, 68, 3-4, 173-196.
Çiftçi, N. B., and E. Bozkurt. 2009. Evolution of the Miocene sedimentary fill of the Gediz Graben, SW Turkey. Sedimentary Geology, 216, 3-4, 49-79.
Civico, R., et al. 2018. Surface ruptures following the 30 October 2016 M-w 6.5 Norcia earthquake, central Italy. Journal of Maps, 14, 2, 151-160.
Clarke, P. J., et al. 1998. Crustal strain in central Greece from repeated GPS measurements in the interval 1989-1997. Geophysical Journal International, 135, 1, 195-214.
Cocard, M., et al. 1999. New constraints on the rapid crustal motion of the Aegean region: recent results inferred from GPS measurements (1993-1998) across the West Hellenic Arc, Greece. Earth and Planetary Science Letters, 172, 1-2, 39-47.
Cogan, M. J., et al. 1998. Shallow structure of the Yadong-Gulu rift, southern Tibet, from refraction analysis of Project INDEPTH common midpoint data. Tectonics, 17, 1, 46-61.
Coleman, M., and K. Hodges. 1995. Evidence for Tibetan Plateau uplift before 14-myr ago from a new minimum age for east-west extension. Nature, 374, 6517, 49-52.
Coney, P. J. (1978). Mesozoic–Cenozoic Cordilleran plate tectonics of. In R. B. Smith and G. P. Eaton (Ed.s.), Mesozoic–Cenozoic Cordilleran plate tectonics of Book (pp. 33-50). Geological Society of America.
Cooke, E. F. 1965. Stratigraphy of Tertiary volcanic rocks in eastern Nevada. Nevada Bureau of Mines Report, 11, pp. 61.
Corti, G. 2009. Continental rift evolution: From rift initiation to incipient break-up in the Main Ethiopian Rift, East Africa. Earth-Science Reviews, 96, 1-2, 1-53.
Cox, A., and R. B. Hart. (1986). Plate Tectonics: How It Works. Wiley-Blackwell.

Craig, T. J., et al. 2011. Earthquake distribution patterns in Africa: their relationship to variations in lithospheric and geological structure, and their rheological implications. Geophysical Journal International, 185, 1, 403-434.
D'Agostino, N. 2014. Complete seismic release of tectonic strain and earthquake recurrence in the Apennines (Italy). Geophysical Research Letters, 41, 4, 1155-1162.
D'Agostino, N., et al. 2014. Gravitational potential energy and active deformation in the Apennines. Earth and Planetary Science Letters, 397, 121-132.
d'Oreye, N., et al. 2011. Source parameters of the 2008 Bukavu-Cyangugu earthquake estimated from InSAR and teleseismic data. Geophysical Journal International, 184, 2, 934-948.
Dannowski, A., et al. 2010. Seismic structure of an oceanic core complex at the Mid-Atlantic Ridge, 22°19′N. Journal of Geophysical Research, 115, B07106.
Darby, B. J., and B. D. Ritts. 2002. Mesozoic contractional deformation in the middle of the Asian tectonic collage: the intraplate Western Ordos fold-thrust belt, China. Earth and Planetary Science Letters, 205, 1-2, Pii s0012-821x(02)01026-9, 13-24.
Davies, J. H. 2013. Global map of solid Earth surface heat flow. Geochemistry Geophysics Geosystems, 14, 10, 4608-4622.
Davis, W. M. 1903. The mountain ranges of the Great Basin. Bulletin of the Museum of Comparative Zoology, 42, 129-177.
DeAngelo, J., et al. 2022. Heat flow maps and supporting data for the Great Basin, USA. U. S. Geological Survey Data Release, https://doi.org/10.5066/P9BZPVUC, accessed 2023.
Della Vedova, B., et al. 1991. Heat flow map of Italy. International Institute for Geothermal Research, CNR-Pisa.
DeMets, C., et al. 2010. Geologically current plate motions. Geophysical Journal International, 181, 1, 1-80.
Deng, Q. D., and H. C. You. (1985). The structural activity and formation mechanism of the down-faulted basins around the Ordos block of. In (Ed.s.), The structural activity and formation mechanism of the down-faulted basins around the Ordos block of Book (pp. 55-78 (in Chinese)). Beijing: Seismological Press.
Déverchère, J., et al. 1993. Seismicity, active faults and stress field of the North Muya Region, Baikal Rift: New insights on the rheology of extended continental lithosphere. Journal of Geophysical Research: Solid Earth, 98, B11, 19895-19912.
Deverchere, J., et al. 2001. Depth distribution of earthquakes in the Baikal rift system and its implications for the rheology of the lithosphere. Geophysical Journal International, 146, 3, 714-730.
Dewey, J. F., et al. 1973. Plate tectonics and evolution of Alpine system. Geological Society of America Bulletin, 84, 10, 3137-3180.
Di Stefano, R., et al. 2011. Three-dimensional Moho topography in Italy: New constraints from receiver functions and controlled source seismology. Geochemistry Geophysics Geosystems, 12, Q09006.
Dickenson, W. R., and W. S. Snyder. 1979. Geometry of subducted slabs related to San Andreas transform. Journal of Geology, 87, 609-628.
Ding, L., et al. 2007. Postcollisional calc-alkaline lavas and xenoliths from the southern Qiangtang terrane, central Tibet. Earth and Planetary Science Letters, 254, 1-2, 28-38.
Doglioni, C. 1991. A proposal of kinematic modelling for W-dipping subductions - possible applications to the Tyrrhenian-Apennines system. Terra Nova, 3, 423-434.
Doglioni, C. 1992. Main differences between thrust belts. Terra Nova, 4, 2, 152-164.
Doglioni, C., and G. Flores. (1997). An introduction of Italian Geology. Lamisco.
Domingues, A., et al. 2016. Ambient noise tomography of the East African Rift in Mozambique. Geophysical Journal International, 204, 3, 1565-1578.
Doser, D. I. 1985. Source parameters and faulting processes of the 1959 Hebgen Lake, Montana, earthquake sequence. Journal of Geophysical Research, 90, B6, 4537-4555.
Doser, D. I. 1988. Source parameters of earthquakes in the Nevada seismic zone, 1915-1943. Journal of Geophysical Research, 93, B12, 15001-15015.
Doser, D. I. 1991. Faulting within the western Baikal rift as characterized by earthquake studies. Tectonophysics, 196, 1-2, 87-107.
Doser, D. I., and R. B. Smith. 1985. Source parameters of the 28 October 1983 Borah-Peak, Idaho, earthquake from body wave analysis. Bulletin of the Seismological Society of America, 75, 4, 1041-1051.

Dugda, M. T., et al. 2007. Thin lithosphere beneath the Ethiopian plateau revealed by a joint inversion of Rayleigh wave group velocities and receiver functions. Journal of Geophysical Research, 112, B8, Article B08305.
Dunn, R. A., et al. 2005. Three-dimensional seismic structure of the Mid-Atlantic Ridge (35°N): Evidence for focused melt supply and lower crustal dike injection. Journal of Geophysical Research, 110, B9, Article B09101.
Dusunur, D., et al. 2009. Seismological constraints on the thermal structure along the Lucky Strike segment (Mid-Atlantic Ridge) and interaction of tectonic and magmatic processes around the magma chamber. Marine Geophysical Research, 30, 2, 105-120.
Ebinger, C. J. 1989. Tectonic Development Of The Western Branch Of The East-African Rift System. Geological Society of America Bulletin, 101, 7, 885-903.
Ebinger, C. J., et al. 1999. Extensional basin geometry and the elastic lithosphere. Philosophical Transactions of the Royal Society a-Mathematical Physical and Engineering Sciences, 357, 1753, 741-762.
Ebinger, C. J., et al. 1991. Mechanical strength of extended continental lithosphere - constraints from the Western Rift System, East-Africa. Tectonics, 10, 6, 1239-1256.
Ebinger, C. J., et al. 1987. Tectonic model of the Malawi Rift, Africa. Tectonophysics, 141, 1-3, 215-235.
Elderfield, H., and A. Schultz. 1996. Mid-ocean ridge hydrothermal fluxes and the chemical composition of the ocean. Annual Review of Earth and Planetary Sciences, 24, 191-224.
Elliott, J. R., et al. 2010. Extension on the Tibetan plateau: recent normal faulting measured by InSAR and body wave seismology. Geophysical Journal International, 183, 2, 503-535.
Elter, P., et al. 1975. Tensional and compressional areas in the recent (Tortoian to present) evolution of the Northern Appennines. Boll. Geophis. Teo. Appl., 42, 3-18.
Emmerson, B., et al. 2006. Seismicity, structure and rheology of the lithosphere in the Lake Baikal region. 167, 3, 1233-1272.
Emre, Ö., et al. (2013). Active Fault Map of Turkey with an Explanatory Text. 1:1,250,000 Scale.
Erickson, A. J. 1970. The measurements and interpretation of heat flow in the Mediterranean and Black Seas. Ph.D. Thesis, Mass. Inst. Technology, p. 272.
Erkan, K. 2015. Geothermal investigations in western Anatolia using equilibrium temperatures from shallow boreholes. Solid Earth, 6, 1, 103-113.
Ersoy, E. Y., and M. R. Palmer. 2013. Eocene-Quaternary magmatic activity in the Aegean: Implications for mantle metasomatism and magma genesis in an evolving orogeny. Lithos, 180, 5-24.
Ewing, J., and M. Ewing. 1962. Reflection profiling in and around the Puerto Rico Trench. Journal of Geophysical Research 67, 12, 4729-4739.
Ewing, M., et al. 1964. Sediment distribution in the oceans: the Mid-Atlantic Ridge. Bulletin of the Geological Society of America, 75, 17-36.
Ewing, M., and B. C. Heezen. 1956. Oceanographic research programs of the Lamont Geological Observatory. Geographical Review, 46, 4, 508-535.
Ewing, M., et al. 1966. Crustal structure of mid-ocean ridges .4. Sediment distribution in south Atlantic ocean and Cenozoic history of Mid-Atlantic Ridge. Journal of Geophysical Research, 71, 6, 1611-+.
Eyidogan, H., and J. Jackson. 1985. A seismological study of normal faulting in the Demirci, Alasehir and Gediz earthquakes of 1969-70 in western Turkey - implications for the nature and geometry of deformation in the continental-crust. Geophysical Journal of the Royal Astronomical Society, 81, 3, 569-607.
Felt, H. (2012). Soundings, The Story of the Remarkable Woman Who Mapped the Ocean Floor. Henry Holt and Co., 352 p.
Fenneman, N. M. 1928. Physiographic Divisions of the United States. Annals of the Association of American Geographers, 18, 4, 261-353.
Fisher, R. L., and R. W. Raitt. 1962. Topography and structure of the Peru-Chile trench. Deep-sea research, 9, 423-443.
Fleischer, R. L., et al. 1968. Mid-Atlantic Ridge - Age And Spreading Rates. Science, 161, 3848, 1339-1342.
Florensov, N. A. (1960). The Baikal Rift Zone (in Russian). Moscow: Nauka.
Florensov, N. A. 1965b. The Baikal Rift Zone. Journal, Rept.,Issue,173-180.
Florensov, N. A. 1969. Rifts of Baikal mountain region. Tectonophysics, 8, 4-6, 443-456.

Forsyth, D. W. 1982. Determinations of focal depths of earthquakes associated with the bending of oceanic plates at trenches. Physics Of The Earth And Planetary Interiors, 28, 2, 141-160.
Foster, A. N., and J. A. Jackson. 1998. Source parameters of large African earthquakes: implications for crustal rheology and regional kinematics. Geophysical Journal International, 134, 2, 422-448.
Fowler, C. M. R. 1976. Crustal structure of Mid-Atlantic Ridge crest at 37° N. Geophysical Journal of the Royal Astronomical Society, 47, 3, 459-491.
Fowler, C. M. R. 1978. Mid-Atlantic Ridge - structure at 45° N. Geophysical Journal of the Royal Astronomical Society, 54, 1, 167-183.
Fowler, C. M. R., and C. E. Keen. 1979. Oceanic crustal structure - Mid-Atlantic Ridge at 45° N. Geophysical Journal of the Royal Astronomical Society, 56, 1, 219-226.
Francheteau, J., et al. 1984. HIgh heat-flow in southern Tibet. Nature, 307, 5946, 32-36.
Fujie, G., et al. 2016. Along-trench variations in the seismic structure of the incoming Pacific plate at the outer rise of the northern Japan Trench. Geophysical Research Letters, 43, 2, 666-673.
Fytikas, M., et al. (1984). Tertiary to Quaternary evolution of volcanism in the Aegean region of. In E. J. Dixon and A. H. F. Robertson (Ed.s.), Tertiary to Quaternary evolution of volcanism in the Aegean region of Book (pp. 687-699). Geol. Soc. .
Fytikas, M. D., and N. P. Kolios. 1979. Preliminary Heat Flow Map of Greece. Journal,Issue,197-205.
Gabrielse, H., et al. 1983. Sonoma Orogeny and Permian To Triassic tectonism in western North-America. Geology, 11, 8, 484-486.
Galli, P., and F. Galadini. 1999. Seismotectonic framework of the 1997-1998 Umbria-Marche (central Italy) earthquakes. Seismological Research Letters, 70, 417-427.
Ganas, A., et al. 2021. Co-seismic and post-seismic deformation, field observations and fault model of the 30 October 2020 Mw 7.0 Samos earthquake, Aegean Sea. Acta Geophysica, 69, 3, 999-1024.
Gansser, A. (1964). The Geology of the Himalayas. New York: Interscience.
Gao, P., et al. 2018. Present-day geothermal characteristics of the Ordos Basin, western North China Craton: new findings from deep borehole steady-state temperature measurements. Geophysical Journal International, 214, 254-264.
Gao, R., et al. 2013. New constraints on crustal structure and Moho topography in Central Tibet revealed by SinoProbe deep seismic reflection profiling. Tectonophysics, 606, 160-170.
Gao, S., et al. 1994. Asymmetric upwarp of the asthenosphere beneath the Baikal Rift-Zone, Siberia. Journal of Geophysical Research-Solid Earth, 99, B8, 15319-15330.
Gao, S. S., et al. 2004. Significant crustal thinning beneath the Baikal rift zone: New constraints from receiver function analysis. Geophysical Research Letters, 31, 20, L20610 (4 pp.).
Garside, L. J., et al. (2005). The upper reaches of the Sierra Nevada auriferous gold channels, California and Nevada of. In H. N. Rhoden, R. C. Steininger and P. G. Vikre (Ed.s.), The upper reaches of the Sierra Nevada auriferous gold channels, California and Nevada of Book (pp. 1-27). Reno, Nevada: Geological Society of Nevada.
Gasparini, C., et al. 1985. Fault-plane solutions and seismicity of the Italian peninsula. Tectonophysics, 117, 1-2, 59-78.
Gaulon, R., et al. 1992. Regional geodynamic implications of the may july 1990 earthquake sequence in southern Sudan. Tectonophysics, 209, 1-4, 87-103.
GEBCO. 2024. Gridded Bathymetry Data: General Bathymetric Chart of the Oceans (GEBCO). https://www.gebco.net/data-products/gridded-bathymetry-data (accessed 2024), (doi:10.5285/f98b053b-0cbc-6c23-e053-6c86abc0af7b).
GEBCO. 2024 General Bathymetric Chart of the Oceans,. https://www.gebco.net/data_and_products/gridded_bathymetry_data/gebco_2019/grid_terms_of_use.html (accessed 2024).
Giardini, D., and L. Beranzoli. 1992. Wave-form modeling of the May 20, 1990 Sudan earthquake. Tectonophysics, 209, 1-4, 105-114.
Gilbert, G. K. (1874). Preliminary geological report (Appendix D: Preliminary geological report by G. K. Gilber, Chief geological Assistant, expedition of 1872 submitted in 1873) of. In (Ed.s.), Preliminary geological report (Appendix D: Preliminary geological report by G. K. Gilber, Chief geological Assistant, expedition of 1872 submitted in 1873) of Book (pp. 48-52). Washington: Government Printing Office.

Gilbert, G. K. 1875. Report upon the geology of portions of Nevada, Utah, California, and Arizona examined in the years 1871-1872. in Part 1 Section I of Vol. III of Report upon geographical and geological exploration and surveys west of the one hundredth meridian., 21-42.
Gilbert, H. J., and A. F. Sheehan. 2004. Images of crustal variations in the intermountain west. Journal of Geophysical Research-Solid Earth, 109, B3, Article B03306, 15.
Global_Volcanism_Program. 2023. (Database) Volcanoes of the world dstributed by Smithsonian Institution and compiled by Venzke, E. https://doi.org/10.5479/si.GVP.VOTW5-2023.5.1, accessed 2024.
Goldsworthy, M., et al. 2002. The continuity of active fault systems in Greece. Geophysical Journal International, 148, 3, 596-618.
Golenetsky, S. I., and L. A. Misharina. 1978. Seismicity and earthquake focal mechanisms in the Baikal rift zone. 45, 1, 71-85.
Golonetski, S. I. 1990. Problems of seismicity of the Baikal rift zone. J. Geodyn., 11, 296-307.
Gori, S., et al. 2018. Surface Faulting Caused by the 2016 Central Italy Seismic Sequence: Field Mapping and LiDAR/UAV Imaging. Earthquake Spectra, 34, 4, 1585-1610.
Gregory, J. W. (1896). The Great Rift Valley. London: John Murray.
Gromme, C. S., et al. 1972. Paleomagnetic correlations and potassium-argon dating of middle tertiary ash-flow sheets in eastern Great Basin, Nevada and Utah. Geological Society of America Bulletin, 83, 6, 1619-&.
Gürboga, S. 2013. 28 March 1970 Gediz earthquake fault, western Turkey: palaeoseismology and tectonic significance. International Geology Review, 55, 10, 1191-1201.
Hall, R. 2002. Cenozoic geological and plate tectonic evolution of SE Asia and the SW Pacific: computer-based reconstructions, model and animations. Journal of Asian Earth Sciences, 20, 4, Pii s1367-9120(01)00069-4, 353-431.
Hamilton, W., and W. B. Meyers. 1966. Cenozoic tectonics of the western United States. Reviews of Geophysics, 4, 4, 509-549.
Harrison, T. M., et al. 1995. Activation of the Nyainqentanghla shear zone - implications for uplift of the southern Tibetan Plateau. Tectonics, 14, 3, 658-676.
Hasterok, D., et al. 2011. Oceanic heat flow; implications for global heat loss. Earth and planetary science letters, 311, 3-4, 386-395.
He, Y., et al. 2022. The 2021 Mw6.7 Lake Hovsgol (Mongolia) Earthquake: Irregular Normal Faulting with Slip Partitioning Controlled by an Adjacent Strike-Slip Fault. Journal, 14,Issue, 10.3390/rs14184553.
Heezen, B. C. 1960. The Rift in the Ocean Floor. Scientific American, 203, 98-110.
Heezen, B. C., et al. 1959. The floors of the oceans 1,. Geological Society of America Special Paper, 65, 122 pp.
Heim, A. (1922). Geologie de Schweiz II(2): Die Schweizer Alper II of. In (Ed.s.), Geologie de Schweiz II(2): Die Schweizer Alper II of Book (pp. 477-1118). Leipzig: Tauchnitz.
Hekinian, R., et al. 1976. Volcanic rocks and processes of the Mid-Atlantic Ridge rift valley near 36 ° 49′ N. Contributions to Mineralogy and Petrology, 58, 1, 83-110.
Henry, C. D., et al. 2012. Eocene-Early Miocene paleotopography of the Sierra Nevada-Great Basin-Nevadaplano based on widespread ash-flow tuffs and paleovalleys. Geosphere, 8, 1, 1-27.
Henry, C. D., and D. A. John. 2013. Magmatism, ash-flow tuffs, and calderas of the ignimbrite flareup in the western Nevada volcanic field, Great Basin, USA. Geosphere, 9, 4, 951-1008.
Herzen, R., and G. Simmons. 1972. 2 heat-flow profiles across Atlantic Ocean. Earth And Planetary Science Letters, 15, 1, 19-&.
Hodgson, I., et al. 2017. Crustal Structure at a young continental rift: a receiver function study from the Tanganyika Rift. Tectonics, 36, 12, 2806-2822.
Hollenstein, C., et al. 2008. Crustal motion and deformation in Greece from a decade of GPS measurements, 1993-2003. Tectonophysics, 449, 1-4, 17-40.
Hsü, K. J., et al. 1975. Glomar challenger returns to the Mediterranean Sea. Geotimes, 20, 8, 16-19.
Huang, P. Y., and S. C. Solomon. 1988. Centroid depths of mid-ocean ridge earthquakes - dependence on spreading rate. Journal Of Geophysical Research, 93, B11, 13445-13477.
Huang, P. Y., et al. 1986. Focal depths and mechanisms of Mid-Atlantic Ridge earthquakes from body wave-form inversion. Journal of Geophysical Research, 91, B1, 579-598.

Hunstad, I., and P. England. 1999. An upper bound on the rate of strain in the Central Apennines, Italy, from triangulation measurements between 1869 and 1963. Earth and Planetary Science Letters, 169, 3-4, 261-267.
Hunstad, I., et al. 2003. Geodetic strain in peninsular Italy between 1875 and 2001. Geophysical Research Letters, 30, 4, 1181.
Hutchinson, D. R., et al. 1992. Depositional and tectonic framework of the rift basins of Lake Baikal from multichannel seismic data. Geology, 20, 7, 589-592.
Hyndman, R. D., et al. 1976. Heat-flow measurements in deep crustal holes on Mid-Atlantic Ridge. Journal Of Geophysical Research, 81, 23, 4053-4060.
Hyndman, R. D., and D. S. Rankin. 1972. Mid-Atlantic Ridge near 45° N. XVIII. heat-flow measurements. Canadian Journal of Earth Sciences, 9, 6, 664-+.
Ichinose, G. A., et al. 2003. Source parameters of eastern California and western Nevada earthquakes from regional moment tensor inversion. Bulletin of the Seismological Society of America, 93, 1, 61-84.
IHFC-DataViewer. 2023. https://ihfc-iugg.org/products/global-heat-flow-database/mapping-visualisation.
Ivanov, A. V. 2004. One rift, two models. Science First Hand, 2, N1, 50-62. (https://scfh.ru/en/papers/one-rift-two-models/) accessed 12-19-2020.
Ivanov, A. V., and E. I. Demonterova. (2009). Tectonics of the Baikal Rift deduced from volcanism and sedimentation: a review oriented to the Baikal and Hovsgol lake systems of. In E. G. Muller and M. A. Grachev (Ed.s.), Tectonics of the Baikal Rift deduced from volcanism and sedimentation: a review oriented to the Baikal and Hovsgol lake systems of Book (pp. 27-54). Berlin, Heidelberg: Springer Berlin Heidelberg.
Ivanov, A. V., et al. 2015. Volcanism in the Baikal rift: 40 years of active-versus-passive model discussion. Earth-Science Reviews, 148, 18-43.
Jachens, R. C., and B. C. Moring. 1990. Maps of the thickness of Cenozoic deposits and the isostatic residual gravity over basement for Nevada. Journal,Issue, 10.3133/ofr90404.
Jackson, J. 1994. Active tectonics of the Aegean region. Annual Review of Earth and Planetary Sciences, 22, 239-271.
Jackson, J., and T. Blenkinsop. 1997. The Bilila-Mtakataka fault in Malawi: An active, 100-km long, normal fault segment in thick seismogenic crust. Tectonics, 16, 1, 137-150.
Jackson, J. A., et al. 1982a. Seismicity, normal faulting, and the geomorphological development of the Gulf of Corinth (Greece) - the corinth earthquakes of February and March 1981. Earth and Planetary Science Letters, 57, 2, 377-397.
Jackson, J. A., et al. 1982b. The Corinth (Greece) earthquakes of February and March 1981. Geophysical Journal of the Royal Astronomical Society, 69, 1, 284-284.
Johnson, J. S. 2005. Volcanism in the Vitim Volcanic Field, Siberia: Geochemical evidence for a mantle plume beneath the Baikal Rift Zone. Journal of Petrology, 46, 7, 1309-1344.
Jolivet, L., et al. 2013. Aegean tectonics: Strain localisation, slab tearing and trench retreat. Tectonophysics, 597, 1-33.
Jones, C. H., et al. 1996. The role of gravitational potential energy in active deformation in the southwestern United States. Nature, 381, 6577, 37-41.
Jones, C. H., et al. 1992. Variations across and along a major continental rift - an interdisciplinary study of the Basin and Range Province, Western USA. Tectonophysics, 213, 1-2, 57-96.
Jones, G. M., et al. 1978. Fault patterns in outer trench walls and their tectonic significance. Journal of Physics of the Earth, 26, Supplement, S85-S101.
Jongsma, D. 1974. Heat-flow in the Aegean Sea. Geophysical Journal of the Royal Astronomical Society, 37, 3, 337-346.
Kahle, H. G., et al. 2000. GPS-derived strain rate field within the boundary zones of the Eurasian, African, and Arabian Plates. Journal of Geophysical Research-Solid Earth, 105, B10, 23353-23370.
Kahle, H. G., et al. 1999. The GPS strain rate field in the Aegean Sea and western Anatolia. Geophysical Research Letters, 26, 16, 2513-2516.
Kanamori. 1971. Seismological evidence for a lithospheric normal faulting - the Sanriku Earthquake of 1933. Phy. Earth Planet. Interiors, 4, 289-300.

Kawada, Y., et al. 2014. Hydrothermal heat mining in an incoming oceanic plate due to aquifer thickening: Explaining the high heat flow anomaly observed around the Japan Trench. Geochemistry, Geophysics, Geosystems, 15, 4, 1580-1599.
Keen, C., and C. Tramontini. 1970. A seismic refraction survey on the Mid-Atlantic Ridge. Geophysical Journal International, 20, 5, 473-491.
Keller, J. V. A., et al. 1994. Anatomy of late orogenic extension - the northern Apennines case. Tectonophysics, 238, 1-4, 275-294.
Kent, G. M., et al. 2025. Melt focusing along lithosphere-asthenosphere boundary below Axial volcano. Nature, 641, 8062.
Kent, P. 1978. Historical background: Early exploration in the East African rift - The Gregroy Rift Valley. Geological Society, London Special Publications, Volume 6, 1-4.
Khil'ko, S. D. (1966). Seismogenic structures of the Kodar system of activated faults (in Russian) of. In (Ed.s.), Seismogenic structures of the Kodar system of activated faults (in Russian) of Book (pp. 171-186). Moscow: Nauka.
Khutorskoi, M. D., and E. A. Teveleva. 2020. Nature of Heat Flow Asymmetry on the Mid-Oceanic Ridges of the World Ocean. Oceanology, 60, 1, 108-119.
King, C. (1870 - 1878). Report of the Geological Exploration of the Fortieth Parallel; Professional Papers of the Engineer Department, U. S. Army; no. 18. Washington: Government Printing Office.
King, C. (1878). Systematic Geology: United States Geological Exploration of the Fortieth Parallel, Clarence King, Geologist in Charge. Washington: Government Printing Office, pp. 796.
Kiselev, A. I. 1987. Volcanism of the Baikal rift zone. 143, 1-3, 235-244.
Klemperer, S. L., et al. 1986. The Moho in the Northern Basin and Range Province, Nevada, along the COCORP 40-degree-n seismic-reflection transect. Geological society of america bulletin, 97, 5, 603-618.
Klootwijk, C. T., et al. 1985. The Himalayan arc - large-scale continental subduction, oroclinal bending and back-arc spreading. Earth and Planetary Science Letters, 75, 2-3, 167-183.
Kreemer, C., et al. 2012. A geodetic strain rate model for the Pacific-North American plate boundary, western United States. Journal, Plate: 48 x 46 inches,Issue.
Krivonogov, S. K., and I. Y. Safonova. 2017. Basin structures and sediment accumulation in the Baikal Rift Zone: Implications for Cenozoic intracontinental processes in the Central Asian Orogenic Belt. Gondwana Res., 47, 267-290.
Kurushin, R. A., et al. (1966). Main neotectonic structures and activated faults (in Russian), of. In (Ed.s.), Main neotectonic structures and activated faults (in Russian), of Book (pp. 71-102). Moscow: Nauka.
Lachenbruch, A. H., and J. H. Sass. (1978). Models of an extending lithosphere and heat flow in the Basin and Range province of. In (Ed.s.), Models of an extending lithosphere and heat flow in the Basin and Range province of Book (pp. 209-250). Boulder Colorado: Geological Society of America.
Lavayssiere, A., et al. 2019. Depth Extent and Kinematics of Faulting in the Southern Tanganyika Rift, Africa. Tectonics, 38, 3, 842-862.
Lavecchia, G., et al. 2024. Slowly deforming megathrusts within the continental lithosphere: a case from Italy. GSA Today, 34, 1, 4-10.
Le Pichon, X., and J. Angelier. 1979. The Hellenic arc and trench system: a key to the neotectonic evolution of the eastern Mediterranean sea. Tectonophysics, 60, 1-42.
Le Pichon, X., and C. Kreemer. (2010). The Miocene-to-Present Kinematic Evolution of the Eastern Mediterranean and Middle East and Its Implications for Dynamics of. In R. Jeanloz and K. H. Freeman (Ed.s.), The Miocene-to-Present Kinematic Evolution of the Eastern Mediterranean and Middle East and Its Implications for Dynamics of Book (pp. 323-351).
Leclerc, F., et al. 2024. Large seafloor rupture caused by the 1956 Amorgos tsunamigenic earthquake, Greece. Communications Earth & Environment, 5, 1, 663.
Lee, W. H. K., et al. 1976. Catalog of historical earthquakes in China compiled from recent Chinese publications. Bulletin of the Seismological Society of America, 66, 6, 2003-2016.
Lindenfeld, M., et al. 2012. Seismicity from February 2006 to September 2007 at the Rwenzori Mountains, East African Rift: earthquake distribution, magnitudes and source mechanisms. Solid Earth, 3, 2, 251-264.
Liu, G., et al. 2021. Rupture Kinematics of the 11 January 2021 Mw 6.7 Hovsgol, Mongolia, Earthquake and Implications in the Western Baikal Rift Zone. Seismological Research Letters, 92, 6, 3318-3326.

Liu, X., et al. 2017. Age of the subducting Pacific slab beneath East Asia and its geodynamic implications. Earth and Planetary Science Letters, 464, 166-174.
Logatchev, N. A. (1974). Sayan-Baikal-Stanavoy upland (in Russian) of. In (Ed.s.), Sayan-Baikal-Stanavoy upland (in Russian) of Book (pp. 16-162). Moscow: Nauka.
Logatchev, N. A. 1984. The Baikal Rift System. Episodes, 7, 1, 38-43.
Logatchev, N. A., and N. A. Florensov. 1978. Baikal system of rift valleys. Tectonophysics, 45, 1, 1-13.
Logatchev, N. A., and Y. A. Zorin. 1987. Evidence and causes of the 2-stage development of the Baikal rift. Tectonophysics, 143, 1-3, 225-234.
Logatchev, N. A., and Y. A. Zorin. 1992. Baikal rift zone: structure and geodynamics. Tectonophysics, 208, 1-3, 273-286.
Logatchev, N. A., et al. 1983. Baikal Rift - active or passive - comparison of the Baikal and Kenya rift zones. Tectonophysics, 94, 1-4, 223-240.
Louderback, G. D. 1904. Basin range structure of the Humboldt region. Geological Society of America Bulletin, 15, 1, 289-346.
Lubimova, E. A. 1969. Heat-flow patterns in the Baikla and other rift zones. Tectonophysics, 8, 457-467.
Lubimova, E. A., and V. A. Shelyagin. 1966. Heat flow through the floor of the Baikal (in Russian). Dokl. Akad. Nauk SSSR,, 171, 1321-1325.
Lucazeau, F. 2019. Analysis and Mapping of an Updated Terrestrial Heat Flow Data Set. Geochemistry Geophysics Geosystems, 20, 8, 4001-4024.
Lucazeau, F., et al. 2006. Heat flow variations on a slowly accreting ridge:: Constraints on the hydrothermal and conductive cooling for the Lucky Strike segment (Mid-Atlantic Ridge, 37°N). Geochemistry Geophysics Geosystems, 7, Article Q07011.
Ludwig, W. J., et al. 1966. Sediments and structure of Japan Trench. Journal Of Geophysical Research, 71, 8, 2121-&.
Lynnes, C. S., and T. Lay. 1988. Source process of the great 1977 Sumba earthquake. Journal of Geophysical Research, 93, B11, 13407-13420.
Lysak, S. V. 1978. The Baikal rift heat flow. 45, 1, 87-93.
Lysak, S. V. 1984. Terrestrial heat-flow in the south of East Siberia. Tectonophysics, 103, 1-4, 205-215.
Lysak, S. V., et al. 1975a. Heat flow of the Baikal rift zone (in Russan). Rifting Problems, Irkutsk, 70-71 (in Russian).
Lysak, S. V., and S. I. Sherman. 2002. Terrestrial heat flow in areas of dynamic influence of faults in the Baikal rift zone. EGU Stephan Mueller Special Publication Series, 2, 153-160.
Ma, X. Y., and D. N. Wu. 1987. Cenozoic extensional tectonics in China. Tectonophysics, 133, 3-4, 243-255.
Macdonald, K. C. 1998. Exploring the global Mid-Ocean Ridge. Oceanus, 41, 1, 2-8.
Macdonald, K. C., and T. M. Atwater. 1978. Evolution of rifted ocean ridges. Earth and Planetary Science Letters, 39, 3, 319-327.
Macgregor, D. 2015. History of the development of the East African Rift System: A series of interpreted maps through time. Journal of African Earth Sciences, 101, 232-252.
MacLeod, C. J., et al. 2002. Direct geological evidence for oceanic detachment faulting:: The Mid-Atlantic Ridge, 15°45′N. Geology, 30, 10, 879-882.
Maheo, G., et al. 2007. Post 4 Ma initiation of normal faulting in southern Tibet. Constraints from the Kung Co half graben. Earth and Planetary Science Letters, 256, 1-2, 233-243.
Makris, J. 1977. Geophysical investigations of the Hellenides. Hamburger Geophysikalische Einzelschriften, 34, 124 pp.
Makris, J., and R. Vees. 1977. Crustal structure of central Aegean sea and islands of Evia and Crete, Greece, obtained by refractional seismic experiments. Journal Of Geophysics-Zeitschrift Fur Geophysik, 42, 4, 329-341.
Malinverno, A., and W. B. F. Ryan. 1986. Extension in the Tyrrhenian sea and shortening in the Apennines as result of arc migration driven by sinking of the lithosphere. Tectonics, 5, 2, 227-245.
Martini, I. P., and M. Sagri. 1993. Tectonosedimentary characteristics of late Miocene-Quaternary extensional basins of the northern Apennines, Italy. Earth-Science Reviews, 34, 3, 197-233.
Masson, D. G. 1991. Fault patterns at outer trench walls. Marine Geophysical Researches, 13, 3, 209-225.
Mats, V. 1993. The structure and development of the Baikal rift depression. Earth-Science Reviews, 34, 2, 81-118.

Mazilov, V. N., et al. 1993. Oligocene deposits of the Tunka basin. Geology and Geophysics, 8, 81-87 (in Russian).
McCaffrey, R., and J. Nabelek. 1998. Role of oblique convergence in the active deformation of the Himalayas and southern Tibet plateau. Geology, 26, 8, 691-694.
McClusky, S., et al. 2000. Global Positioning System constraints on plate kinematics and dynamics in the eastern Mediterranean and Caucasus. Journal of Geophysical Research, 105, B3, 5695-5719.
McConnell, R. B. 1967. The East African rift system. Nature, 215, 578-581.
McConnell, R. B. 1972. Geological development of the rift system of Eastern Africa. Geological Society American bulletin, 83, q, 2549-2572.
McKee, E. H. 1971. Tertiary igneous chronology of Great Basin of western United-States - implications for tectonic models. Geological Society of America Bulletin, 82, 12, 3497-&.
McKee, E. H., and D. C. Noble. 1986. Tectonic and magmatic development of the Great Basin of the western United States during late Cenozoic time. Modern Geology, 10, 39-49.
McKee, E. H., and M. I. Silberman. 1970. Geochronology of Tertiary igneous rocks in central Nevada. Geological Society of America Bulletin, 81, 8, 2317-&.
McKenzie, D. 1972. Active tectonics of Mediterranean region. Geophysical Journal of the Royal Astronomical Society, 30, 2, 109-185.
McKenzie, D. 1978. Active tectonics of Alpine-Himalayan Belt - Aegean sea and surrounding regions. Geophysical Journal of the Royal Astronomical Society, 55, 1, 217-+.
McKenzie, D. P. 1970. Plate Tectonics of Mediterranean region. Nature, 226, 5242, 239-&.
Meade, B. J., et al. 2002. Estimates of seismic potential in the Marmara Sea region from block models of secular deformation constrained by global positioning system measurements. Bulletin of the Seismological Society of America, 92, 1, 208-215.
Mel'Nikova, V. I., et al. 2012. The 2008 Kultuk earthquake with M w = 6.3 in the south of Baikal: Spatial-temporal analysis of seismic activation. 48, 7-8, 594-614.
Mercier, J. L., et al. 1987. Change from late tertiary compression to quaternary extension in southern Tibet during the India-Asia collision. Tectonics, 6, 3, 275-304.
Michetti, A. M., et al. 1996. Trench investigations of the 1915 Fucino earthquake fault scarps (Abruzzo, central Italy): Geological evidence of large historical events. Journal of Geophysical Research-Solid Earth, 101, B3, 5921-5936.
Middleton, T. A., et al. 2017. Extension rates across the northern Shanxi Grabens, China, from Quaternary geology, seismicity and geodesy. Geophysical Journal International, 209, 2, 535-558.
Middleton, T. A., et al. 2016. A major, intraplate, normal-faulting earthquake: The 1739 Yinchuan event in northern China: 1739 Yinchuan Earthquake, northern China. Journal of Geophysical Research, 121, 1, 293-320.
Misharina, L. A. 1963. The investigatons of mechanism of hypocentres of aftershocks of middle Baikal earthquake, Aug 29. Bull. Seismol. Comm., 5, 81-94 (in Russian?).
Misharina, L. A. (1967). Stresses in the earth's crust in rift zones Moscow: Nauka (in Russian).
Mohamed, A., and M. Al Deep. 2021. Depth to the bottom of the magnetic layer, crustal thickness, and heat flow in Africa: Inferences from gravity and magnetic data. Journal of African Earth Sciences, 179, 104204.
Mohapatra, G. K., and R. A. Johnson. 1998. Localization of listric faults at thrust fault ramps beneath the Great Salt Lake Basin, Utah: Evidence from seismic imaging and finite element modeling. Journal of Geophysical Research-Solid Earth, 103, B5, 10047-10063.
Molnar, P. 1988. A review of geophysical constraints on the deep-structure of the Tibetan Plateau, the Himalaya and the Karakoram, and their tectonic implications. Philosophical Transactions of the Royal Society a-Mathematical Physical and Engineering Sciences, 326, 1589, 33-88.
Molnar, P., and W. P. Chen. 1983. Focal depths and fault plane solutions of earthquakes under the Tibetan Plateau. Journal of Geophysical Research, 88, NB2, 1180-1196.
Molnar, P., et al. 1973. Fault plane solutions of shallow earthquakes and contemporary tectonics in Asia. Earth and Planetary Science Letters, 19, 2, 101-112.
Molnar, P., and H. Lyon-Caen. 1989. Fault plane solutions of earthquakes and active tectonics of the Tibetan Plateau and its margins. Geophysical Journal International, 99, 1, 123-153.

Molnar, P., and P. Tapponnier. 1975. Cenozoic tectonics of Asia - effects of a continental collision. Science, 189, 4201, 419-426.
Molnar, P., and P. Tapponnier. 1977. The collision between India and Eurasia. Scientific American, 236, 4, 30-41.
Molnar, P., and P. Tapponnier. 1978. Active tectonics of Tibet. Journal of Geophysical Research, A, Space Physics, 83, B11, 5361-5375.
Mongelli, F., et al. 1989. Interpretation of heat-flow density of the Apennine chain,Italy. Tectonophysics, 164, 2-4, 267-280.
Morley, C. K., et al. 1992. Tectonic Evolution Of The Northern Kenyan Rift. Journal of the Geological Society, 149, 333-348.
Müller, R. D., et al. 2008. Age, spreading rates, and spreading asymmetry of the world's ocean crust. Geochemistry Geophysics Geosystems, 9, Q04006.
Nábelek, J., et al. 2009. Underplating in the Himalaya-Tibet Collision Zone Revealed by the Hi-CLIMB Experiment. Science, 325, 5946, 1371-1374.
Nakamura, Y., et al. 2023. Incoming plate structure at the Japan Trench subduction zone revealed in densely spaced reflection seismic profiles. Progress in earth and planetary science, 10, 1, 45.
Nason, R. D., and W. H. K. Lee. 1962. Preliminary Heat-Flow Profile across the Atlantic. Nature, 196, 4858, 975-975.
Navin, D. A., et al. 1998. The RAMESSES experiment - II. Evidence for accumulated melt beneath slow spreading ridge from wide-angle refraction and multichannel reflection seismic profiles. Geophysical Journal International, 135, 3, 746-772.
Ni, J., and J. E. York. 1978. Late Cenozoic tectonics of Tibetan Plateau. Journal of Geophysical Research, 83, NB11, 5377-5384.
Nielsen, C., and H. Thybo. 2009a. Lower crustal intrusions beneath the southern Baikal Rift Zone: Evidence from full-waveform modelling of wide-angle seismic data. 470, 3-4, 298-318.
Nielsen, C., and H. Thybo. 2009b. No Moho uplift below the Baikal Rift Zone: Evidence from a seismic refraction profile across southern Lake Baikal. Journal of Geophysical Research-Solid Earth, 114, B08306, 22.
Nikolayev, V. G., et al. 1985. The sedimentary section beneath Lake Baikal. International Geology Review, 27, 449-459.
NOAFAULTS. 2024. NOAFAULTS KMZ layer version 60 (National Observatory of Athens). https://zenodo.org/records/13168947, accessed October 2024.
Nocquet, J.-M. 2012. Present-day kinematics of the Mediterranean: A comprehensive overview of GPS results. Tectonophysics, 579, 220-242.
Nolan, T. B. 1943. The Basin and Range Province in Utah, Nevada, and California. Professional Paper, 197-D, 141-196.
Nyblade, A. A. 1997. Heat flow across the East African Plateau. Geophysical Research Letters, 24, 16, 2083-2086.
Nyst, M., and W. Thatcher. 2004. New constraints on the active tectonic deformation of the Aegean. Journal of Geophysical Research-Solid Earth, 109, B11, B11406.
Obana, K., et al. 2012. Normal-faulting earthquakes beneath the outer slope of the Japan Trench after the 2011 Tohoku earthquake: Implications for the stress regime in the incoming Pacific plate. Geophysical Research Letters, 39, L00g24.
Obana, K., et al. 2019. Seismic velocity structure and its implications for oceanic mantle hydration in the trench-outer rise of the Japan Trench. Geophysical Journal International, 217, 3, 1629-1642.
Obana, K., et al. 2021. Seismicity around the trench axis and outer-rise region of the southern Japan Trench, south of the main rupture area of the 2011 Tohoku-oki earthquake. Geophysical Journal International, 226, 1, 131-145.
Obrutchev, V. A. 1938. Geology of Siberia. USSR Acad. Sci. Moscow/Lenigrad, 3, 1357 pp. (in Russian).
Oddone, E. 1915. Gli elementi fisici del grande terremoto marsicano fucense del 13 gennaio 1915. Boll. Soc. Sism. It., 19, 71-216.
Okal, E. A., et al. 2016. The Showa Sanriku earthquake of 1933 March 2: a global seismological reassessment. Geophysical Journal International, 206, 3, 1492-1514.

Okal, E. A., et al. 2009. The 1956 earthquake and tsunami in Amorgos, Greece. Geophysical Journal International, 178, 3, 1533-1554.

Oreskes, N. (2003). Plate Tectonics: An Insider's History of the Modern Theory of the Earth. CRC Press, 448 pp.

Ovsyuchenko, A. N., et al. 2024. The Khubsugul Earthquake of January 12, 2021, <i>M</i>w = 6.7, Northern Mongolia: Geological Effects and Tectonic Position of the Source (vol 511, pg 566, 2023). Doklady Earth Sciences, 514, 1, 195-195.

Ozdemir, S., and M. O. Karslioglu. 2019. Soft clustering of GPS velocities from a homogeneous permanent network in Turkey. Journal of Geodesy, 93, 8, 1171-1195.

Pakiser, L. C. 1963. Structure of the crust and upper mantle in the western United States. Journal of Geophysical Research, 68, 20, 5747-5756.

Pan, S., and F. Niu. 2011. Large contrasts in crustal structure and composition between the Ordos plateau and the NE Tibetan plateau from receiver function analysis. Earth and Planetary Science Letters, 303, 3-4, 291-298.

Pan, Y., and W. S. F. Kidd. 1992. Nyainqentanglha Shear Zone - a late Miocene extensional detachment in the southern Tibetan Plateau. Geology, 20, 9, 775-778.

Pancha, A., et al. 2006. Comparison of seismic and geodetic scalar moment rates across the Basin and Range province. Bulletin of the Seismological Society of America, 96, 1, 11-32.

Pantosti, D., and G. Valensise. 1993. Source geometry and long-term behavior of the 1980, Irpinia earthquake fault based on field geologic observations. Annali Di Geofisica, XXXVI, 1, 41-49.

Papadakis, G., et al. 2016. Non-extensive statistical physics applied to heat flow and the earthquake frequency-magnitude distribution in Greece. Physica A-statistical mechanics and its applications, 456, 135-144.

Papoulia, J., and J. Makris. 2010. Tectonic processes and crustal evolution on/offshore Western Peloponnese derived from active and passive seismics. Bulletin of the Geological Society of Greece, 43, 1, 357-367.

Pavlovsky, E. V. 1948. A comparison of the tectonics of Meso-Cenozoic structures of East Siberia and the East African rift (in russian). Proc. Acad. Sci USSR, Ser. Geol, no. 5, 25-38.

Peltzer, G., et al. 1985. Neogene and Quaternary faulting in and along the Qinling Shan. Nature (London), 317, 6037, 500-505.

Petit, C., et al. 1997. On the structure and mechanical behaviour of the extending lithosphere in the Baikal Rift from gravity modelling. 149, 1-4, 29-42.

Petit, C., and J. Deverchere. 1995. Velocity structure of the Northern Baikal Rift, Siberia, from local and regional earthquake travel-times. Geophysical Research Letters, 22, 13, 1677-1680.

Petit, C., and J. Déverchère. 2006. Structure and evolution of the Baikal rift: A synthesis. Geochemistry, Geophysics, Geosystems, 7, 11, n/a-n/a.

Petit, C., et al. 1996. Present-day stress field changes along the Baikal rift and tectonic implications. Tectonics, 15, 6, 1171-1191.

Pfister, M., et al. 1998. Geothermal reconnaissance of the Marmara Sea region (NW Turkey): surface heat flow density in an area of active continental extension. Tectonophysics, 291, 1-4, 77-89.

Planert, L., et al. 2009. Along- and across-axis variations in crustal thickness and structure at the Mid-Atlantic Ridge at 5°S obtained from wide-angle seismic tomography: Implications for ridge segmentation. Journal of Geophysical Research, 114, B09102.

Poort, J., and J. Klerkx. 2004. Absence of a regional surface thermal high in the Baikal rift; new insights from detailed contouring of heat flow anomalies. Tectonophysics, 383, 3-4, 217-241.

Powell, J. W. 1874. Report of exploration in 1873 of the Colorado of the West and its tributaries. Journal,Issue.

Powell, J. W. (1876). Report on the geology of the eastern portion of the Uinta Mountains and a region of country adjacent thereto. With Atlas. Washington: Government Printing Office, 218.

Priestley, K. F., et al. 1982. Crust and upper mantle structure in the northwest Basin and Range province. Bulletin of the Seismological Society of America, 72, 3, 911.

Prodehl, C. 1979. Crustal structure of the Western United States. Journal, 1034,Issue,62.

Proffet, J. M. J. 1977. Cenozoic geology of the Yerington distric, Nevada, and implications for the nature and origin of Basin and Range faulting. Geological Society of America Bulletin, 88, 247-266.

Prokopenko, A. A., et al. 2005. Basin-wide sedimentation changes and deglacial lake-level rise in the Hovsgol basin, NW Mongolia. Quaternary International, 136, 1, 59-69.
Purdy, G. M., and R. S. Detrick. 1986. Crustal structure of the Mid-Atlantic Ridge at 23-degrees-n from seismic refraction studies. Journal of Geophysical Research, 91, B3, 3739-3762.
Puzyrev, N. N., et al. 1970. Crustal seismic investigation in the Baikal rift zone. Journal of Geomagnetism and Geoelectricity, 22, 1-2, 169-175.
Puzyrev, N. N., et al. 1973. Deep seismic investigations in Baikal Rift Zone. Tectonophysics, 20, 1-4, 85-95.
Puzyrev, N. N., et al. 1978. Deep-structure of Baikal and other continental rift zones from seismic data. Tectonophysics, 45, 1, 15-22.
Qin, C. Y. 2002. The thickness of seismogenic layer under the areas surrounding the Ordos block, Northern China. Pure and Applied Geophysics, 159, 11-12, 2613-2628.
Qin, C. Y., et al. 1999. Spatial distribution of time-independent seismicity in China. Pure and Applied Geophysics, 154, 1, 101-119.
Radziminovich, N. A. 2010. Focal depths of earthquakes in the Baikal region: A review. Izvestiya, Physics of the Solid Earth, 46, 3, 216-229.
Radziminovich, N. A., et al. 2013. Seismicity of the Baikal rift system from regional network observations. 62, 146-161.
Radziminovitch, N., et al. 2005. The 1999 M w 6.0 earthquake sequence in the southern Baikal rift, Asia, and its seismotectonic implications. 161, 2, 387-400.
Radziminovitch, N. A., et al. 2006. Seismicity and seismotectonic deformations of the crust in the Southern Baikal basin. 42, 11, 904-920.
Raitt, R. W., et al. (1955). Tonga Trench * of. In A. Poldervaart (Ed.s.), Tonga Trench * of Book (pp. 0). Geological Society of America.
Rasskazov, S. V., et al. 1997. Evolution of magmatism in the northeastern Baikal rift system. Petrology, 5, 2, 101-120.
Rasskazov, S. V., et al. 2002. Late Cenozoic Volcanism in the Baikal Rift System: Evidence for Formation of the Baikal and Khubsugul Basins due to Thermal Impacts on the Lithosphere and Collision-Derived Tectonic Stress. International Symposium - Speciation in Ancient Lakes, SIAL III - Irkutsk, September 2-7, 2002, 4, 33-38.
Reilinger, R., et al. 2006. GPS constraints on continental deformation in the Africa-Arabia-Eurasia continental collision zone and implications for the dynamics of plate interactions. Journal of Geophysical Research-Solid Earth, 111, B5, B05411.
Reilinger, R. E., et al. 1997. Global Positioning System measurements of present-day crustal movements in the Arabia-Africa-Eurasia plate collision zone. Journal of Geophysical Research-Solid Earth, 102, B5, 9983-9999.
Ren, C., et al. 2022. Rupture process of the 2020 Mw = 6.9 Samos, Greece earthquake on a segmented fault system constrained from seismic, geodetic, and tsunami observations. Tectonophysics, 839, 229497.
Research Group of SSB. (1988 (in Chinese)). Active Fault System around Ordos Massif Beijing: Seismological Press.
Roberts, R. J. 1968. Tectonic framework of the Great Basin. Mo. Univ., Res. J., 101-119.
Russell, I. C. 1885. Geological history of Lake Lahontan, a Quaternary lake of northwestern Nevada. Journal, XI,Issue,288.
Rychkova, K. M., and S. S. S. Mongush. 2018. The Distribution of Heat and Mas Flux in the Southwesternmost Baikal Rift Zone. Journal of Volcanology and Seismology, 12, 3, 187-196.
Sakellariou, D., and K. Tsampouraki-Kraounaki. (2016). Offshore faulting in the Aegean Sea: a synthesis based on bathymetric and seismic profiling data.
Sandwell, D. T., et al. (2002). Bathymetry from Space:Oceanography, Geophysics, and Climate. Bethesda, Maryland: Geosciences Professional Services, 24 pp.
Sankov, V. A., et al. 2014. Contemporary horizontal movements and seismicity of the south Baikal Basin (Baikal rift system). Izvestiya. Physics of the Solid Earth, 50, 6, 785-794.
Saria, E., et al. 2014. Present-day kinematics of the East African Rift. Journal of Geophysical Research-Solid Earth, 119, 4, 3584-3600.
Sass, J. H., et al. 1971. Heat flow in the western United States. Journal of Geophysical Research, 76, 26, 6376-6413.

Sass, J. H., et al. 2005. Summary of Supporting Data for USGS Regional Heat-flow Studies of the Great Basin, 1970-1990. U. S. Geological Survey Open-File Report, 2005-1207, https://pubs.usgs.gov/of/2005/1207/.

Sauermilch, I., et al. 2018. Pre-rift sedimentation of the Lomonosov Ridge, Arctic Ocean at 84°N - A correlation to the complex geologic evolution of the conjugated Kara Sea. Journal Of Geodynamics, 118, 49-54.

Saunders, P., et al. 1998. Variations in the crustal structure beneath western Turkey. Geophysical Journal International, 134, 2, 373-389.

Scholz, C. H., and J. Campos. 1995. On the Mechanism of Seismic Decoupling and Back-Arc Spreading at Subduction Zones. Journal of Geophysical Research-Solid Earth, 100, B11, 22103-22115.

Seeber, L., and J. Armbruster. (1981). Great detachment earthquakes along the Himalayan arc and long-term forecasting of. In D. W. Simpson and R. P. G. (Ed.s.), Great detachment earthquakes along the Himalayan arc and long-term forecasting of Book (pp. 259-279). Am. Geophys. Union.

Seeber, L., and J. G. Armbruster. 1984. Some elements of continental subduction along the Himalayan front. Tectonophysics, 105, 1-4, 263-278.

Sempere, J. C., et al. 1990. Segmentation of the Mid-Atlantic Ridge between 24-degrees-n and 30-degrees-40'n. Nature, 344, 6265, 427-431.

Sengor, A. M. C., et al. (1985). Strike-slip faulting and related basin formation in zones of tectonic escape: Turkey as a case study of. In K. T. Biddle and N. Christie-Blick (Ed.s.), Strike-slip faulting and related basin formation in zones of tectonic escape: Turkey as a case study of Book (pp. 227-265). Society of ecomonic paleontoligsts and mineralogists.

Sengor, A. M. C., et al. 2005. The North Anatolian Fault: a new look. Annual Review of Earth and Planetary Sciences, 33, 37-112.

Seno, T., and D. G. Gonzalez. 1987. Faulting caused by earthquakes beneath the outer slope of the Japan Trench. Journal Of Physics Of The Earth, 35, 5, 381-407.

Seno, T., and Y. Yamanaka. (1996). Double seismic zones, compressional deep trench-outer rise events, and superplumes of. In (Ed.s.), Double seismic zones, compressional deep trench-outer rise events, and superplumes of Book (pp. 347-355). AGU.

Serpelloni, E., et al. 2005. Crustal velocity and strain-rate fields in Italy and surrounding regions: new results from the analysis of permanent and non-permanent GPS networks. Geophysical Journal International, 161, 3, 861-880.

Serpelloni, E., et al. 2006. GPS measurement of active strains across the Apennines. Annals of Geophysics, 49, 1, 319-329.

Serpelloni, E., et al. 2007. Kinematics of the western Africa-Eurasia plate boundary from focal mechanisms and GPS data. Geophysical Journal International, 169, 3, 1180-1200.

Severinghaus, J., and T. Atwater. 1990. Cenozoic geometry and thermal state of the subducting slabs beneath western North America. Geological Society of America Memoir, 176, 1-22.

Shah, A. K., and O. S. Boyd. 2018c. Depth to Basement and Thickness of Unconsolidated Sediments for the Western United States—Initial Estimates for Layers of the U.S. Geological Survey National Crustal Model. U. S. Geological Survey Open-File Report, 2018-115, 13 p.

Shaw, B., and J. Jackson. 2010. Earthquake mechanisms and active tectonics of the Hellenic subduction zone. Geophysical Journal International, 181, 2, 966-984.

Shaw, P. R. 1992. Ridge segmentation, faulting and crustal thickness in the Atlantic-Ocean. Nature, 358, 6386, 490-493.

Shchetnikov, A. A., et al. 2012. Late Quaternary geology of the Tunka rift basin (Lake Baikal region), Russia. Journal of Asian Earth Sciences, 46, 195-208.

Shor, G. G., and R. I. Fisher. 1961. Middle America Trench: Seismic-Refraction Studies. Geological Society of America Bulletin, 72, 721-730.

Shudofsky, G. N. 1985. Source mechanisms and focal depths of east-african earthquakes using rayleigh-wave inversion and body-wave modeling. Geophysical Journal of the Royal Astronomical Society, 83, 3, 563-614.

Simao, N., et al. 2010. Regional seismicity of the Mid-Atlantic Ridge: observations from autonomous hydrophone arrays. Geophysical Journal International, 183, 3, 1559-1578.

Singh, A., et al. 2017. Crustal Structure Beneath India and Tibet: New Constraints From Inversion of Receiver Functions. Journal Of Geophysical Research, 122, 10, 7839-7859.
Singh, S. C., et al. 2006. Discovery of a magma chamber and faults beneath a Mid-Atlantic Ridge hydrothermal field. Nature, 442, 7106, 1029-1032.
Sinha, M. C., et al. 1997. Evidence for accumulated melt beneath the slow-spreading Mid-Atlantic ridge. Philosophical Transactions of the Royal Society A-Mathematical Physical And Engineering Sciences, 355, 1723, 233-253.
Sinton, J. M., and R. S. Detrick. 1992. Mid-ocean ridge magma chambers. Journal Of Geophysical Research, 97, B1, 197-216.
Smith, D. K., and J. R. Cann. 1992. The role of seamount volcanism in crustal construction at the Mid-Atlantic Ridge (24°30'N). Journal of Geophysical Research, 97, B2, 1645-1658.
Smith, D. K., and J. R. Cann. 1993. Building the crust at the Mid-Atlantic Ridge. Nature, 365, 6448, 707-715.
Smith, D. K., et al. 2006. Widespread active detachment faulting and core complex formation near 13°N on the Mid-Atlantic Ridge. Nature, 442, 7101, 440-443.
Smith, R. B., and R. L. Bruhn. 1984. Intraplate extensional tectonics of the Eastern Basin-Range - inferences on structural style from seismic-reflection data, regional tectonics, and thermal-mechanical models of brittle-ductile deformation. Journal of Geophysical Research, 89, NB7, 5733-5762.
Sodoudi, F., et al. 2006. Lithospheric structure of the Aegean obtained from P and S receiver functions. JOURNAL OF GEOPHYSICAL RESEARCH-SOLID EARTH, 111, B12, B12307.
Solonenko, V. P. (1977). Seismic Zonation of Eastern Siberia and its Geological and Geophysical Bases. (of. In (Ed.s.), Seismic Zonation of Eastern Siberia and its Geological and Geophysical Bases. (of Book (pp. pp. 303). Novosibirsk: Nauka.
Sonder, L. J., and C. H. Jones. 1999. Western United States extension: How the West was widened. Annual Review of Earth and Planetary Sciences, 27, 417-+.
Speed, R. C., and N. H. Sleep. 1982. Antler orogeny and foreland basin - a model. Geological Society of America Bulletin, 93, 9, 815-828.
Stamps, D. S., et al. 2018. A Geodetic Strain Rate Model for the East African Rift System. Scientific Reports, 8:732, 732, 1-8.
Staub, R. 1924. Der Bau des Alpen:. Geologie Karte Schweiz, 52, 272.
Stauder, W. 1968. Tensional character of earthquake foci beneath the Aleutian Trench with relation to sea-floor spreading. Journal of Geophysical Research (1896-1977), 73, 24, 7693-7701.
Stein, C. A., and S. Stein. 1994. Constraints on hydrothermal heat-flux through the oceanic lithosphere from global heat-flow. Journal of Geophysical Research, 99, B2, 3081-3095.
Stewart, J. H. 1971. Basin And Range Structure - System Of Horsts And Grabens Produced By Deep-Seated Extension. Geological Society of America Bulletin, 82, 4, 1019-1043.
Stewart, J. H. (1978). Basin and Range structure in western north America: A review of. In R. B. Smith and G. P. Eaton (Ed.s.), Basin and Range structure in western north America: A review of Book (pp. 1-31). Boulder, CO: Geological Society of America.
Stewart, J. H. 1980. Regional tilt patterns of late Cenozoic Basin-Range fault blocks, Western United-States. Geological Society of America Bulletin, 91, 8, 460-464.
Stewart, J. H. 1989. Geology of Nevada: A discussion to accompany the Geologic Map of Nevada. Nevada Bureau of Mines and Geology Special Publication 4, Cenozoic Tectonics, 105-115.
Stewart, J. H. (1998). Regional characteristics, tilt domains, and extensional history of the late Cenozoic Basin and Range province, western North America of. In J. E. Faulds and J. H. Stewart (Ed.s.), Regional characteristics, tilt domains, and extensional history of the late Cenozoic Basin and Range province, western North America of Book (pp. 47-44). Boulder, Colorado: Geological Society of America.
Stewart, J. H., and F. G. Pool. (1974). Lower Paleozoic and uppermost Precambrian Cordilleran miogeocline, GreatBasin, western United States of. In W. R. Dickenson (Ed.s.), Lower Paleozoic and uppermost Precambrian Cordilleran miogeocline, GreatBasin, western United States of Book (pp. 27-57). Society of Economic Paleontologists and Mineralogists.
Straub, C., and H. G. Kahle. 1994. Global positioning system (gps) estimates of crustal deformation in the Marmara Sea region, northwestern Anatolia. Earth and Planetary Science Letters, 121, 3-4, 495-502.
Straub, C., et al. 1997. GPS and geologic estimates of the tectonic activity in the Marmara Sea region, NW Anatolia. Journal of Geophysical Research-Solid Earth, 102, B12, 27587-27601.

Suess, E. (1891). Die Bruche des ostlichen Africa, of. In (Ed.s.), Die Bruche des ostlichen Africa, of Book (pp. 555-584). Wien, Denkschr.: Akad. Wiss.

Suvorov, V. D., et al. 2002. Structure of the crust in the Baikal rift zone and adjacent areas from Deep Seismic Sounding data. Tectonophysics, 351, 1-2, 61-74.

Sykes, L. R. 1967. Mechanism of earthquakes and nature of faulting on mid-oceanic ridges. Journal Of Geophysical Research, 72, 8, 2131-&.

Sykes, L. R. (2019). Plate Tectonics and Great Earthquakes: 50 Years of Earth-Shaking Events. Columbia University Press, 272 pp.

Tao, W., and Z. Shen. 2008. Heat flow distribution in Chinese continent and its adjacent areas. Progress in Natural Science, 18, 843-849.

Tapponnier, P., et al. 1981. Field evidence for active normal faulting in Tibet. Nature (London), 294, 5840, 410-414.

Tapponnier, P., and P. Molnar. 1976. Slip-line field-theory and large-scale continental tectonics. Nature, 264, 5584, 319-324.

Tapponnier, P., and P. Molnar. 1977. Active faulting and tectonics in China. Journal of Geophysical Research, 82, 20, 2905-2930.

Tapponnier, P., and P. Molnar. (1977). Rigid plastic indentation; the origin of syntaxis in the Himalayan Belt of. In C. Jest (Ed.s.), Rigid plastic indentation; the origin of syntaxis in the Himalayan Belt of Book (pp. 431-432). Paris, France: Centre National de la Recherche Scientifique.

Tapponnier, P., and P. Molnar. 1979. Active faulting and Cenozoic tectonics of the Tien Shan, Mongolia, and Baykal regions. Journal of Geophysical Research, 84, NB7, 3425-&.

Taylor, M., and A. Yin. 2009. Active structures of the Himalayan-Tibetan orogen and their relationships to earthquake distribution, contemporary strain field, and Cenozoic volcanism. Geosphere, 5, 3, 199-214.

Tectonics_Observatory. 2009. Seafloor Age. Journal,Issue.

Teleki, S. 1895. Count Samuel Teleki East African diaries, in Hungarian, 1886-95; with English translations, 1961-1965. MSS 94, Special Collections, MSU Libraries, Michigan State University, East Lansing, MI.

ten Brink, U. S., and M. H. Taylor. 2002. Crustal structure of central Lake Baikal: Insights into intracontinental rifting. Journal of Geophysical Research-Solid Earth, 107, B7, 2132, 15.

Thatcher, W. 2003. GPS constraints on the kinematics of continental deformation. International Geology Review, 45, 3, 191-212.

Thatcher, W., et al. 1999. Present-day deformation across the Basin and Range province, western United States. Science, 283, 1714-1718.

Thieblemont, D. 2016. Carte Geologique de L'Afrique (Geological Map of Africa). 1:10 milliion scale, Printing sponsored by African Minerals Development Centre (AMDC).

Thompson, G. A., and D. B. Burke. 1974. Regional Geophysics of the Basin and Range Province. Annual Review of Earth and Planetary Sciences, 2, 1, 213-238.

Thompson, G. A., et al. (1989). Geophysics of the western Basin and Range province of. In L. C. Pakiser and W. Mooney (Ed.s.), Geophysics of the western Basin and Range province of Book (pp. 177-203).

Tilmann, F., et al. 2004. Microearthquake seismicity of the Mid-Atlantic Ridge at 5°S:: A view of tectonic extension -: art. no. B06102. Journal Of Geophysical Research, 109, B6, B06102.

Tozer, B., et al. 2019. Global Bathymetry and Topography at 15 Arc Sec: SRTM15+. Earth and Space Science, 6, https://doi.org/10.1029/ 2019EA000658.

Trexler, J. H., et al. 2003. Widespread effects of middle Mississippian deformation in the Great Basin of western North America. Geological Society of America Bulletin, 115, 10, 1278-1288.

Trexler, J. H., et al. 2004. Late Paleozoic tectonism in Nevada: Timing, kinematics, and tectonic significance. Geological Society of America Bulletin, 116, 5-6, 525-538.

Tsampouraki-Kraounaki, K., et al. (2022). Seismic stratigraphy and structure of Myrtoon basin: preliminary results.

Tucholke, B. E., et al. 2008. Role of melt supply in oceanic detachment faulting and formation of megamullions. Geology, 36, 6, 455-458.

UNAVCO. 2020. Tectonic motions of the Western United States. University NAVSTAR Consortium (UNAVCO) Velocity Map Poster Series, https://www.unavco.org/education/outreach/giveaways/velocity-map-posters/velocity-map-posters.html (accessed 2022).

Uyeda, S., and H. Kanamori. 1979. Back-arc opening and the mode of subduction. Journal of Geophysical Research, 84, NB3, 1049-1061.

Vinnik, L. P., et al. 2017. Crust and mantle of the Baikal Rift Zone from P- and S-wave receiver functions. Geodynamics & Tectonophysics, 8, 4, 695-709.

von Hohnel, L. (1894). Discovery of Lakes rudolof and Stephanie: a narrative of Count Samuel Teleki's exploring and hunting expedition in Eastern Equatorial Africa in 1887 ad 1888 (Translated by Nancy Bell (n. D'anvers). London: Longmans, Green and Co. (and New York: 15 East 16th Street).

Vonherzen, R. P., and V. Vacquier. 1967. Terrestrial heat flow in Lake Malawi Africa. Journal of Geophysical Research, 72, 16, 4221-+.

Vvedenskaya, A. V. (1961). Peculiarities of the stress state in the foci of Pribaikal earthqakes (in Russian) of. In (Ed.s.), Peculiarities of the stress state in the foci of Pribaikal earthqakes (in Russian) of Book (pp. 666-669 (in Russian)). Izvestiya: Akademi Nauk, USSR.

Wallace, R. E. (1984). Fault scarps formed during the earthquakes of October 2, 1915, in Pleasant Valley, Nevada, and some tectonic implications of. In (Ed.s.), Fault scarps formed during the earthquakes of October 2, 1915, in Pleasant Valley, Nevada, and some tectonic implications of Book (pp. A1-A33). Reston, VA: U. S. Geological Survey.

Wallace, R. E. 1984. Patterns and timing of late Quaternary faulting in the Great Basin province and relation to some regional tectonic features. Journal of Geophysical Research, 89, 5763-5769.

Wang, C. Y., et al. 2014. Lateral variation of crustal structure in the Ordos block and surrounding regions, North China, and its tectonic implications. Earth and Planetary Science Letters, 387, 198-211.

Wang, F. B., and B. Y. Li. (1982). The lower boundary of the Quaternary in the Himalayan region in China of. In Q. R. A. o. China (Ed.s.), The lower boundary of the Quaternary in the Himalayan region in China of Book (pp. 13-16). Beijing: China Ocean Press.

Wang, Q., et al. 2001. Present-day crustal deformation in China constrained by Global Positioning System Measurements. Science, 294, 574-577.

Wang, S. Q., et al. 2017. Geothermal resources in Tibet of China: current status and prospective development. Environmental Earth Sciences, 76, 6, 239.

Wang, T., et al. 2021. Crustal structure beneath the Ethiopian Plateau and adjacent areas from receiver functions: Implications for partial melting and magmatic underplating. Tectonophysics, 809, 228857.

Wang, Y., et al. (1982). Some features of the active faults in the northern part of Ningxia Autonomous Region. Beijing: Seismological Publishing House, 154-161 (in Chinese).

Wesnousky, S. G., et al. 1984. Historical seismicity and rates of crustal deformation along the margins of the Ordos block, north China. Bulletin of the Seismological Society of America, 74, 5, 1767-1783.

Westaway, R. 1992. Seismic moment summation for historical earthquakes in Italy - tectonic implications. Journal of Geophysical Research-Solid Earth, 97, B11, 15437-15464.

Westaway, R., and J. Jackson. 1984. Surface faulting in the southern Italian Campania-Basilicata earthquake of 23 November 1980. Nature, 312, 5993, 436-438.

Wheeler, G. M. (1875). Report Upon Geographical and Geological Surveys West of the one Hundredth Meridian. Washington: Government Printing Office.

Wheildon, J., et al. 1994. Heat-flow in the Kenya rift-zone. Tectonophysics, 236, 1-4, 131-149.

Williams, H., et al. 2001. Age and composition of dikes in Southern Tibet: New constraints on the timing of east-west extension and its relationship to postcollisional volcanism. Geology, 29, 4, 339-342.

Willis, B. (1936). East African plateaus and rift valleys. Wahsington: Carnegie Institute.

Wolfe, C. J., et al. 1995. Microearthquake characteristics and crustal velocity structure at 29 degrees N on the Mid-Atlantic Ridge: The architecture of a slow spreading segment. Journal of Geophysical Research, 100, B12, 24449-24472.

Wolfe, J. A., and P. Molnar. 1997. Paleobotannical evidence for high altitudes in Nevada during the Miocen. Science, 276, 1672-1675.

Xu, Y., et al. 2018. The CE 1303 Hongdong Earthquake and the Huoshan Piedmont Fault, Shanxi Graben: Implications for Magnitude Limits of Normal Fault Earthquakes. Journal of Geophysical Research: Solid Earth, 123, 4, 3098-3121.

Yakovlev, A. V., et al. 2007. Moho depths and three-dimensional velocity structure of the crust and upper mantle beneath the Baikal region, from local tomography. Russian Geology and Geophysics, 48, 2, 204-220.

Yamano, M., et al. 2014. Heat flow anomaly on the seaward side of the Japan Trench associated with deformation of the incoming Pacific plate. Earth and Planetary Science Letters, 407, 196-204.

Yang, Z., and W.-P. Chen. 2010. Earthquakes along the East African Rift System: A multiscale, system-wide perspective. Journal of Geophysical Research-Solid Earth, 115, B12309.

Yang, Z. H., and W. P. Chen. 2008. Mozambique earthquake sequence of 2006: High-angle normal faulting in southern Africa. Journal of Geophysical Research, 113, B12, B12303.

Ye, H., et al. 1987. The Cenozoic tectonic evolution of the great north China; two types of rifting and crustal necking in the great north China and their tectonic implications. Tectonophysics, 133, 217-227.

Ye, H., and W. Zhang. (1983). The history and deformation mechanism of Cenozoic crustal movement in North China [in Chinese] of. In J. Ren (Ed.s.), The history and deformation mechanism of Cenozoic crustal movement in North China [in Chinese] of Book (pp. 130-139 (in Chinese)). Beijing: Publishing House of Academy of Sciences.

Yin, A., and T. M. Harrison. 2000. Geologic evolution of the Himalayan-Tibetan orogen. Annual review of earth and planetary sciences, 28, 211-280.

Yu, C.-Q., et al. 2012. Thick crust beneath the Ordos plateau: Implications for instability of the North China craton. Earth and Planetary Science Letters, 357, 366-375.

Zhang, B. C., et al. 1986. Fault scarps related to the 1739 earthquake and seismicity of the Yinchuan graben, Ningxia Huizu Zizhiqu, China. Bulletin of the Seismological Society of America, 76, 5, 1253-1287.

Zhang, P. Z., et al. 2004. Continuous deformation of the Tibetan Plateau from global positioning system data. Geology, 32, 9, 809-812.

Zhang, Y. Q., et al. 1998. Extension in the graben systems around the Ordos (China), and its contribution to the extrusion tectonics of south China with respect to Gobi-Mongolia. Tectonophysics, 285, 1-2, 41-75.

Zhang, Z. J., et al. 2013. Seismic structure and rheology of the crust under mainland China. Gondwana Res., 23, 4, 1455-1483.

Zhang, Z. J., et al. 2004. Crustal structure of seismic velocity in southern Tibet and east-westward escape of the crustal material - An example by wide-angle seismic profile from Peigu Tso to Pumoyong Tso. Science in China Series D-Earth Sciences, 47, 6, 500-506.

Zhao, B., et al. 2017. Contemporary kinematics of the Ordos block, North China and its adjacent rift systems constrained by dense GPS observations. Journal of Asian Earth Sciences, 135, 257-267.

Zhao, G. D., et al. 2020. Moho Beneath Tibet Based on a Joint Analysis of Gravity and Seismic Data. Geochemistry Geophysics Geosystems, 21, 2, e2019GC008849.

Zheng, Y., et al. 2011. Crust and uppermost mantle beneath the North China Craton, northeastern China, and the Sea of Japan from ambient noise tomography. Journal of Geophysical Research-Solid Earth, 116, B12312.

Zielke, O., and M. R. Strecker. 2009. Recurrence of Large Earthquakes in Magmatic Continental Rifts: Insights from a Paleoseismic Study along the Laikipia-Marmanet Fault, Subukia Valley, Kenya Rift. Bulletin of the Seismological Society of America, 99, 1, 61-70.

Zorin, Y., and L. Cordell. 1991. Crustal extension in the Baikal rift zone. Tectonophysics, 198, 1, 117-121.

Zorin, Y. A. 1966. On the deep structure of theBaikal epression basd on geophysical data (in Russian). Isv. Akad. Nauk SSSR, , Ser. Geol., no. 7, 76-85.

Zorin, Y. A. 1999. Geodynamics of the western part of the Mongolia-Okhotsk collisional belt, Trans-Baikal region (Russia) and Mongolia. Tectonophysics, 306, 1, 33-56.

Zorin, Y. A., et al. 1989. Thickness of the lithosphere beneath the Baikal rift zone and adjacent regions. 168, 4, 327-337.